Beam Behaviour of Hybrid Steel Sections

Prepared by:
Diana E. Makwecha

Supervised by:
Dr Alvin Masarira

Department of Civil Engineering
University of Cape Town
2007

This dissertation is submitted to the University of Cape Town
in partial fulfilment of the requirements for the degree of
Master of Science in Engineering

To the memory of my father,

Daniel Dick Tiisai Makweche.

Declaration

I know the meaning of plagiarism and declare that all of the work in the document, save for that which is properly acknowledged, is my own.

Signed by candidate ..29/05/2007..

Diana E. Makweche Date

Acknowledgements

I would like to extend my sincere thanks to the following people for their support throughout the duration of this programme:

- Dr Alvin Masarira for supervising my research
- Prof. George Ekama and University Council for their financial assistance;
- Dr Salie Mahoi for helping me with some of the modelling aspects;
- Mrs Eunice Makweche and Schona Makweche for their financial support;
- Jeanine McGill, Joanne Stocks and my bible study group for their prayers and encouragement;
- Precillar Moyo and
- My colleagues within the Structures Research Group.

Abstract

Doubly symmetric hybrid beams with I-section profiles are composed of higher steel flanges while the web usually contains lower strength, conventionally manufactured steel. This arrangement confers greater strength to the flanges which are fundamental in generating bending resistance to the applied loads.

Although hybrid beams offer many potential benefits, such as savings in material and costs, existing codes of practice contain few guidelines on how to design such members. Apart from the lack of design guidelines, recommendations in many steel design codes apply only to steel grades with specified yield strength less than 460MPa.

The purpose of the research was, firstly, to examine the development of stresses and strains within the flanges and web in order to establish how this differs from that in homogeneous members. It was also necessary to investigate the effectiveness of various hybrid combinations (with steels of varying yield strength in webs and flanges), the influence of different width to thickness ratios on hybrid beam behaviour, and the possibility of extrapolating existing design guidelines so that they can be used for higher grade steels.

This comparative study was achieved through finite element analysis of 2m and 4m hybrid beams using the finite element analysis software ABAQUS. Data and results extracted included Mises stresses, strains and deflections.

This research shows that for some aspects of hybrid design, namely width to thickness ratios and section classification, extrapolation may not be conservative. Furthermore, it confirms the recommendation that the flange yield moment be taken as the characteristic hybrid beam strength as failure, due to material yielding, and unloading occur quite rapidly after the ultimate load has been achieved.

Recommendations were made, in the form of suggestions of new slenderness classification limits geared to accommodate higher strength steels.

Contents

Dedication i

Declaration ii

Acknowledgements iii

Abstract iv

1 Introduction and Literature Review 1

1.1 Background……1

1.2 Literature Review……4

1.3 Problem Definition……16

2 Methodology 18

2.1 Introduction…… 18

2.2 Characteristics of ABAQUS……19

2.2.1 Introduction……19

2.2.2 ABAQUS Element Library……19

2.2.3 Material Model……20

2.2.4 Geometric Nonlinearities……22

2.2.5 Types of Analysis……23

2.2.6 Input and Output……24

2.3 Model Description……24

2.3.1 Introduction……24

2.3.2 Beam Geometry……24

2.3.3 Elements and Meshing……25

2.3.4 Boundary Conditions and Loading……26

2.4 Material Types and Characteristics of Steels Used in the Hybrid Beams……..…27

2.4.1 Introduction……27

2.4.2 Material Data…… ..30

2.4.3 Steel Properties…… ...38

2.4.3.1 Modulus of Elasticity…… ..38

2.4.3.2 Poisson's Ratio…… …41

2.4.3.3 Shear Modulus…… …41

3 The Behaviour of Beams in Bending…… ...42

3.1 Introduction…… … …42

3.2 General Beam Theory……..…… … .42

3.2.1 Bending of a Homogeneous Member…… …42

3.2.2 Width to Thickness Ratios and the Elastic Buckling of Webs and Flanges of Unstiffened Beams……..…...45

3.3 Hybrid Steel Sections Configurations……..…....47

3.3.1 Introduction…….....47

3.3.2 Development of Stresses across the Hybrid 4 Cross-Section…….....….48

3.4 Determination of Hybrid 4 Beam Moment from First Principles……..50

4 Comparative Analysis and Investigation of Hybrid Beams……...54

4.1 Introduction…….....54

4.2 Influence of Width to Thickness Ratios on Bending Behaviour…… .56

4.2.1 Introduction…… .56

4.2.1.1 Model Data……..…. 56

4.2.1.2 Limiting Width to Thickness Ratios from Design Codes.....57
4.2.1.3 Classification of Flanges and Webs.....60
4.2.2 ABAQUS Analysis Results.....61
4.2.3 Theoretical Numerical Results.....66
4.2.4 Summary of Results.....71
4.3 Influence of Length on Bending Behaviour.....72
4.3.1 Introduction.....72
4.3.1.1 Model Data.....72
4.3.2 ABAQUS Results.....72
4.3.2.1 Two Metre Beams with 350MPa Flanges.....72
4.3.2.2 Two Metre Beams with 460MPa Flanges.....73
4.3.2.3 Two Metre Beams with 550MPa Flanges.....75
4.3.2.4 Two Metre Beams with 690MPa Flanges.....77
4.3.2.5 Two Metre Beams with 700MPa Flanges.....82
4.3.2.6 Four Metre Beams with 350MPa Flanges.....87
4.3.2.7 Four Metre Beams with 460MPa Flanges.....88
4.3.2.8 Four Metre Beams with 550MPa Flanges.....89
4.3.2.9 Four Metre Beams with 690MPa Flanges.....91
4.3.2.10 Four Metre Beams with 700MPa Flanges.....94
4.3.3 Summary of ABAQUS Results.....100
4.3.4 Theoretical Numerical Results.....101
4.3.4.1 Two Metre Beams with 350MPa Flanges.....108
4.3.4.2 Two Metre Beams with 460MPa Flanges.....108
4.3.4.3 Two Metre Beams with 550MPa Flanges.....109

4.3.4.4 Two Metre Beams with 690MPa Flanges.....111

4.3.4.5 Two Metre Beams with 700MPa Flanges.....113

4.3.4.6 Four Metre Beams with 350MPa Flanges.....116

4.3.4.7 Four Metre Beams with 460MPa Flanges.....116

4.3.4.8 Four Metre Beams with 550MPa Flanges.....117

4.3.4.9 Four Metre Beams with 690MPa Flanges.....119

4.3.4.10 For Metre Beams with 700MPa Flanges.....121

4.3.5 Summary of Theoretical Numerical Results.....124

4.4 Influence of Hybrid Configuration on Bending Behaviour.....125

4.4.1 Introduction.....125

4.4.1.1 Model Data.....126

4.4.2 ABAQUS Results.....126

4.4.3 Summary of Results.....129

4.5 Verification of Bending Equations.....130

4.5.1 Verification Using the Equation Presented by

Frost and Schilling (1964).....131

4.5.2 Verification Using the Equations Presented by Frost

and Schilling (1964) and the Joint ASCE-AASHO

Committee on Flexural members (1968).....132

4.6 Determination of New Width to Thickness Ratios.....134

4.6.1 Width to Thickness Ratios for Flanges.....134

4.6.2 Width to Thickness Ratios for Webs.....136

5 Recommendations.....139

5.1 Conclusions……139

5.2 Recommendations……..140

Bibliography……141

1 Introduction and Literature Review

1.1 Background

One of the objectives of engineering design is to create efficient systems in order to reduce costs. This often involves making adequate use of the available resources, developing new methods, coming up with better designs, and conducting research aimed at identifying, and even creating, more suitable materials.

This trend is also evident in structural steel analysis and design. Steel is widely regarded as a versatile material in construction as it allows for greater innovation as compared to other materials. The history of large construction in metal began very humbly in the early eighteenth century. The first road bridge made completely of cast iron (the Ironbridge) was completed in 1779 in England. Prior to that time, bridges had been designed exclusively in brick, timber and stone in structural systems that ensured that the actions in the members were mainly compressive. Cast iron revolutionised bridge design, in particular, as it allowed for arrangements where ties and beams played a greater role.

As structures became larger and more complex, some points of concern were raised regarding cast iron. The low yield stress, which is in the region of 120 megaPascals (MPa), and low ductility were two important ones as they directly influenced the load-carrying capacity of structures. Corrosion and the tendency of the metal to rust were also under scrutiny.

Progressively, the need for particular properties to facilitate economical and safe design led manufacturers into developing new materials which would address the yield stress and ductility shortcomings presented by the use of cast iron. The development of the modern steel production process yielded the first conventional steels which were capable of sustaining yield stresses in the order of magnitude of approximately 250MPa.

From the 1950's the 500MPa class steels were being used in bridge construction in Japan (Miki et al, 2002) and by the 1970's steel grades of 800MPa had been developed. During the same period 690MPa steels were developed and employed in

bridge construction in North America (Bjorhovde, 2004). One example of such steels is COR-TEN Type T-1 which was first used in bridge construction in 1962 (Bjorhovde, 2004). These are high strength steels as they have yield strengths in excess of 450MPa. At the outset, their high yield stresses were obtained very simply by increasing the percentage Carbon content.

While those grades at the lower end of the strength spectrum, which may be referred to as mild steels, exhibited acceptable levels of ductility, it became clear that those at the upper end tended to be quite brittle. In effect, the Carbon that added strength had a highly deleterious effect on the ductility. In addition, high preheating temperatures had to be employed during welding, coupled with other stringent measures. These measures included inert gaseous environments that contained very low levels of hydrogen (Adonyi, 1998) in order to ensure that the welds were of a high quality. This made welding a complicated and an expensive operation and the strict conditions demanded were more closely approximated in machine shops rather than on site. However, the higher yield strengths of steel made slender girder cross-sections possible but also led to serviceability problems such as excessive deflections and increased vibration.

These factors dissuaded some designers and stakeholders within the construction industry from utilising these steels. Researchers in academia and industry, however, continued investigating ways of improving the characteristics of the materials. The term *high performance steels* (HPS) was coined to describe those that possessed particular, desirable properties. Such qualities ranged from higher yield strength to enhanced corrosion resistance and improved weldability. *Weldability* is a term used to describe the ease with which steel lends itself to joining by welding methods without excessive hydrogen cracking (MacDougall et al, 2004).

The added corrosion resistance made HPS amenable to use without the need for protective coats of paint while the increased weldability made it possible to lower, and even eliminate, the need for high preheat temperatures. These successes were made possible by new thermo-mechanical controlled processes (TMCP). These have replaced the traditional quenching and tempering processes and work by closely regulating temperatures and deformations during steel production (Miki et al., 2002).

The first step was to manipulate the chemical composition of the steel. Modern HPS contain significantly lower percentages of carbon and small amounts of micro-alloying elements such as Aluminium and Molybdenum have been added to make up for the loss of strength. TMCP has the added advantage of producing steel plates that have a much finer grain structure (Datta and Mishra, 2001) and longer mill lengths (Lwin, 2002).

Despite these advances many steel design codes, including the Eurocode (EN 1993-1-1), the American Institute of Steel Construction Load and Resistance Factor Design (AISC LRFD, 1999; 2005) and the South African National Standard (SANS 10162-1, 2004) state that design recommendations according to these codes apply only to steel grades with specified yield strength less than 460MPa. This fact has always been a hindrance to those designers who recognise the potential benefits of using HPS and yet have no clear design guidelines. This state of affairs persists in spite of the large volume of research indicating that HPS design can be approached much in the same manner as that of conventional mild steels.

Extrapolating existing design methods and equations for use in HPS has been addressed in various literary studies (Ricles et al., 1998; Thomas and Earls, 2003). Other research areas that have been scrutinised have covered the strength aspects of flexural capacity (Frost and Schilling, 1964), as quantified by either yield or plastic moment of girders; rotational capacity (Greco and Earls, 2003), which is a measure of a beams ability to sustain the high levels of ductility required for plastic analysis; and shear capacity or, alternatively, a beam's resistance to concentrated patch loads (Lagerqvist and Johansson, 1996). Stability aspects identified encompassed lateral bracing and slenderness limits. Additionally, connections (welding and bolting), residual stresses and initial imperfections (Clarin, 2004), fatigue performance (Hildebrand and Schliebner, 2004) and hybrid behaviour (Frost and Schilling, 1964) all have received some attention.

The main focus of this thesis is hybrid beam behaviour. The most commonly used hybrid beams comprise of high strength flanges and mild steel webs. These composites came about, in part, due to the appreciation that homogeneous HPS beams are rather uneconomical because of the higher material cost. Further, it is clear that

flanges play a far greater role in resisting bending moments and, hence, it is conceivable that the moment resistance would be increased if the flange material yield stress were increased.

Some facets of hybrid beams have been studied, for example their rotation capacity (Greco and Earls, 2003), ultimate bending strength (Frost and Schilling, 1964) and shear strength (Carskaddan, 1968). However, there has been little discussion, particularly in design codes, that delves into the development and distribution of stresses and strains through a hybrid cross-section. Indeed, how the hybrid characteristic strength is determined remains unclear as codes of practice do not contain relevant guidelines.

1.2 Literature Review

The structural strength and stability behaviour of typical high strength steel (McDermott, 1969; Sause and Fahnstock, 2001) and hybrid members (Carskaddan, 1968; Greco and Earls, 2003) has been investigated in several different ways in order to ascertain whether they exhibit the required performance. Such desirable behaviour includes the ability to achieve the full yield or plastic moment capacity of the section; adequate resistance to concentrated loading; sufficient resistance to deformation; and the ability to exhibit the necessary levels of ductility. In addition, these properties should be present under both static and dynamic loading conditions.

The strength of homogeneous flexural members is taken as the yield moment or the plastic moment, depending on the width to thickness ratios of the constituent plates. Beams of class 1 (SANS 10162-1, 2004; EN 1993-1-1) or compact (AISC LRFD, 1999; AISC Spec., 2005) cross-section show adequate ductile behaviour and can achieve the theoretic plastic moment ($M_p = \sigma_y Z$, where σ_y and Z are the material yield stress and plastic modulus, respectively). Beams of classes 3 and 4 (SANS 10162-1, 2004; EN 1993-1-1) or those which are non-compact (AISC LRFD, 1999; AISC Spec., 2005) may achieve only the yield moment ($M_y = \frac{\sigma_y I}{y}$, where σ_y is the yield stress, I is the moment of inertia of the section, and y is the distance from the neutral axis).

Further restrictions are placed on high strength steel beams, with specified minimum yield stress exceeding 450MPa, in that even those which have been classified as compact are regarded as not being able to achieve the plastic moment. This means that plastic analysis and design are not permitted (AISC LRFD, 1999; AISC Spec., 2005). This stipulation is rather severe because it means that a great deal of the reserve strength that comes with the higher strength steel is not utilised at all; and this applies to both homogeneous and hybrid beams. It has been argued that possible material and cost savings are compromised by the guideline and some experimental work (Sause and Fahnstock, 2001) has been conducted in order to try and demonstrate that the assumption is conservative.

At first glance, it appears that the above constraint merely seeks to limit the yield stress of the flange and web steel. In reality, it is based on the realisation that high strength steels have limited ductility. This is substantiated by a further guideline which states that a minimum rotation capacity of three is required (AISC Spec., 2005) for all beams that are to be designed using plastic methods. The rotation capacity is essentially a measure of the amount of plastic deformation that will take place before a structure starts to unload and is defined as defined as $R = \frac{\theta_u}{\theta_p} - 1$ (see Figure 1.1); where R is the rotation capacity, θ_p is the theoretical rotation at which the full plastic capacity is achieved based on elastic beam stiffness and θ_u is the rotation when moment capacity drops below M_p on the unloading branch of the moment-curvature plot (Greco and Earls, 2003). θ is the hypothetical end rotation of the beam. It may well be due to the fact that tension flange fractures observed in the past (McDermott. 1969; Ricles et al., 1998) have motivated the passing of this recommendation.

Notwithstanding, numerous literature addressing the ultimate strength of high strength and hybrid beams and their ability to reach these prescribed levels of deformation have illustrated various degrees of success on the part of the researchers. Some of the research considers the effect of slenderness (Beg and Hladnik, 1996; Barth et al., 2000) while others regard the influence of both slenderness and bracing arrangements (Earls, 1999; Thomas and Earls, 2003; Greco and Earls, 2003) as significant.

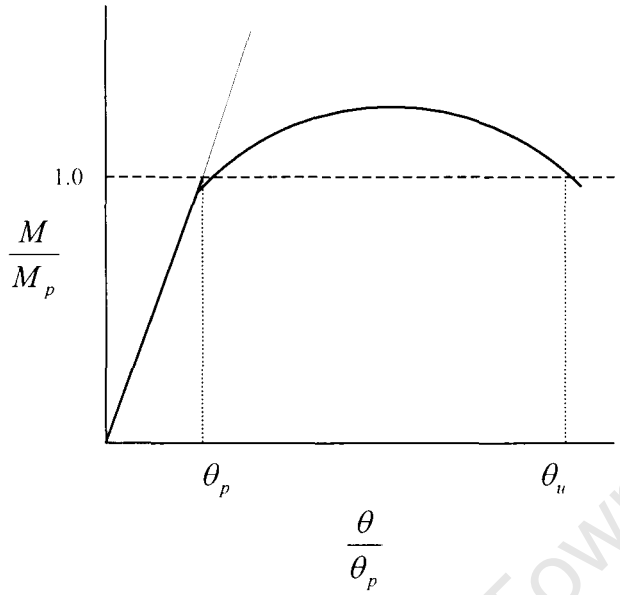

Figure 1.1 Rotation Capacity (Greco and Earls, 2003)

This subject has been the focus of much debate. While it is an accepted fact that stocky members are more likely to fail by yielding while more slender ones will fail through buckling at loads far below the yield values, failure can be manipulated through the application of lateral bracing. With this interaction between web, flange and lateral bracing, predicting the girder response becomes far more complex.

There are, however, reservations regarding the ability of high strength steel beams to sustain high strains. A number of investigations concluded that the minimum rotation could not be achieved under the existing guidelines in American Association of State Highway and Transportation Officials (AASHTO) and American Institute of Steel Construction (AISC) design codes (Thomas and Earls, 2003; Greco and Earls, 2003). It was shown that there was substantial flange and web interactions within a certain range of slenderness (Thomas and Earls, 2003). These findings are of relevance to hybrids as this behaviour may be magnified due to the differing yield stresses of flange and web. Some suggestions put forward advocated the revision of lateral bracing spacing such that the aspect ratio (the ratio of the distance between beam centre and brace position to beam depth) was either 0.5 (Earls, 1999) or 1 (Thomas

and Earls, 2003; Greco and Earls, 2003). The moment rotation would decrease beyond these limits (Sause and Fahnstock, 2001).

An independent analysis (Kato, 1990) presented equations derived for the maximum elongation of a standard tapered specimen, such as that used in tensile tests. The findings confirmed that the rotation capacity of higher strength steels decreases with increasing yield ratio. The yield ratio (YR) is defined as the ratio of yield strength to ultimate tensile strength. Furthermore it was illustrated that steel which exhibited elastic-perfectly plastic material behaviour, with a yield ratio of unity, would not undergo extension in the plastic region but would most likely fracture at the yield point (Kato, 1990).

Other factors that have been thought to influence moment rotation include yield stress (Earls, 2000; Green et al., 2002), the strain hardening modulus (Earls, 2000; Green et al., 2002), loading condition (Green et al., 2002), yield plateau length of the stress-strain curve (Earls, 2000) and yield ratio (Ricles et al., 1998; Barth et al., 2000; Green et al., 2002). It was concluded that increased yield stress signalled a corresponding decrease in ductility as did cyclic loading. When HSLA-80 (a North American high strength-low alloy steel with 552MPa yield stress) girders were compared with A36 (a North American 248.4MPa steel) girders it was discovered that the HSLA-80 girders suffered losses in rotation capacity of up to 83%. The greatest losses were experienced during cyclic loading (Green et al., 2002). High yield ratio was also found to cause reduced ductility (Green et al., 2002). Grade A36, with yield ratio of 0.69, had significantly higher levels of ductility (R=13.7) than HSLA-80, with yield ratio between 0.88 and 0.9, (R=3.2) for the same geometry (Ricles et al., 1998). The tension flange fractures (McDermott. 1969; Ricles et al., 1998) occurred where the yield ratio was approximately 0.9.

In the investigation into the effects of yield plateau (Earls, 2000), it was observed that an increase in the yield plateau length corresponded to an increase in rotation capacity. This is to be expected since the physical interpretation of this phenomenon is that the material of the beam is experiencing large increases of strain (or deformation) at a constant stress. It was also found that a longer yield plateau meant a decrease in moment capacity. A possible explanation could be that the stress

associated with a particular strain would be lower if a yield plateau is present (Earls, 2000).

It is worth noting that several researchers (McDermott, 1969; Sause and Fahnstock, 2001) conducted their studies in such a way that they first analysed and proportioned their test specimens according to plastic methods and then tested the specimens to ascertain whether the theoretical ultimate loads are achieved. Some beams were able to attain their design plastic moments (Mans et al., 2001) while the vast majority were not (Carskaddan, 1969; Sause and Fahnstock, 2001).

Most stability concerns have revolved around the fact that high strength steel sections are more slender to the extent that lateral torsional and local buckling are likely to be more prominent. Questions have also been raised on whether the existing section classification, as given in most design codes, could be extended for use on high strength steel sections.

One of the earliest submissions was that the existing limits could be maintained and that all that was required was a modification factor (McDermott, 1969). This factor would depend on the yield strength of the reference steel grade as well as that of the higher strength steel. A 690MPa steel could be safely designed in this manner (McDermott, 1969). It appears that this factor is equivalent to the epsilon factor (e) given in Eurocode 3 (EC3). The only difference is that the EC3 restricts the application of this ratio to steel with yield strength less than 460MPa.

In addition to meeting flexural strength and ductility requirements, hybrid beams must also be able to resist shearing forces. Though a large proportion of the experimental studies on hybrid beams were conducted in three and four point bending, few actually consider the effects of transverse forces acting on the webs of flexural members. Compact webs in hybrid beams, in which local buckling had been eliminated as a mode of failure, were found to fail at shears slightly less than the design plastic shear capacity (Frost and Schilling, 1964). This may be due to the fact that the extreme fibres of the web are already in a state of yield under bending stresses such that they are unable to resist the added shear.

Quite surprisingly, the presence of shear forces was discovered to have a larger bending strength reduction on homogeneous beams than on hybrid ones (Frost and Schilling, 1964). This conclusion was likely the basis for the recommendation that hybrid beams be designed separately for shear and bending (Frost and Schilling, 1964), the qualification being that the flange and web lie within certain width to thickness ratios. These width to thickness ratios would, in turn, vary depending on the material yield stress.

Another view point was that the ultimate strength of an unstiffened beam was possibly the shear buckling strength. (Carskaddan, 1968). After an experimental investigation of several different hybrids, results showed that beams with less slender flanges and webs actually failed by yielding (Carskaddan. 1968).

The effects of static, concentrated loads on the flanges of bridge girders have been an area of some focus since it has been established that this type of loading introduces stresses into the web that could reduce the overall stability of the web if the loads are of a sufficiently large magnitude (Lagerqvist, 1998). Sometimes referred to as 'patch loads', these concentrated loads are introduced during the launching of the girder (Lagerqvist and Johansson, 1996; Lagerqvist, 1998).

Three different load cases have been identified and these are *patch loading,* where a single concentrated load acts on one flange; *opposite patch loading*, where two loads act in the same plane but on either flange; and *end patch loading*, which is a single load acting near the girder end (Lagerqvist and Johansson, 1996). Under varying web slenderness and length of applied patch load, experimental results showed that both high strength and conventional steel grades deformed in the same manner (Lagerqvist and Johansson, 1996). It could not be shown conclusively that high strength steel girders were more resistant to patch loads (Lagerqvist and Johansson, 1996; Tryland et al., 1999).

Welding practices have an adverse effect on member behaviour but this has to be weighed against the fact that it is also the most versatile method of forming members. Consequently, many authors have carried out extensive work on the subject (Adonyi, 1998; Atkins et al., 2002). A primary objective has been to find those conditions

under which high quality welds can be achieved at relatively low cost and to demonstrate that high performance steels do have the increased weldability that the manufacturers claim. On the whole, these appraisals have yielded positive results. One report found that Submerged Arc Welding with no pre-heat could be used to join HPS 70W (a high performance 483MPa steel), up to a thickness of 50mm, provided that the levels of diffusible hydrogen were sufficiently low (Adonyi, 1998). In comparison, conventional A709 Grade 70 required a minimum pre-heat of 100°C to prevent cold cracking (Adonyi, 1998). The importance of correct storage, handling and usage of low-hydrogen consumables was emphasised. Moreover, cooling rates of weld metal and the heat affected zone (HAZ) were found to influence cracking to a large extent and by increasing the overall heat input, it was discovered that the cooling rate could be reduced to such levels that hardness was minimised (Adonyi, 1998).

Another report investigated the susceptibility of four different welding processes to cracking in the presence of differing levels of diffusible hydrogen (Atkins et al., 2002). Submerged arc welding was concluded to be the best process as it exhibited zero cracking at all levels with a minimum preheat of only 52°C.

With all the input from researchers, it was possible to generate a document, the HPS Designer's Guide (Lwin, 2002), which gave clear recommendations to fabricators working with HPS 70W. The guidelines were framed only for HPS 70W so it is clear that there is need for research to include other strength grades and hybrid beams.

In isolation, welding poses a challenge and, in hybrid construction, welding base metals of unequal yield strengths has presented an even greater one. *Mismatch* welds are those where the two metals being joined metals have different yield strengths such as are found in hybrid girders (Hildebrand and Schliebner, 2004). The stresses present at the weld due to the different microstructures have the potential to quite adversely affect the fatigue life of the weld (Hildebrand and Schliebner, 2004). Typically, the higher the yield strength of the base metal, the lower the fatigue life of a weld (Hildebrand and Schliebner, 2004).

While not favoured in steel bridge construction, bolted connections of high strength steels have received some attention. Some 25 tests were carried out on bolted connections in shear. The aim of the study was to confirm that the edge distance and bolt spacing in Eurocode 3 Part 1.1 for the Swedish steel grades S235 and S355 could also be used for grade S460 (Puthli and Fleischer, 2001). The conclusion was that not only could high strength bolted connections be designed according to the existing standard, but that both the edge distance and the bolt spacing could even be reduced.

Stresses occurring within structural members are frequently attributable to physical loading conditions; however, there is another type of stress which is sometimes overlooked. Residual stresses are generally introduced in members through welding and have the potential of undermining load-carrying capacity. Though often undetectable, they can sometimes be of such magnitude that they cause visible distortions, or initial imperfections, in the form of out-of-straightness of flange and web elements.

Since different steels would not have identical magnitudes of residual stresses it is possible that distortions of a member cross section will be more severe for hybrid girders. There appears to be some evidence of this as some measured imperfections within hybrid members were of greater magnitude (Carskaddan, 1969). Apart from the ability to cause sudden failure, it is likely that imperfections predetermine the mode of failure of the member. This was clearly demonstrated where thick flanges were welded to relatively slender webs in hybrid beams. The distortions were so extreme that, when the beams were loaded in shear, they influenced the position of the shear buckles (Carskaddan, 1968).

Establishing whether a relationship existed between material strength and longitudinal residual stresses was the objective of a series of tests carried out on welded box specimens (Clarin, 2004). Three steel grades, with yield strengths ranging from 420MPa to 1100MPa, were used. There was no linear relationship between the magnitude of residual stress and increasing material strength, though it was confirmed that the ratio of residual stress to material strength decreases with increasing material strength (Clarin, 2004). No evidence was found to support the assumption that tensile residual stresses could approach the material strength for higher yield steels. It was

determined that although the residual stresses in the high strength steel plates were somewhat larger than those in the conventional strength plates, when taken as dimensionless quantities they were smaller (Clarin, 2004).

Another aspect that falls within the realm of extrapolation is whether or not serviceability limit states as they stand can be useful in the design of high strength steels. In order to carry the same loading, a conventional steel member would require far more material than its counterpart built in high strength steel. The resulting section would be deeper and, therefore, much stiffer and subject to smaller deflections. The problem identified with high strength members is that their slender sections very easily exceed current deflection limits and other serviceability limits such as vibration.

During the early days of research in the behaviour of high strength steel, the theory of elasticity was used to examine the differences between mild and high strength steel. Various expressions were derived for cross sectional area, elongation, deflection, and section modulus for two materials with differing yield stress and modulus of elasticity (Haaijer, 1961). For tension members, the expressions showed that the required area of cross section was inversely proportional to the yield stress which, simply put, means that a smaller area is needed as the yield stress increases. The implication was that elongation (and hence, deflection) was directly proportional to the yield stress. In real terms this translates to: if two steels have yield stresses such that their ratio is R, then their elongations should be in the same ratio, provided they have the same modulus of elasticity. This does not appear to agree with measured values (Haaijer, 1961) as in one particular instance the ratio of the yield stresses was 3 and that of elongations was 0.8. An explanation would be that any such theoretic relationships would be valid within the material elastic region and would fall away once yielding began.

For beams and girders under the action of similar moments, a smaller section modulus is required for high strength steel than for mild steel (Haaijer, 1961). However, where the modulus of elasticity is equal, the smaller moment of inertia of the higher strength material experiences an increase in deflections (Haaijer, 1961). The extensions of

690MPa steel tension members were a maximum of 200% greater than similar members made of the 228MPa steel (Haaijer, 1961).

For all practical purposes, such deflections would be too excessive and this is problematic as design codes, like the AASHTO LRFD, have no prescribed limits for deflection (Wasserman, 2002). Limits were effectively ignored in the design of a bridge along State Route 53 in Tennessee and it was noted that the allowable deflection for the span was exceeded (Wasserman, 2002).

There are distinctions between homogeneous and hybrid high strength steel beams which would require further investigation. On examination of a plot of bending moment versus midspan deflection (Carskaddan, 1969) it appears that, in general, the homogeneous girders carried larger loads and, hence, sustained greater moments than their equally slender hybrid counterparts but also had smaller midspan deflections.

Yet another facet of this predicament brought to light was that slender sections would be carrying a larger live load proportion; such that wind induced vibrations would be of greater concern (Fortner, 1999).

Cost considerations, like structural efficiency, have played a large role in the decision-making processes linked to the use of high strength steel. One of the earliest studies asserted that using higher strength steels was justifiable given that the relative increase in yield strength far outstripped that of the cost (Haaijer, 1961). The steels under consideration had yield stresses varying from about 228MPa to 690MPa and included carbon steels, high-strength low-alloy steels and constructional alloy steels. Higher strength steels were more favourably priced in that the increase in strength was not directly proportional to the increase in price but, unfortunately, a more recent study (Greco and Earls, 2003) has found that this is not the case any more. At the time, however, this appeared to indicate that materials-related costs would be appreciable (Haaijer, 1961). With the 228MPa steel as the reference material, it was found that the maximum weight saving was 67% for the 690MPa steels and this was coupled with material cost savings of 20%. It is important to note that these results were gained from a theoretical study and it is not clear if the relevant slenderness and deflection limits that would govern structural members, for practical purposes, were

upheld. Typically, steels with higher yield stresses allow greater cost savings in long span girders where the dead weight is larger. Hybrid girders were found to be more economical than homogeneous girders. The web to total area ratio influenced the overall cost of hybrids (Haaijer, 1961) implying that the high material costs of deep homogeneous beams can be reduced significantly by using mild steel in the web.

HPS bridges that had been constructed in the various states within North America have afforded the opportunity to further investigate the area of sustainability. For example, cost savings realised in Tennessee due to the substitution of conventional steel with HPS-70W (a 483MPa steel) were in the region of US$78,000 which represented approximately 10% of the total construction costs. This corresponded to a 24% saving in weight (Wasserman et al., 1998). Judicious use of a combination of conventional and high strength steel in bridge designs has made material savings of up to 30% a reality (Wasserman, 2002).

One practical way in which the use of high strength steel has facilitated engineering gains in the U.S. state of Oregon is by allowing addition of extra lanes in the highway below HPS bridge structures (Madonna, 2001) and effectively increasing the overhead clearance. This is because longer, unsupported spans are now possible.

Most studies have considered the adequacy of traditional structural elements but a few have discussed innovative structural systems that could possibly be incorporated in the design of high strength steel. One such suggestion was girders with corrugated webs that could potentially allow greater section depths while another approach would be tubular flanges filled with cement grouting (Kulicki, 2000). Sandwich panels consisting of two high strength web plates and suitable filler would significantly reduce the web thickness (Driver et al., 2002). It was envisioned that this girder configuration would allow the use of more slender steel webs; resulting in a materials saving. The cavities would subsequently be filled with a cementitious or epoxy grout (Driver et al., 2002). One disturbing observation was that such double-plate and stiffened webs failed suddenly without any local buckling.

In summary, whether or not a high strength beam can sustain its plastic moment is not an isolated matter. It is closely linked to the deformation capacity of the beam.

Fundamental material principles clearly show that stress is a function of the strain and while the strains remain below their yield values, yielding and plastification cannot occur. This is true for all flexural members regardless of the steel grade which is why the rotation capacity requirements, set by Eurocode 3 and the American Institute of Steel Construction (AISC) specifications, are universal. This being the case, the stipulation that a minimum rotation capacity of three must be assured before plastic methods are applied cannot be said to be unreasonable for high strength steel. On the other hand, limiting plastic methods for all sections with yield stress greater than 450MPa does not appear justified. One would assume that once a beam has achieved sufficient rotation there would no longer be any reason to prevent the use of plastic analysis.

Even though a large proportion of the tests available in literature were conducted on homogeneous high strength beams and girders (Earls, 2001; Sause and Fahnstock, 2001; Mans et al., 2001) and not on hybrids, it may still be possible to draw some conclusions about hybrid beam behaviour. For example, it may be concluded that since higher strength steels exhibit less ductility than conventional steel grades (Kato, 1990; Green et al., 2002), the flanges of hybrid beams may similarly be unable to generate sufficient strains. This is based on the fact that in all beams, regardless of whether they are homogeneous or hybrid, the strain is always proportional to the distance from the neutral axis and, hence, in both homogeneous and hybrids beams the high strength steel in the flanges will be unable to exhibit large deformation capacity.

The correct classification of cross-section plays a crucial role in ensuring that adequate resistance to local buckling is provided. This topic, too, needs rationalization as many different slenderness limits have been proposed.

One of the outstanding questions that needs to be addressed deals with the extent to which the design codes which are currently in use can be applied to design of high strength and, especially, hybrid members. The areas of greatest interest are the prediction of ultimate flexural strength, slenderness classes (with reference to stability against local buckling) and deflection limits. At first the outlook was that the higher

strength steels required no special provisions but a more conservative approach is now advocated. Within their own particular sphere of concern, various researchers have tried to answer this question with varying degrees of success.

In conclusion, even a cursory glance at the available literature quickly highlights the fact that researchers, both in academia and industry, recognize the usefulness of the better quality materials that are now available for steel construction. What is also quite apparent is the fact that in comparison, far less information is available to those who would be interested in hybrid construction. The few sources that do exist deal, more or less, with similar issues revolving around whether specific flexural members should or should not reach the plastic moment. There is, however, very limited information regarding how these members should be analysed and designed in the first place. Recommendations and equations, related to bending strength, presented by individual authors need to be compiled in order to come up with a formal document that may be used by designers. In addition, the way in which stresses and strains develop in hybrids needs to be more closely investigated.

1.3 Problem Definition

Due to the elevated unit cost of high strength steel, it would be unlikely that designers would consider designing a homogeneous high strength steel structure of any great proportions. Hybrid beams offer a solution in that they can provide the structural benefits associated with high strength steel and yet be economical. In order for hybrids to be effective the following need to be understood:

(i) Development of stresses and strains within the flanges and web from the onset of loading;

The analysis of homogeneous cross-sections is well understood in that the stresses and strains vary linearly through the depth of the section until the material yield stress is reached at the outermost fibre. In a hybrid cross-section yielding will almost always begin at the web-flange interface (the exception is where the yield strengths of the web and flange material are close such that an almost homogeneous behaviour results). This makes analysis more complicated.

(ii) **The influence of different width to thickness ratios on the behaviour of unstiffened hybrid beams;**

This topic is complex as it requires that there be prescribed section classification limits for hybrid sections. It is important to investigate how this can be done given that the classification would need to incorporate two different steel grades.

(iii) **The extent to which current design and recommendations that are presented in the various design codes and literature can be extrapolated for use in hybrid beam design;**

The focus will be on the aspects such as design for bending and local buckling.

(iv) **The effectiveness of the commonly used hybrid configuration;**

For bending members, theory shows that the most beneficial arrangement is when most of the material is positioned as far away from the neutral axis as possible. This has led to a hybrid configuration which incorporates two high strength steel flanges and a mild steel web. Other arrangements have been suggested in literature and it would is necessary to establish whether the commonly accepted arrangement is the most effective.

2 Methodology

2.1 Introduction

This research is a comparative study of hybrid beam behaviour and how this is different from homogeneous behaviour, in terms of the development of stresses across a section and load-carrying capacity. This comparative form has been adopted because hybrid beams are made up of two different materials and so it is often difficult to draw direct parallels between hybrid beam and homogeneous beam characteristics, such as their ultimate strength. The analysis of unstiffened hybrid beams in bending was carried out by means of finite element modelling.

Both homogeneous high strength and hybrid beam behaviour have been studied using finite element analysis (Thomas and Earls, 2003; Greco and Earls, 2003). The areas of research have been quite diverse and ranged from rotation capacity (Earls, 2001; Green et al, 2002) to fatigue tests of high strength steel welds (Hildebrand and Schliebner, 2004). On the whole, finite element modelling has been found to yield results (Green et al, 2002) that mirror those derived from laboratory tests.

Finite element analysis involves the creation of a model that represents an actual structure in terms of both the geometry and position within space, or within a system. The model structure is then loaded and its response, whether in terms of moments or displacements, under the action of the loads is measured. Some type of verification of the model is usually performed in order to ensure that the results generated are reasonably accurate. This verification generally involves carrying out tests on fabricated specimens and comparing the measured values with those given as output from the finite element analysis. Sometimes, however, verification is accomplished by comparing the results generated by one finite element package against those generated by another finite element package.

There are a number of reasons why researchers have turned to finite element analysis, the major reason often being monetary cost savings. Higher strength steel grades tend to cost more, per unit weight, than conventional steel grades. Fabricating beams for the purposes of carrying out practical testing can become quite expensive. Generally,

acquiring a licensed finite element package can be expensive yet there are many advantages to be gained. Unlike a single manufactured specimen, say a beam, which can be tested to failure only once, finite element packages allow multiple researchers to generate many models which can be run as many times as needed in order to generate a large reserve of results. The results can be generated relatively quickly as no physical fabrication is required. Where a physical structure would require extraction of measurements using sensitive equipment, finite elements models are able to yield numerous accurate output values simultaneously and with little effort on the part of the researcher. In practical terms, numerical modelling eliminates the need for large amounts of testing space in the laboratory, reduces steel material wastage, and does not require the specialist labour and welding conditions necessary for the welding of high strength steel members.

The finite element modelling package used in the study, ABAQUS (versions 6.4-3 and 6.5-1 © 2004), was developed by Hibbitt, Karlsson and Sorensen Inc. and is now registered under ABAQUS, Inc.

2.2 Characteristics of ABAQUS

2.2.1 Introduction

The analyses were run using the general purpose ABAQUS/Standard and post-processing of results was carried out with the aid of ABAQUS/Viewer. This software package has many functionalities which make it a useful tool in solving a wide range of engineering problems of varying complexity. The range of elements and material models also allow users to approximate real systems as closely as possible.

2.2.2 ABAQUS Element Library

The fundamental concept behind elements is that they allow a fairly large structure to be subdivided into a number of smaller units whose behaviour is easy to analyse. The overall behaviour of the system can then be found by summing the deformations of the units. Choosing the correct element, therefore, is of the utmost importance as a suitable element should have the relevant degrees of freedom at the nodes in order to be able to capture the deformations.

Shell elements, which were used in his study, are suitable for use where the thickness of the structure is less than one tenth the typical global dimensions which may be the distance between the supports. The linear S4R element, a three-dimensional shell, can be used for a broad spectrum of problems and has four corner nodes with a single integration point at the centre. The 'R' signifies reduced integration (ABAQUS, Inc., 2004), which has the effect of reducing computational time. There are six degrees of freedom at each node; translations in the x, y, and z directions and the corresponding rotations about these axes.

S4R takes into account membrane strains and allows the thickness to change as the element deforms (ABAQUS, Inc., 2004). The reference surface for this element is the middle surface but this can be offset to either the top or bottom face as the need arises, say where a connection is required between a flange and a web.

The shell normal is determined by noting the nodal connectivity and applying the right hand rule as is demonstrated in Figure 2.1. Quantities that vary through the thickness of the shell can be conveniently based on this system.

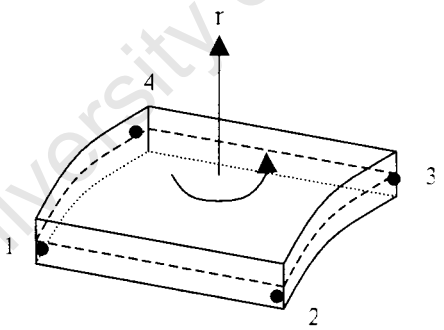

Figure 2.1 Representation of a Typical Shell Element

2.2.3 Material Model

With ABAQUS, it is possible to simulate linear and nonlinear, isotropic and anisotropic material properties. Once a material has been created and named, it can subsequently have a density, Poisson's Ratio, and Young's modulus assigned to it.

Often a material property is a constant, in which case this material would be easily characterised. However, sometimes a function may need to be defined. An example is

when the strain-hardening curve of a material needs to be prescribed. In such a case, the values of stress are input as functions of the strain. As with any discretisation process, a more accurate definition of the strain-hardening curve is obtained when the intervals are smaller. ABAQUS then interpolates between the given values, assuming linearity between such given data points (ABAQUS, Inc., 2004). Beyond the given values it is presumed that the magnitude is constant as is illustrated in Figure 2.2.

In analyses where a material, such as steel, is strained beyond its proportional limit, 'elastic' and *'plastic'* options (ABAQUS, Inc., 2004) need to be assigned to the steel. The von Mises isotropic yielding model is used.

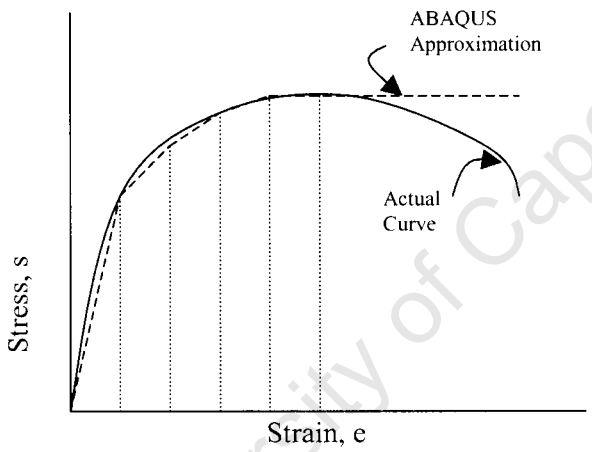

Figure 2.2 Representation of material definition in ABAQUS

ABAQUS uses the true, or logarithmic, strain and true stress for the material model (ABAQUS, Inc., 2004), and these quantities are given by

$$\varepsilon_{true} = \ln(1 + \varepsilon_{direct}) \text{ and } \sigma_{true} = \sigma_{direct}(1 + \varepsilon_{direct}) \quad 2.1$$

where ε_{true} is the true strain, ε_{direct} is the direct strain, σ_{true} is the true stress, and σ_{direct} is the direct stress. The direct stress is the stress due to a tensile or compressive force and can be represented as

$$\sigma_{direct} = \frac{F}{A} \quad 2.2$$

where F is the force normal to the area, A. Direct, or engineering, strain is given by

$$\varepsilon_{direct} = \frac{\Delta l}{l} \qquad 2.3$$

where l and Δl are length and change in length, respectively.

Where the material experiences plasticity this can be described within the material model by the input of plastic strain values. Plastic strain is specified as

Plastic strain, ε_{pl} = total strain, ε_{total} – elastic strain, ε_e. 2.4

Young's modulus (E), which is the slope of the stress-strain curve in the elastic region, can be simply represented. A constant value can be assumed until the yield point (B in Figure 2.3). Thereafter, a level yield plateau follows. Alternatively, the yield plateau may be given a slight gradient (BC in Figure 2.3) which is maintained throughout the analysis.

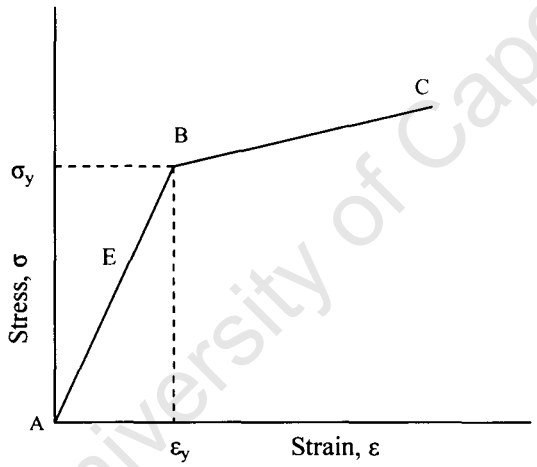

Figure 2.3 Material Model Incorporating Elastic Modulus and Tangent Modulus of Constant Value

2.2.4 Geometric Nonlinearities

All structural members and systems, however strictly monitored the fabrication process, contain imperfections which may take the form of warping or skewness of plates that are intended to be straight. In an initially perfect finite element mesh, these imperfections can be approximated. One method found to be of great use is that of superimposing a low energy buckling mode onto the mesh. The first step is to carry out a linear eigenvalue analysis on the structure in order to determine the buckled

modes with the lowest frequencies. Subsequently either the first mode or a combination of the modes is introduced to the mesh. Such a combination could take the form

$$\Delta x_i = \sum_{i=1}^{m} \omega_i \Phi_i \text{ (ABAQUS, 2004)} \qquad 2.5$$

Where the $\Phi's$ are the mode shapes and the $\omega's$ are the scaling factors.

2.2.5 Types of Analysis

ABAQUS has the capability to perform two different types of analyses and these depend on the expected behaviour of the system, or structure. '*Linear perturbation*' steps produce linear response only while *'general'* steps have the potential to produce either linear or nonlinear reactions (ABAQUS, Inc., 2004). Furthermore, these can be divided into static and dynamic classes. The Riks solver is helpful in solving highly nonlinear problems, especially where buckling is expected to occur.

Fundamentally this method is similar to the Newton-Raphson Method and is particularly useful where the load-deflection curve is highly nonlinear in nature. Generally, a problem has been solved if a single equilibrium path has been found such that it is described by the nodal variables and the proportional load factor. It is imperative that the increment size be restricted so that the radius of convergence is not exceeded.

The Riks solver works on the principle that both loads and displacements are unknown. Since these two have to be resolved, a third parameter, known as the arc length, is used to track the state of the system at any point (ABAQUS, Inc., 2004). Loading applied to the structural system at any given time increment is a certain fraction of the total applied load. This can be represented as

$$N_{current} = N_{initial} + \alpha\left(N_{applied} - N_{initial}\right) \qquad 2.6$$

where N is the load and α is the load proportionality factor.

In order to avoid the bifurcation which occurs at the critical buckling load, imperfections are introduced. The function of these irregularities in the mesh is to induce a certain reaction within the structure below the critical load.

2.2.6 Input and Output Data

ABAQUS/Standard allows the user to write scripts, or programmes, which translates into greater control over input variables and analysis procedure. The input of node and elemental structuring can be done according to the user's needs and in the same token; an output which is directly pertinent can be requested. The ABAQUS/Viewer conveniently displays the final solution or the state of the system at any increment if this information is required.

2.3 Model Description

2.3.1 Introduction

While one of the objectives of this study was to examine the manner in which hybrid beams develop stresses in bending, this could not be looked at in isolation. This study would, therefore, be a comparative study using homogeneous high strength beams. Where there were points of overlap, for example where the flanges of the hybrids share the same steel grade, further comparison was made between the hybrid beams themselves.

2.3.2 Beam Geometry

The starting point was to extract dimensions of beams from tests conducted by other researchers. These beams had been physically fabricated and tested in laboratories. The aim was to use this data as a framework within which to come up with beam dimensions that would be comparative to results from other researchers.

The standard beam has an I-section profile consisting of two identical flanges and a web. The web is connected to the top and bottom flanges in an ideal connection which approximates a weld. This connection enables the web to transfer shear forces and maintain the distance between flanges so that the beam acts as a unit. Different combinations of steel grades were specified for the flanges and web depending on whether the beam in question was homogeneous or hybrid. Two separate beam lengths were selected, the motive being to observe the change in behaviour as a function of length. Flange and web thickness were varied in order to study the effect of varying slenderness.

2.3.3 Elements and Meshing

Identical meshes of the four node shell element, S4R, were used for all beams that were to be subsequently compared. In essence, a shell element is created when a linear quadrilateral element is superimposed on a flat, plate element.

This quadrilateral element is detailed below in Figure 2.4. The components of displacement, as shown by the arrows, are restricted to straight lines only such that deformations, u and v, in the x and y directions can be fully described by linear expressions.

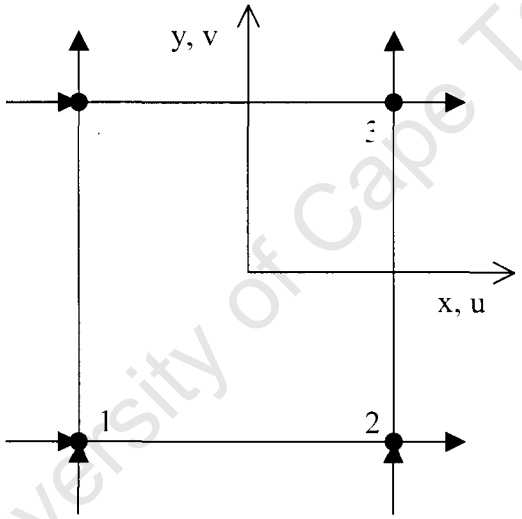

Figure 2.4 Layout of a Quadrilateral Element

The displacement field is given by

$$u = \beta_1 + \beta_2 x + \beta_3 y + \beta_4 xy \qquad 2.7$$

and

$$v = \beta_5 + \beta_6 x + \beta_7 y + \beta_8 xy \qquad 2.8$$

where the β_i's are displacement amplitudes. From elastic theory, the strains in the x and y directions are

$$\varepsilon_x = \frac{\partial u}{\partial x} \qquad 2.9$$

$$\varepsilon_y = \frac{\partial v}{\partial y} \qquad 2.10$$

After differentiating 2.7 with respect to x and 2.8 with respect to y the results give

$$\frac{\partial u}{\partial x} = \varepsilon_x = \beta_2 + \beta_4 y \qquad 2.11$$

and

$$\frac{\partial v}{\partial y} = \varepsilon_y = \beta_7 + \beta_8 x \qquad 2.12$$

respectively. The shear strain, γ_{xy} is given by the equation

$$\gamma_{xy} = \frac{\partial u}{\partial y} + \frac{\partial v}{\partial x} = (\beta_3 + \beta_6) + \beta_4 x + \beta_8 y \qquad 2.13$$

Expressions 2.11 and 2.12 above are linear and highlight the fact that while the variation in strain through the depth of the section can be captured, the response of the element under pure bending would be approximated as shown in Figure 2.5(b) below.

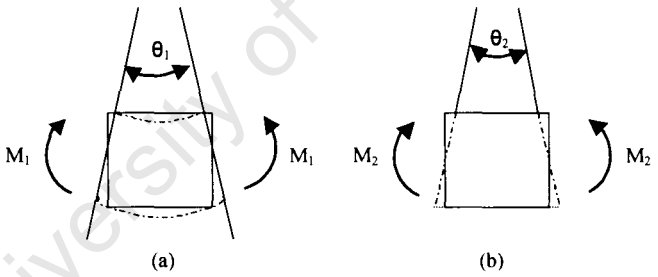

Figure 2.5 (a) Correct Deformation (b) Deformation of the Quadrilateral Element

The sides of the quadrilateral are unable to deform in the correct manner with the consequence that the right angles are not preserved as is assumed in theory. Because these spurious mode shapes are difficult to identify, methods have to be devised by which they can be prevented. Although the element is likely to underestimate deflections, this effect can be minimised by mesh refinement (Cook, 1995).

2.3.4 Boundary Conditions and Loading

Simple support conditions were created at each beam end and bending was about an axis perpendicular to the longitudinal axis of the beam. Loading on the top flange

consisted of a single line load down the centre of the flange which arrangement introduced both bending and shearing stresses (see Figure 2.6).

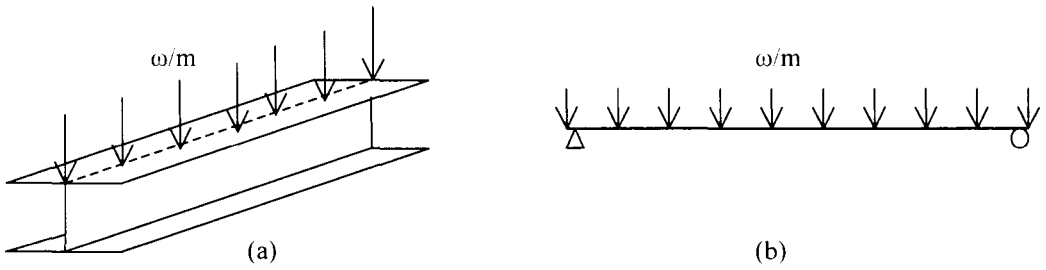

Figure 2.6 Representation of Simply Supported Beam Set-up Acting Under a Uniformly Distributed Load

2.4 Material Types and Characteristics of Steels Used in the Hybrid Beams

2.4.1 Introduction

The beams considered in this study were composed of combinations of six different steel grades ranging from 248.4MPa to 700Mpa (see Table 2.1). The steel grades used were labelled from A to F for convenience. To differentiate the different hybrid beams the following coding was used to label them:

XY-HYBa-ß, X is the steel grade in the web and Y is the steel grade in the flange as given in Table 2.1. a is the hybrid type number and ß is the beam length.

One of the desired objectives was to verify whether the behaviour of members would evolve in a gradual and measurable manner as the strength of the constituent material increased, hence the range of steels. All stress and strain data for these steels was obtained from literature.

Table 2.1 Summary of Material Types and Characteristics

Steel	Type	Yield stress (Mpa)	Description
A	ASTM A36	248.4	This North American steel has a nominal specified yield stress of 248.4Mpa. For the purposes of the numerical study, a yield stress of 269Mpa was assumed with the ultimate stress being 548Mpa. Details of this and other steels can be found in Section 2.4.2.
F	Grade 350W	350	Grade 350 was introduced into the South African market in 2005 with the intention of replacing the 300Mpa steel which was currently in use. It is expected that, with its higher yield strength of 350Mpa, material savings of up to 16.7% will be realised for larger sections (Creamer, 2005). Vanadium and niobium are two of the micro-alloys (Creamer, 2005) that have been added to increase the yield strength. There is no loss of weldability when compared to the 300Mpa steel.
B	Domex 460MC	460	With low carbon content and the micro alloying elements niobium, titanium and vanadium, Domex 460MC has a fine grain structure which allows ultimate strengths of up to 670Mpa. No preheating is necessary when welding.
C	Domex 550W	550	Domex 550W has a minimum ultimate strength of 600N/mm^2 and can be welded without preheating as well. This weathering steel forms a coat of protective oxide which effectively stops further attack by the atmosphere. The high strength, improved impact toughness and favourable weldability make Domex 550W a feasible option for use in the fabrication of rail wagons, steel bridges and buildings.

D	ASTM A514	690	This low alloy, quenched and tempered steel has a nominal yield stress of 690Mpa. Its highly valued properties, apart from high strength, include reasonable toughness at low temperatures and resistance to atmospheric corrosion. Applications of this steel can be found in bridge construction, cranes and earthmoving equipment.
E	Domex 700W	700	Domex 700W can be welded without preheating. Yield and ultimate stresses are 700Mpa and 750Mpa respectively which make it useful in bridge structures where long spans and reduced dead load are needed.

2.4.2 Material Data

Tables of nominal stress, measured in megaPascals (MPa), and nominal strain, expressed as a percentage, which were obtained from literature were used to generate the curves in Figures 2.7 to 2.12. This data was for tensile tests in which the steel was tested parallel to the rolling direction. No statistical information was provided in the source literature. The strain values were first converted to dimensions of millimetre per millimetre (mm/mm) and then the nominal stress was used to calculate the true stress with the aid of the equation

$$\sigma_t = \sigma_n(1+\varepsilon_n) \qquad 2.14$$

where σ_t is the true stress, σ_n is the nominal stress and ε_n is the nominal strain. The true strain is calculated as

$$\varepsilon_t = \ln(1+\varepsilon_n) \qquad 2.15$$

with ε_t as the true strain. In effect, Equations 2.14 and 2.15 are similar to Equation 2.1, the only difference being that the direct stress is here referred to as the nominal stress and the direct strain is referred to as the nominal strain. Finally, the plastic strain is determined as follows

$$\varepsilon_{pl} = \varepsilon_t - \frac{\sigma_t}{E} \qquad 2.16$$

Equation 2.16 is similar to Equation 2.4, with true strain being taken as the total strain value. The elastic strain is calculated by dividing the true stress by the modulus of elasticity.

Steel A: ASTM Steel Grade A36

Table 2.2 Chemical Composition of A36

C	Si	Mn	P	S	Cu	Fe
0.29[a]	0.28	1.03	0.04	0.05	0.2	98

[a] Note: all values are percentages (%) of the total composition

Table 2.3 Mechanical Properties of A36

Yield Stress $\sigma_{y\ (N/mm^2)}$	Ultimate Tensile Strength $\sigma_{u\ (N/mm^2)}$	Elongation %
250[b]	400-550	23

[b] Nominal yield stress as specified by the manufacturer

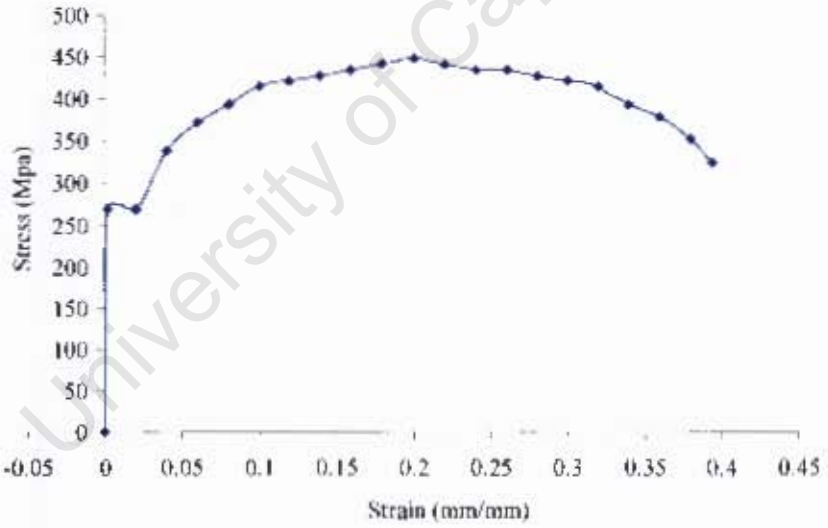

Figure 2.7 Stress-Strain Curve for A36 Steel

Steel F: Grade 350W

Table 2.4 Chemical composition of Grade 350W

C	Mn	P	S	Cr	Si	Cu	V	Mo	Ni
0.12*	0.5	0.15	-	1.25	0.75	0.55	-	-	0.65

*These values represent the maximum allowable percentages and, therefore, do not add up to 100%

Table 2.5 Mechanical properties of Grade 350W

Yield Stress $\sigma_{y\ (N/mm^2)}$	Ultimate Tensile Strength $\sigma_{u\ (N/mm^2)}$	Elongation %
350	480	24

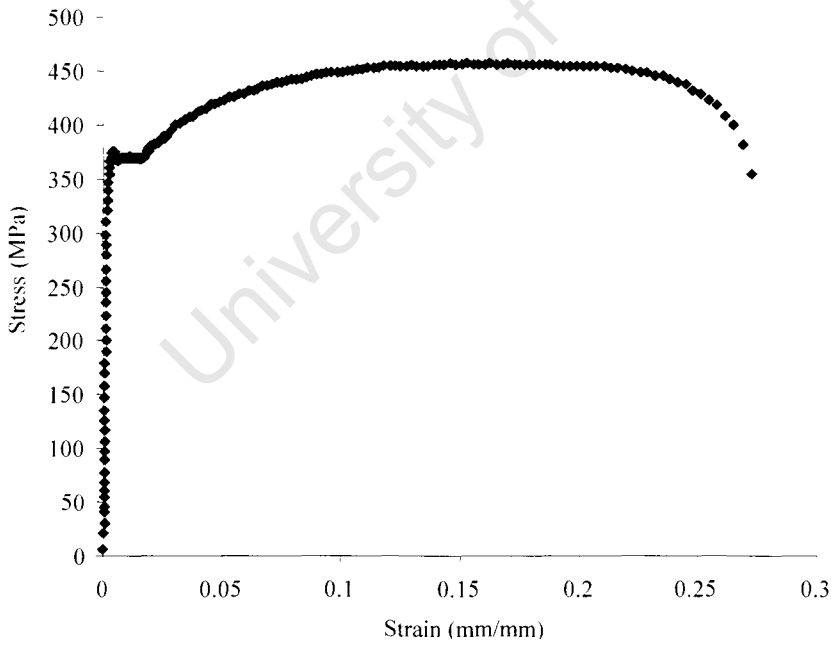

Figure 2.8 Stress-Strain Curve for Grade 350W

Steel B: Domex 460MC

Table 2.6 Chemical composition of Domex 460MC

C	Si	Mn	P	S	Al	Nb	V	Ti
0.1[a]	0.1	1.5	0.025	0.01	0.015	0.09	0.2	0.15

Table 2.7 Mechanical properties of Domex 460MC

Yield Stress $\sigma_{y\ (N/mm^2)}$	Ultimate Tensile Strength $\sigma_{u\ (N/mm^2)}$	Elongation %
460	520-670	19

Impact toughness as measured using the Charpy V-notch test: 27J at -40°C

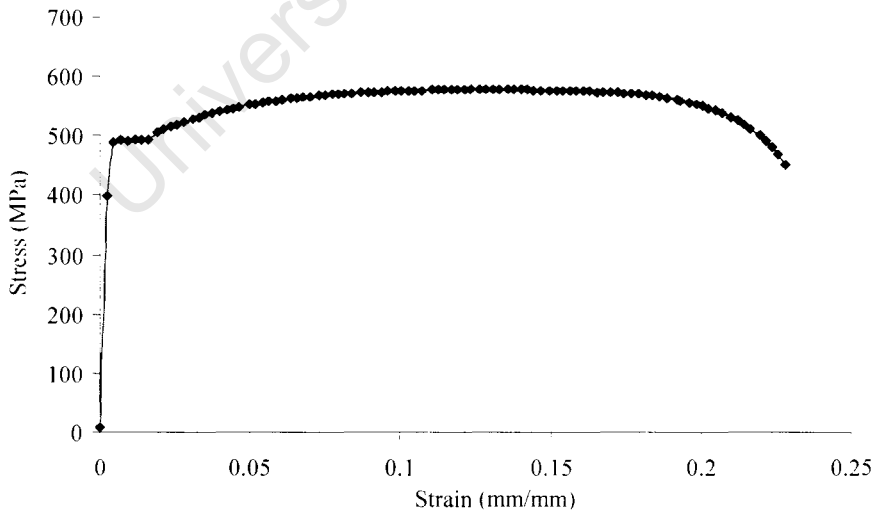

Figure 2.9 Stress-Strain Curve for Domex 460MC

Steel C: Domex 550W

Table 2.8 Chemical composition of Domex 550W

C	Si	Mn	P	Cu	Cr	Microalloys
0.1[a]	0.45	0.8	0.12	0.35	0.95	present

Table 2.9 Mechanical properties of Domex 550W

Yield Stress $\sigma_{y\ (N/mm^2)}$	Ultimate Tensile Strength $\sigma_{u\ (N/mm^2)}$	Elongation %
550	600	18

Impact toughness as measured using the Charpy V-notch test: 27J at -40°C

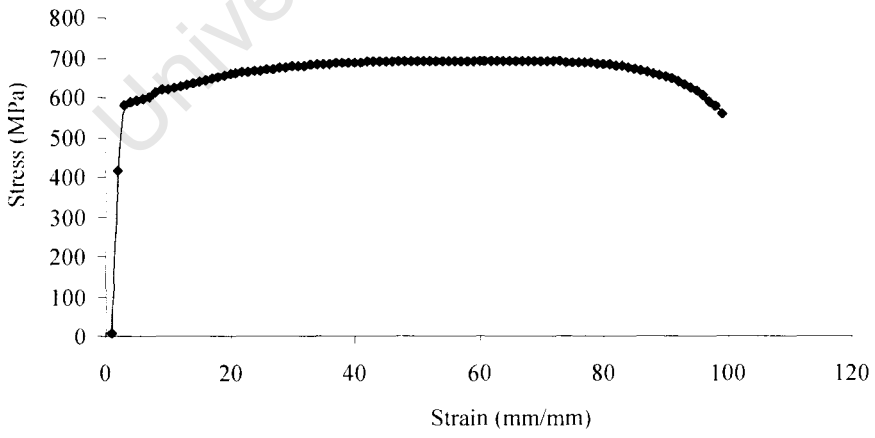

Figure 2.10 Stress-Strain Curve for Domex 550W

Steel D: ASTM A514

Table 2.10 Chemical composition of ASTM A514 steel

C	Si	Mn	P	S	Ni	Mo	B	Cr	Fe
0.21*	0.35	0.7	0.035	0.04	1.5	0.6	0.005	1.2	96.73

*These values represent the maximum allowable percentages and, therefore, do not add up to 100%

Table 2.11 Mechanical properties of ASTM A514 steel

Yield Stress $\sigma_{y\ (N/mm^2)}$	Ultimate Tensile Strength $\sigma_{u\ (N/mm^2)}$	Elongation %
690	828	18

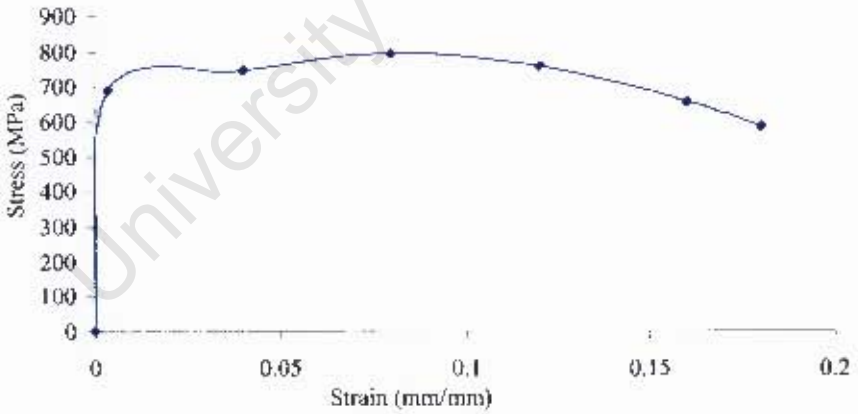

Figure 2.11 Stress-Strain Curve for A514

Steel E: Domex 700W

Table 2.12 Chemical composition of Domex 700W

C	Si	Mn	Cu	Cr	Micro alloys
0.1[a]	0.5	1.25	0.3	0.6	present

[a] Note: all values are percentages (%) of the total composition

Table 2.13 Mechanical properties of Domex 700W

Yield Stress σ_y (N/mm^2)	Ultimate Tensile Strength σ_u (N/mm^2)	Elongation %
700	750	12

Impact toughness as measured using the Charpy V-notch test: 27J at -20°C

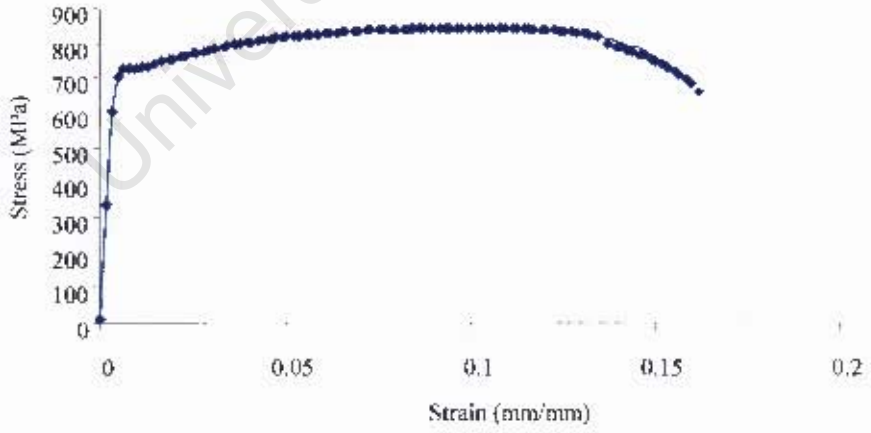

Figure 2.12 Stress-Strain Curve for Domex 700W

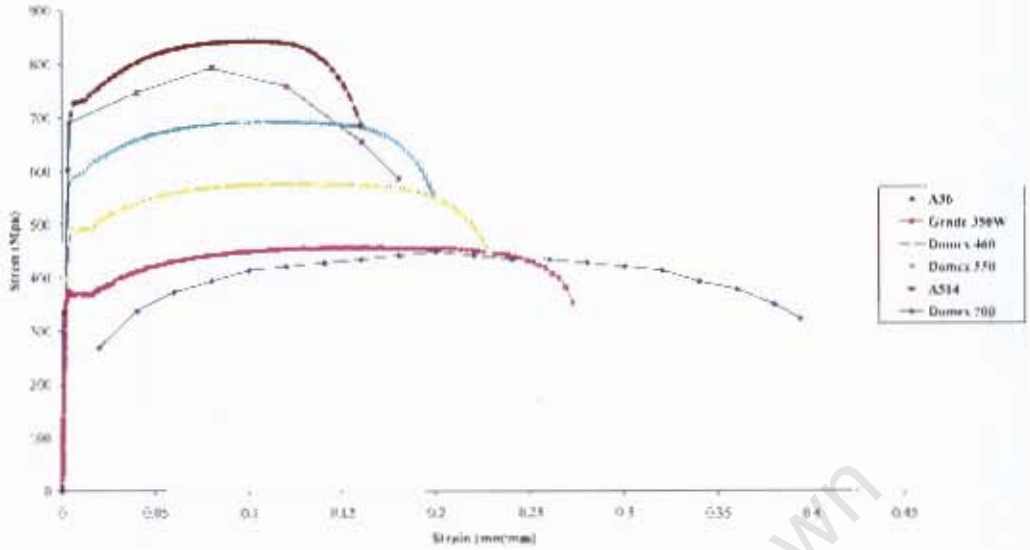

Figure 2.13 Comparison of Stress-Strain Curves for All Steels

2.4.3 Steel Properties

2.4.3.1 Modulus of Elasticity

Typical values of Young's Modulus of Elasticity (E) for steel range from 190 to 210GPa with the average value being approximately 200GPa. A value of 210GPa was chosen to represent the linear section of the stress-strain curve for all steels as calculated values of E tended to be considerably less than the typical values. Beyond the linear region, the tangent modulus was calculated from the nominal stress-strain curve. The discrete points at which this was done were selected so as to coincide with the regularly spaced values of plastic strain which were entered into the ABAQUS model.

This approach is a more accurate approximation to the actual behaviour than the simplified material model detailed previously in Section 2.2.3. Values of plastic strain were specified at constant intervals in order to prevent the ABAQUS finite element software from interpolating the material data between given points, thereby generating a curve of unknown shape. This was also done to remove the extra computational expense that would be required in order for ABAQUS to carry out this regularisation.

Stress and strain data was graphed in a scatter plot by first identifying the three distinct portions, namely the linearly-elastic range, the plateau region and finally the strain-hardening curve. These were plotted as separate series so that different trend lines could be added to each distinct area. Once the equations of the trend lines were established, the derivatives were obtained at discrete points required by the ABAQUS material model. The value of the tangent modulus was not permitted to become negative.

The ABAQUS material model assumes a constant Young's Modulus (E) until the steel begins to yield. A value of 210GPa was used for the analysis. Beyond the yield point, any variables which describe the behaviour of the steel must be input as a function of the plastic strain. Calculated values of E for the different steels are shown in Tables 2.14 to 2.19.

Table 2.14 Calculated Mechanical Properties of A36

Tangent Modulus E_t (x10^9) Pa	**Plastic strain ε_{pl}**
210	0.000
77.5	0.025
73.4	0.050
69.2	0.075
64.9	0.100
60.7	0.125
56.4	0.150
52.2	0.175
48.0	0.200
43.9	0.225
39.9	0.250
36.0	0.275

Table 2.15 Calculated Mechanical Properties of Grade 350W

Tangent Modulus E_t (x10^9) Pa	**Plastic strain ε_{pl}**
210	0
2.4	0.01
2.4	0.02
1.7	0.03
1.1	0.04
0.8	0.05
0.8	0.06

Table 2.16 Calculated Mechanical Properties of Domex 460MC

Tangent Modulus E_t (x10^9) Pa	**Plastic strain ε_{pl}**
210	0
2.3	0.01
2.3	0.02
1.4	0.03
0.7	0.04
0.7	0.05

Table 2.17 Calculated Mechanical Properties of Domex 550W

Tangent Modulus E_t (x10^9) Pa	**Plastic strain ε_{pl}**
210	0
2.6	0.01
1.9	0.02
0.7	0.03
0.7	0.04

Table 2.18 Calculated Mechanical Properties of A514

Angent Modulus E_t (x10^9) Pa	**Plastic strain ε_{pl}**
210	0.0
1.6	0.01
1.6	0.02
1.6	0.03
2.1	0.04
1.7	0.05
1.2	0.06
0.6	0.07
0.6	0.08

Table 2.19 Calculated Mechanical Properties of Domex 700W

Tangent Modulus E_t (x10^9) Pa	**Plastic strain ε_{pl}**
210	0
2.8	0.01
2.8	0.02
2.3	0.03
1.8	0.04
1.3	0.05
1.0	0.06
0.8	0.07
0.8	0.08

2.4.3.2 Poisson's Ratio

Poisson's ratio was assumed to demonstrate similar behaviour both in tension and compression and an average value of 0.3 was selected.

2.4.3.3 Shear Modulus

An average shear modulus of 77.5MPa was used.

3 The Behaviour of Beams in Bending

3.1 Introduction

Analysis of hybrid members requires a shift in perspective as a number of commonly used terms become ambiguous. An example would be what is generally referred to as the *yield moment* of a homogeneous beam. This is the characteristic strength of a beam designed by elastic methods. The yield moment causes the outermost fibres of the cross-section to reach the material yield stress under bending action.

Yield moment, with reference to hybrids, becomes somewhat meaningless. Firstly, this is because the cross-section consists of two separate materials so it is not immediately clear which material is being referred to; and secondly, because yielding commences at the extreme fibres of the web and not the flanges. With this last point in mind, it would be tempting to take the characteristic strength of hybrid beams as that moment which causes initial web yielding. As previously noted, this moment is so insignificant (Frost and Schilling, 1964) that it can hardly be used in the same manner as *yield moment* for homogeneous beams. It was, thus, proposed that the characteristic strength of a hybrid beam be either the flange yield moment or the plastic moment (Frost and Schilling, 1964).

3.2 General Beam Theory

3.2.1 Bending of a Homogeneous Member

Prior to yielding, a homogeneous, simply supported beam with a uniformly distributed load such as that in Figure 3.1 will have a midspan moment equal to

$$M_u = \frac{\omega_u L^2}{8} \qquad 3.1$$

with ω representing the magnitude of the distributed load. Yielding changes the beam's response to loading, in that part of the load contributes to permanent material deformation rather than deflection of the beam cross-section, such that the equilibrium equations used in statics are no longer adequate to predict behaviour. By assuming that web yielding causes little deviation in the beam's initially linear load-deflection response (Frost and Schilling, 1964), it can be concluded that equation 3.1 can also be used for hybrid beams up until the flange yield moment.

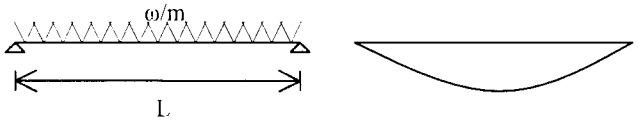

Figure 3.1 (a) Simply Supported Beam acting under a UDL
(b) Bending Moment Diagram

Yielding begins at the extreme fibres of the flanges and as the loading is increased, the region of yielding extends inwards towards the neutral axis of the section. The midspan moment just as the flange starts yielding can be calculated using the equation

$$M = \frac{\sigma I}{y} \qquad 3.2$$

where y is the distance from the neutral axis, σ is the stress and I is the moment of inertia. The relation remains valid as long as the stress distribution is linear. The symmetry of the section ensures that the neutral axis always lies halfway down the section depth.

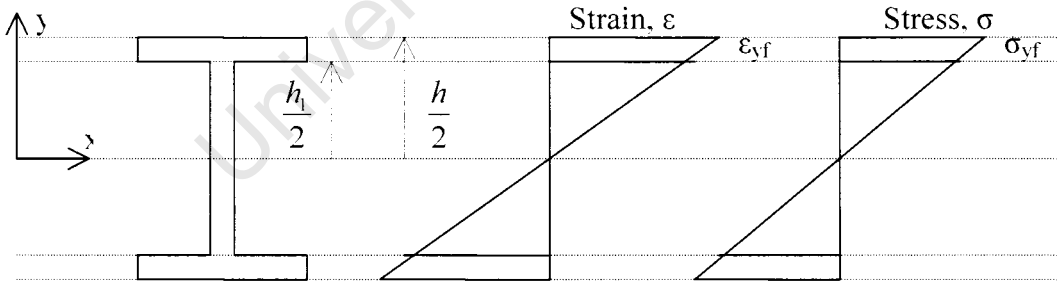

Figure 3.2 Strain, ε, and Stress, σ, at Flange Yielding

Figure 3.2 shows the strain and stress distribution when flange yielding commences and strains are assumed to remain linear such that

$$\varepsilon_x = \frac{-y}{\rho} = -y\kappa \qquad 3.3$$

is valid.

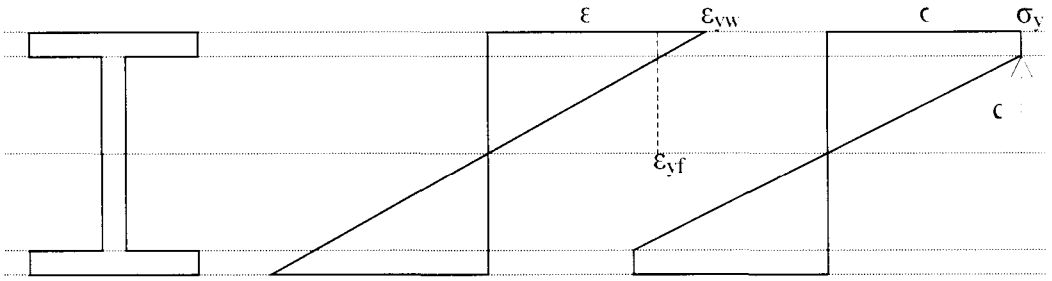

Figure 3.3 Strain, ε, and Stress, σ, at Web Yielding

In the relationship between strain and curvature given in Equation 3.3, ρ is the radius of curvature; κ is the curvature and y is the distance from the neutral axis to the reference point. In those portions of the beam section which are still elastic at this stage, the relationship

$$\varepsilon = \frac{-\sigma}{E} \qquad 3.4$$

is also valid. Hence, the following can be written for the flange;

$$\frac{-c}{\rho} = \frac{-\sigma_{yf}}{E} \qquad 3.5$$

where c represents the 'elastic core' depth. This is the region of the cross-section located near the neutral axis of the section that has not yet yielded. This can be expressed as

$$c = \rho\frac{\sigma_{yf}}{E} \qquad 3.6$$

In a homogeneous cross-section at flange yielding, the elastic core depth is equal to the section depth.

Equations 3.3 to 3.6 can be similarly used in order to come up with expressions governing the distribution of stresses at the onset of web yielding. Taking a stress value of σ_{yw} at the top of the web, Equation 3.5 can be rewritten as

$$\frac{-\sigma_{yw}}{E} = \frac{-y}{\rho} \tag{3.7}$$

and

$$\sigma_{yw} = \frac{yE}{\rho} \tag{3.8}$$

Here, y is the distance from the neutral axis to a reference point now lying specifically within the web. Although the separate terms 'σ_{yf}' and 'σ_{yw}' have been used, in a homogeneous section they are equal and would be replaced by with 'σ_y'. The terms are of more relevance in hybrid sections.

3.2.2 Width to Thickness Ratios and the Elastic Buckling of Webs and Flanges of Unstiffened Beams

Classification of homogeneous sections into Class 1, 2 or 3 is a straightforward process. The flange and web are separately assessed and the section is given a classification equivalent to the lowest grouping obtained by either the flange or the web. Hybrid sections, on the other hand, appear to pose a challenge as there are two separate materials that need to be considered. The question that arises then is whether special arrangements need to be made to accommodate the materials.

On the surface this seems a reasonable enough question but then again it is important to note that elastic buckling phenomena is purely of geometric significance. Material properties, such as the modulus of elasticity and Poisson's Ratio, are constant as long as the material remains below its yield strength. Once the material begins to yield and inelastic buckling occurs then the nature of the problem changes and it is then that the differing yield strengths may have an effect.

Buckling strength is dependent on the plate dimensions and support conditions. The limiting width to thickness ratio, below the yield point, can be found by simply considering Euler's critical buckling equation

$$\sigma_{cr} = \frac{k_\sigma \pi^2 E}{12(1-\nu^2)} \cdot \left(\frac{t}{b}\right)^2 \tag{3.9}$$

where σ_{cr} is the critical buckling stress, k_σ is the buckling coefficient, E is the modulus of elasticity, t is the plate thickness, b is the plate width, and ν is the Poisson's Ratio.

Below the critical buckling limit, the material yields before buckling occurs. The normalised plate slenderness is expressed as

$$\lambda_p = \sqrt{\frac{f_y}{\sigma_{cr}}} \qquad 3.10$$

Where λ_p is the plate slenderness, and f_y is the material yield strength.

Substituting equation 3.9 into 3.10 gives

$$\lambda_p = \sqrt{\left(\frac{f_y.12(1-\nu^2)}{\pi^2.E.k_\sigma}\left(\frac{b}{t}\right)^2\right)} = 1.1\frac{b}{t}\sqrt{\frac{f_y}{Ek_\sigma}} \qquad 3.11$$

with ν=0.3.

In a long plate, such as a flange, compression is uniform and the buckling coefficients are as shown in the table below. The short loaded edges of the plate would be simply supported while the longer unloaded edges would have the support conditions described in Table 3.1.

Table 3.1 Values of Buckling Coefficient for Various Edge Conditions

Description of Supports	$\mathbf{k_\sigma}$
Both edges simply supported	4.00
One edge fixed, the other free	1.28
One edge simply supported, the other free	0.43
Both edges free	b^2/a^2
Both edges fixed	6.97
One edge fixed, the other simply supported	5.40
All edges hinged in bending (e.g. web)	23.9

The symbol a, as it appears in the table, is the plate length such that $\frac{a}{b}$ represents the aspect ratio; b being the width of the plate. These values would be valid for aspect ratios far greater than one, such as in unstiffened plates.

Limits for each slenderness class are set by assigning various ranges for the modified plate slenderness. For example, the Eurocode sets the following ranges (Kulevan.ac.be, 2006);

(i) $0.46 \leq \lambda_{p1} \leq 0.6$, with a value of 0.5 taken for compression members

(ii) $\lambda_{p1} \leq \lambda_{p2} \leq \lambda_{p3}$, with a prescribed value of 0.6

(iii) $0.5 \leq \lambda_{p3} \leq 0.9$, with a prescribed value of 0.74

Where λ_{p1}, λ_{p2}, and λ_{p3} are the modified plate slenderness values for classes 1, 2, and 3, respectively. Substituting these values into Equation 3.11 gives the limiting slenderness values for plates subject to compression as they appear in the Eurocode. Unfortunately these same values cannot be used for plates of yield strength greater than 460MPa so there is a need for the proposal of new limits.

3.3 Steel Hybrid Section Configurations

3.3.1 Introduction

Figure 3.4 shows examples of commonly used hybrid configurations. Hybrid 4 (HYB4) is the most used arrangement in practice as it provides additional strength to the flanges in both negative and positive moment regions.

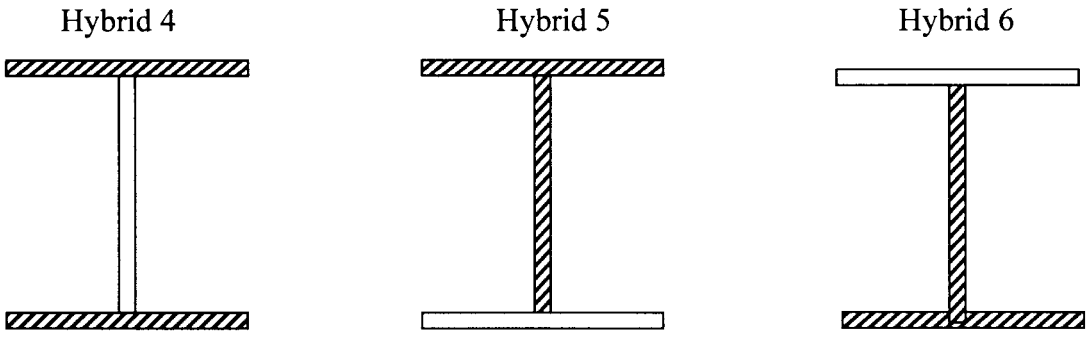

Figure 3.4 Hybrid Configurations

Due to the symmetry of the cross-section, Hybrid 4 is also the easiest to analyse as the neutral axis always passes through the centre. Hybrid 5 (HYB5) is suitable for negative moment regions while Hybrid 6 (HYB6) works best in positive moment regions. Given the versatility of the Hybrid 4 arrangement, this configuration was chosen as the basis of the comparison of between hybrid and homogeneous members.

3.3.2 Development of Stresses across the Hybrid 4 Cross-Section

Consideration of a section of the beam at the middle of the span from the onset of loading reveals a variation of stresses such as that shown in Figure 3.5.

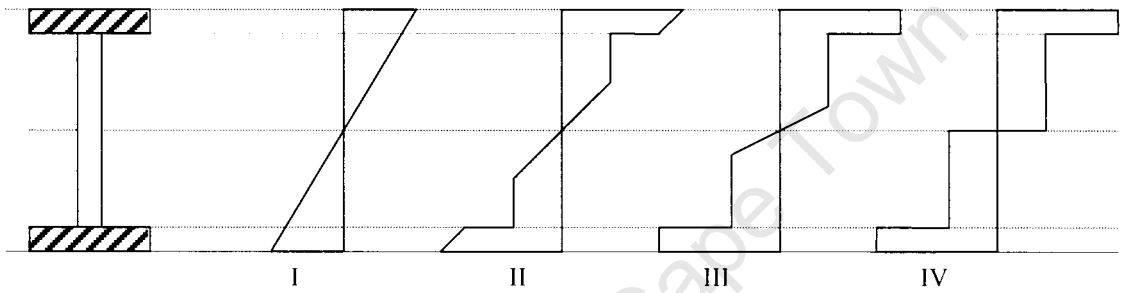

Figure 3.5 Changes in Stress Distribution with Increased Bending Moment

Stress distribution I shows the section as the web reaches its material yield stress. At this stage the flange is still behaving elastically. As the load is increased, in diagram II, the extreme fibres of the flange reach the material yield stress. The extreme fibres of the web are yielding progressively up till that point. Complete flange yielding is shown in figure III at which stage only the core of the web remains elastic. IV shows a hybrid section that has completely plastified. This stage marks the point where the maximum moment at the centre of the span is equal to the plastic moment.

Stages I to IV are further illustrated on the moment- curvature plot in Figure 3.6. Changes in the distribution of stress as described in Figures 3.5 and 3.6 are purely qualitative. There is, however, no design code that provides equations with which the bending moments at stages I through III can be calculated. Some suggestions (Frost and Schilling, 1964; Joint ASCE-AASHO Committee on Flexural Members, 1968) have, however, been made.

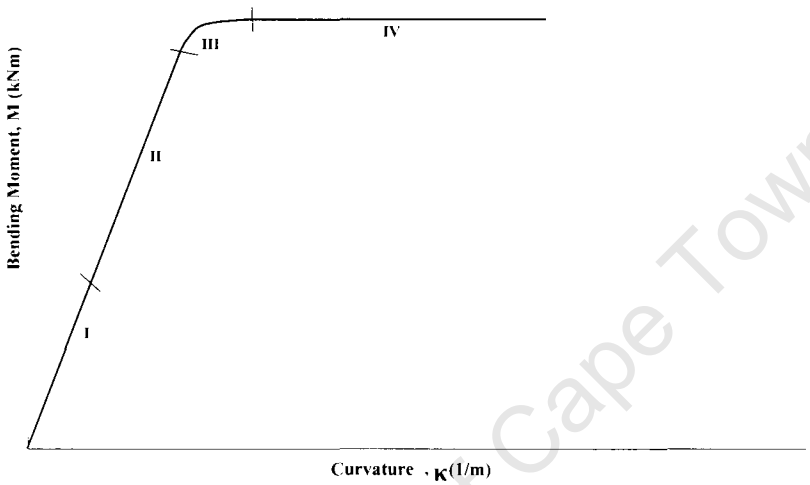

Figure 3.6 Moment-Curvature Plot showing Stages of Stress Distribution

The relationship

$$M_{yw} = \sigma_{yw} S \frac{d}{h_w} \text{ (Frost and Schilling, 1964),} \qquad 3.12$$

where σ_{yw} is the yield stress of the web material, S is the section modulus, d is the section depth, and h_w is the web depth, was recommended as accurately predicting the web yielding moment of a hybrid beam.

For predicting the moment causing flange yielding, the formulae

$$M_{yf} = \frac{2I_f}{d}\sigma_{yf} + Z_w \sigma_{yw} - \frac{t_w d^2}{12}\left(\frac{\sigma_{yw}^3}{\sigma_{yf}^2}\right) \text{ (Frost and Schilling, 1964)} \qquad 3.13$$

and

$$M_{yf} = M_y\left[\frac{12+\beta(3\alpha-\alpha^3)}{12+2\beta}\right]$$ (Joint ASCE and AASHO Committee on Flexural Members, 1968) 3.14

have been suggested. In the above equations, σ_{yw} and σ_{yf} represent the material yield stresses of the web and flange, respectively. The moment of inertia of the flanges is given as I_f, d is the section depth, Z_w is the plastic modulus of the web, and t_w is the web thickness. M_y is the yield moment of a homogeneous beam, of the same cross-section as the hybrid beam, made of the flange steel. The symbol α represents the ratio of the web yield stress to the flange yield stress, and β is the ratio of the cross-sectional area of the web to that of one flange.

3.4 Determination of Hybrid Beam Moment from First Principles

A 2m hybrid beam with 700MPa flanges and 248.4MPa web is selected to examine the development of stresses across a typical hybrid section. The chosen beam represents the most extreme case where the web yield stress is far less than the flange yield stress and, hence, all other hybrids investigated in this research would be adequately covered. The beam dimensions and properties are as given below:

Flange yield stress, σ_{yf} = 700 MPa

Web yield stress, σ_{yw} =248.4 MPa

Flange width, b_f = 0.2m

Flange thickness, t_f = 0.006m

Web height, $h_w = h_1$= 0.18m

Web thickness, t_w = 0.005m

Section moment of inertia, I_{xx} = 23.2 x 10^6 mm^4

Section depth, h = 0.192m

Young's Modulus, E = 210 GPa (for both steels)

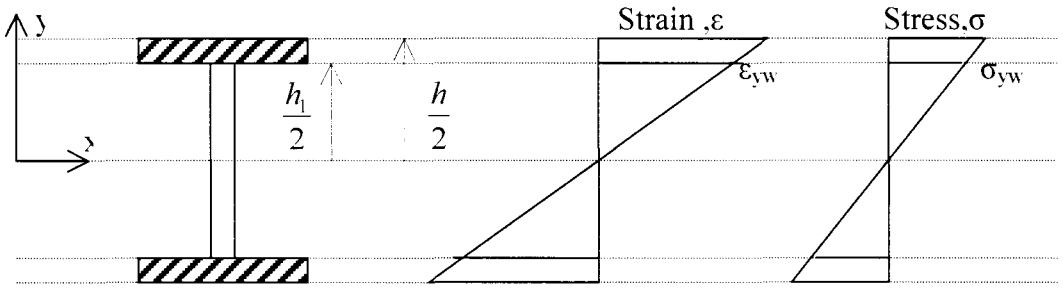

Figure 3.7 Strain and Stress Distribution at Web Yielding in a Hybrid Beam

The web begins yielding first (Figure 3.7) and Equation 3.2, $M = \frac{\sigma I}{y}$, can be used to calculate the moment causing web yielding. So the web yield moment is given as,

$$M_{yw} = \frac{248.4 \times 23.2 \times 10^6}{90} = 64kNm$$

Equation 3.8 can be rearranged as shown in Equation 3.15

$$c = \rho \frac{\sigma_{yw}}{E} \qquad 3.15$$

with c, the elastic core depth, substituted for y. Since the beam acts as a unit ρ, the radius of curvature is the same for flange and web. Equations 3.6 and 3.15 can be used to obtain

$$\sigma_{yf} = y \frac{\sigma_{yw}}{c} \qquad 3.16$$

which gives the relationship between the flange yield stress and the elastic core depth as the flange begins to yield (Figure 3.8). Here, y is the distance from the neutral axis to a reference point now lying in the flange.

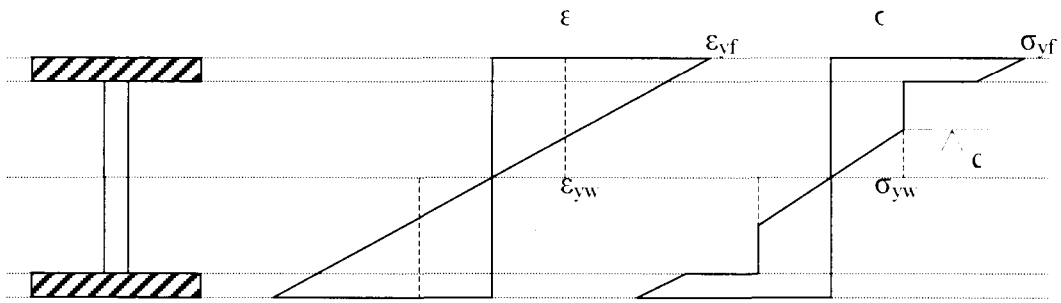

Figure 3.8 Strain and Stress Distribution at Flange Yielding in a Hybrid Beam

The elastic core depth, c, can only be determined by physical measurement and to ascertain to what extent the web has yielded is a complex challenge. Hypothetically, it is possible that the conventional steel web is in complete plastification by the time the higher strength steel flanges begin yielding. If this were the case then Equation 3.16 would be meaningless as c would be equal to zero and the expression would be undefined.

It is, therefore, necessary to verify whether Equation 3.16 is valid for the hybrid beams investigated in this study. Verifying Equation 3.16 for the most severe case where the hybrid is composed of a 248.4MPa web and a 700MPa web would ensure that the equation is relevant for all other hybrid combinations. The procedure involves the selection of a value of c which is sufficiently small as to approximate a fully yielded web. Substituting the small value of c and the web yield stress into Equation 3.16 generates a value of the flange stress, σ_f. If this value of σ_f is less than the flange yield stress, 700MPa in this case, then this confirms that the web has yielded completely prior to flange yielding. If, on the other hand, the value of σ_f is greater than 700MPa then this indicates that the web will only reach total plastification after the flanges have begun yielding. The process of verification is illustrated below.

The first step is to assume that the web is in fact in total plastification. A minimum value of c, say 1mm, is chosen. Substituting this value into the flange equation 3.16 gives

$$\sigma_f = \frac{0.096 \times 248.4}{0.001} = 23846.4MPa > 700MPa$$, the flange yield stress

This result confirms that the assumption that the web has yielded completely is wrong as σ_f is far greater than the flange yield stress. The value of c at the commencement of flange yielding can now be found by substituting the actual value of σ_{yf} into 3.16.

$$700 = \frac{0.096 \times 248.4}{c} \Rightarrow c = 0.034m$$

The moment associated with the stress distribution can then be calculated by separate consideration and subsequent summation of the couples C_1 and T_1, C_2 and T_2, and C_3 and T_3 as shown in Figure 3.9.

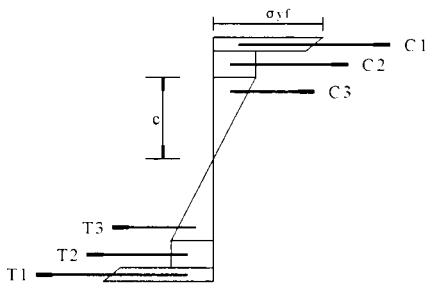

Figure 3.9 Calculation of Flange Yield Moment

4 Comparative Analysis and Investigation of Hybrid Beams

4.1 Introduction

Analysis was conducted using two separate methods. Firstly, the finite element package ABAQUS was used to model the behaviour of a number of simply supported homogeneous and hybrid beams under a uniformly distributed load. This portion of the investigation yielded loads and corresponding deflections, as well as visualisations of the stress distributions across the member. Secondly, the moments and curvatures of the same homogeneous and hybrid beams were calculated based on theory.

ABAQUS/CAE which has an interactive graphical user interfaces use automatic meshing techniques. This means that the user has no control over the node and element numbering. Extracting valuable data, such as stresses and deflections can then become quite difficult as the node and element labels at the desired output location are unknown. However, ABAQUS/Standard allows a user to write their own programme, or script, which enables the exact ordering and numbering of the nodes and elements of each model. Initially an attempt was made to seed all beams with imperfections but this was discontinued in the 4m beams as there was no sensitivity to the imperfections and both seeded and unseeded beams gave similar results.

Work carried out using ABAQUS included the analysis of:

(i) 2m Homogeneous beams incorporating all steel grades

(ii) 4m Homogeneous beams incorporating all steel grades

(iii) 2m Hybrid 4 (HYB4) beams incorporating different combinations of steel grades

(iv) 4m Hybrid 4 (HYB4) beams incorporating different combinations of steel grades

(v) 2m Hybrid 4 (HYB4) beams (Steels A and E) with varying width to thickness ratios

(vi) 4m Hybrid 4 (HYB4) beams (Steels A and E) with varying width to thickness ratios

(vii) 2m hybrid (Steels A and E) with varying hybrid configuration

The theoretical numerical analysis consisted of calculation of the yield and plastic moments of both homogeneous and hybrid beams using the relationships previously derived in Chapter 3. Verification of the hybrid bending equations was also performed in this portion of the study. Calculations were performed manually and using spreadsheets.

Work carried out using numerical methods included the analysis of:

(i) 2m Homogeneous beams incorporating all steel grades

(ii) 4m Homogeneous beams incorporating all steel grades

(iii) 2m Hybrid 4 (HYB4) beams incorporating different combinations of steel grades

(iv) 4m Hybrid 4 (HYB4) beams incorporating different combinations of steel grades

(v) 2m Hybrid 4 (HYB4) beams (Steels A and E) with varying width to thickness ratios

(vi) 4m Hybrid 4 (HYB4) beams (Steels A and E) with varying width to thickness ratios

4.2 Influence of Width to Thickness Ratios on Bending Behaviour

4.2.1 Introduction

To demonstrate the effect of the width to thickness ratio only the Hybrid 4 (HYB4) configuration was used. Furthermore, only the Steel A (248.4MPa) and Steel E (700MPa) combination was considered as it provided the greatest difference in material yield strength. The width to thickness ratios were achieved by varying the thicknesses of the plates while keeping the width constant. Lengths of 2m and 4m were chosen to try and identify whether the behaviour of the beams would change with an increase in span length.

4.2.1.1 Model Data

Tables 4.1 and 4.2 below summarise the data for the beams used in this part of the study.

Table 4.1 Dimensions for 2m Beams with Varying Flange and Web Thickness

Combination	Flange (mm)		Web (mm)	
	Width, b_f	Thickness, t_f	Height, h_w	Thickness, t_w
0	200	6	180	5
1	200	10	180	5
2	200	15	180	5
3	200	12	180	4
4	200	12	180	8
5	200	12	180	10

Table 4.2 Dimensions for 4m Beams with Varying Flange and Web Thickness

Combination	Flange (mm)		Web (mm)	
	Width, b_f	Thickness, t_f	Height, h_w	Thickness, t_w
0	200	10	300	8
1	200	15	300	10
2	200	20	300	8
3	200	20	300	12
4	200	20	300	13
5	200	20	300	14

4.2.1.2 Limiting Width to Thickness Ratios from Design Codes

Normally, a homogeneous beam cross-section is assigned a section classification according to the lowest classification of either the web or flange. For example, if the web is in class 3 and the flange is in class 1, then the beam cross-section is classified as class 3. With hybrid beams, the process of classification is not as clear cut as that for homogeneous sections.

Despite this dilemma, it was still necessary to obtain some indication of the width to thickness, b/t, ratios of the flanges and webs of the hybrid beams. With this view in mind, the b/t ratios of flanges and webs detailed in Tables 4.1 and 4.2 were calculated using the SANS 10162-1, Eurocode 3 and AISC LRFD extracts below.

Extract from SANS 10162-1 Table 1

Width to thickness $\left(\frac{b_1}{t}\right)$ ratios for elements in compression.

Table 4.3 Section Classification According to SANS 10162-1

Element	Class 1 plastic design	Class 2 compact	Class 3 Non-compact
Flanges of I-sections	$\frac{145}{\sqrt{f_y}}$	$\frac{170}{\sqrt{f_y}}$	$\frac{200}{\sqrt{f_y}}$
Webs in flexural compression	$\frac{1100}{\sqrt{f_y}}$	$\frac{1700}{\sqrt{f_y}}$	$\frac{1900}{\sqrt{f_y}}$

For flanges,

$$b_1 = \frac{b_f}{2} \qquad 4.1$$

and for the web

$$b_1 = h_w \qquad 4.2$$

where h_1 the clear distance between the flanges.

Extract from Eurocode 3

Width to thickness $\left(\frac{c}{t}\right)$ ratios for elements in compression.

Table 4.4 Section classification according to Eurocode 3

Element	Class 1	Class 2	Class 3
Internal compression part	$\frac{c}{t} \le 72\varepsilon$	$\frac{c}{t} \le 83\varepsilon$	$\frac{c}{t} \le 124\varepsilon$
Outstand flange	$\frac{c}{t} \le 9\varepsilon$	$\frac{c}{t} \le 10\varepsilon$	$\frac{c}{t} \le 14\varepsilon$

Classes 1 and 2 can be designed plastically up to 460MPa.

For flanges,

$$c = \frac{b_f - 2r - t_w}{2} \qquad 4.3$$

where r is the fillet radius, and for webs

$$c = h_w - 2r \qquad 4.4$$

$$\varepsilon = \sqrt{\frac{235}{f_y}} \qquad 4.5$$

up to yield stress of 460MPa.

Extract from AISC LRFD

Width to thickness $\left(\frac{b_1}{t}\right)$ ratios for elements in compression.

Table 4.5 Section Classification According to AISC LRFD

Element	Compact	Non-compact
Flanges of I-shaped hybrid or welded beams in flexure	$0.38\sqrt{\frac{E}{f_y}}$	$0.95\sqrt{\frac{E}{(F_L/k_c)}}$
Web in flexural compression	$3.76\sqrt{\frac{E}{f_y}}$	$5.70\sqrt{\frac{E}{f_y}}$

For flanges, $b_1 = \frac{b_f}{2}$ and for the web, $b_1 = h_w$.

F_L is the smaller of $(F_{yf} - F_r)$ or F_{yw}

F_r is the compressive residual stress in flange (= 114MPa for welded shapes)

$$k_c = \frac{4}{\sqrt{(h/t_w)}};\ 0.35 \le k_c \le 0.763 \qquad 4.6$$

4.2.1.3 Classification of Flanges and Webs

Tables 4.6 and 4.7 show the calculated width to thickness ratios for the flange and web combinations given in Tables 4.1 and 4.2. Reference to the codes in question highlights the fact that the flanges cannot be classified as the material yield strength is greater than 460MPa. In all instances, the web is classified as class1, or compact, under all three design codes.

Table 4.6 Flange and Web Width to Thickness (b/t) Ratios for 2m Beams

Combination	**Beam**	**Flange (700MPa)**		**Web (248.4Mpa)**
		SANS/ LRFD	**Eurocode**	
0	HYB4-2	16.7	16.3	36.0
1	HYB4-2-1	10	9.8	36.0
2	HYB4-2-2	6.7	6.5	36.0
3	HYB4-2-3	8.3	8.2	45.0
4	HYB4-2-4	8.3	8.0	22.5
5	HYB4-2-5	8.3	7.9	18.0

Table 4.7 Flange and Web Width to Thickness (b/t) Ratios for 4m Beams

Combination	**Beam**	**Flange (700MPa)**		**Web (248.4MPa)**
		SANS/ LRFD	**Eurocode**	
0	HYB4-4	10.0	9.6	37.5
1	HYB4-4-1	6.7	6.3	30.0
2	HYB4-4-2	5.0	4.8	37.5
3	HYB4-4-3	5.0	4.7	25.0
4	HYB4-4-4	5.0	4.7	23.1
5	HYB4-4-5	5.0	4.7	21.4

4.2.2 ABAQUS Results

The data extracted from the ABAQUS analyses was used to plot curves of the load per unit length, ω, versus the midspan deflection, d. Under normal circumstances the moment, as calculated by the equation $M = \frac{\omega l^2}{8}$ (for a simply supported beam acting under a uniformly distributed load), would be plotted against deflection or curvature. However, this formula is valid only within the elastic region and the moment-deflection response curve would need to be truncated. Using load-deflection curve enables the entire progress of the analysis to be captured, even when the beam response becomes non-linear. In the same token, values of curvature could not be extracted as the approximated simple support conditions did not permit this.

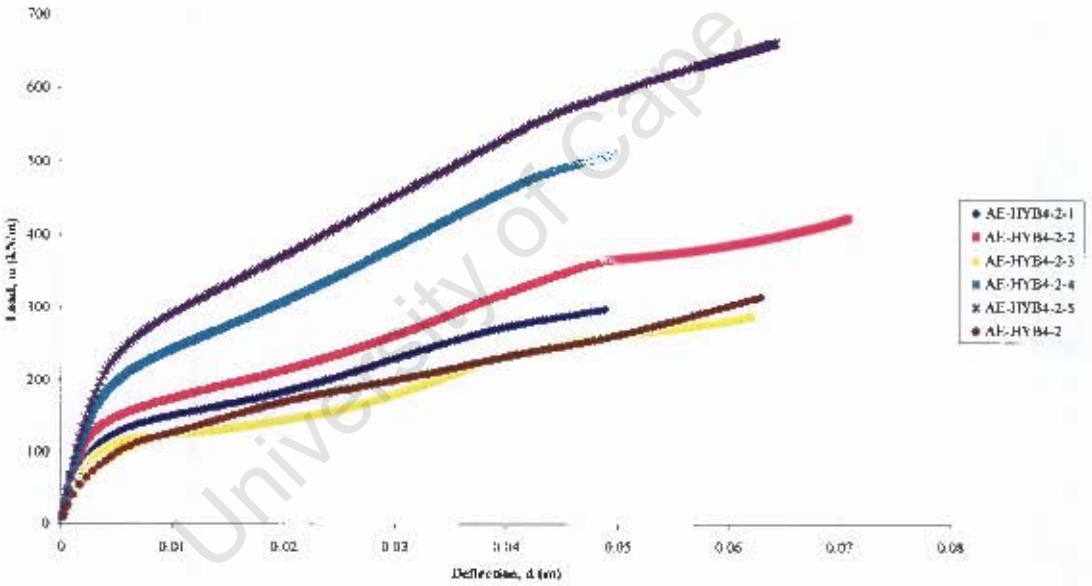

Figure 4.1 Comparison of Load-Deflection Response for 2m Hybrid Beams with Varying Flange and Web Thickness

When plotted as a function of the load per unit length, ω, and midspan deflection, d, the ABAQUS results for the 2m beams (Figure 4.1) predict that AE-HYB4-2-5, which has the smallest b/t ratio of web and the second least slender flanges, will be able to carry the greatest load. This same beam was the only one to reach its flange yield moment. AE-HYB4-2-3, with the most slender web, and AE-HYB4-2, with the most slender flanges, will carry the least load.

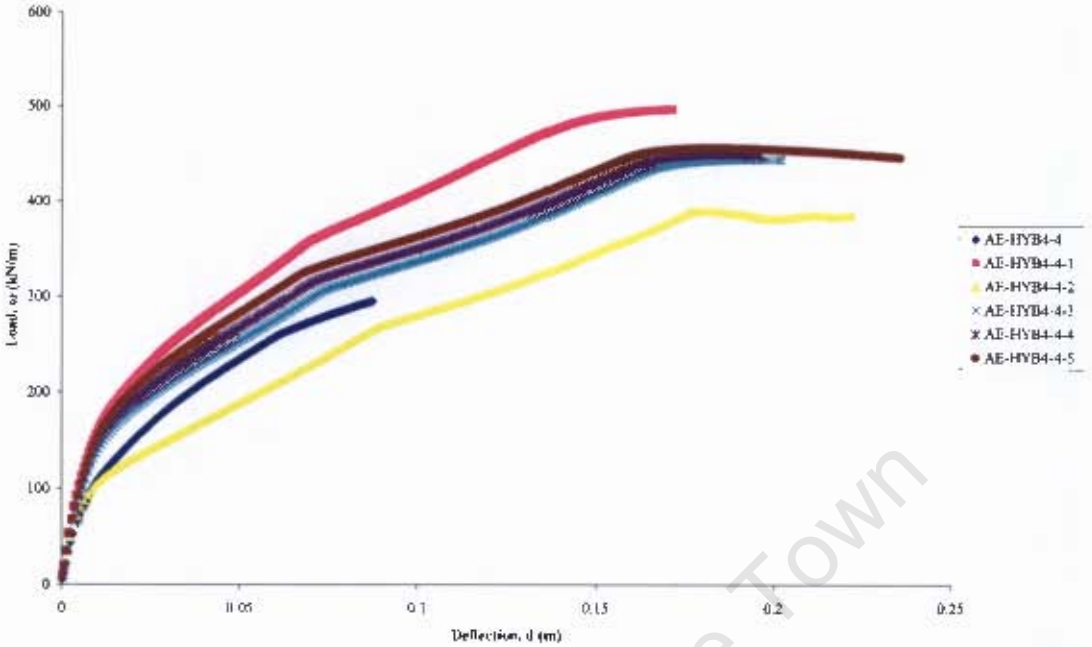

Figure 4.2 Comparison of Load-Deflection Response for 4m Hybrid Beams with Varying Flange and Web Thickness

Within the 4m beam series shown in Figure 4.2, ABAQUS results indicate that AE-HYB4-4-1, with a flange b/t ratio of 6.7 and web b/t ratio of 30, will carry the greatest load. What could be termed the *'most compact section'* in relative terms manages to sustain an ultimate load that is appreciably less than that of AE-HYB4-4-1. Furthermore, AE-HYB4-4-1 and AE-HYB4-4 were the only two beams to reach their flange yield and yield moments, respectively. This suggests that simply designing stockier thicker flanges and webs will not necessarily equate to a larger ultimate strength in bending. AE-HYB4-4-2 will carry the least load as it has a width-thickness ratio of web equal to 37. Certain analyses (Figure 4.1 and 4.2) terminated prematurely due to difficulties in convergence. This was possibly due to thick flanges and webs which increased model stiffness.

Figure 4.3 shows a visual taken at the end of the analysis. Since the beam consists of two different materials the fact that the web has exceeded it material yield stress is not immediately clear by simply referring to the colour legend. Closer inspection of the Mises stress values themselves is necessary.

Figure 4.3 shows a visual extracted at the last load increment. At this stage, the bottom flange stresses are between 400MPa and 500MPa as seen from the key in the figure. This implies that the tension flange has already reached its material yield strength and is now unable to sustain further loads. The web will also have reached its yield stress and is in plastification. The compression flange is just reaching its yield stress at this point. Theoretically the tension and compression flanges should yield at the same stress. In practice, the compression flange can potentially yield at higher stresses if local buckling is prevented.

What is immediately clear from Figure 4.3 is that the starts to buckle near the supports where the shear has a maximum value (due to the distributed transverse load). This effect is magnified in AE-HYB4-2-3 which has the most slender web (width-thickness ratio of 45) but is also evident in Figures 4.4 and 4.5.

Figure 4.3 Stress Distribution in Hybrid Beam AE-HYB4-2-3

Figure 4.4 Stress Distribution in Hybrid Beam AE-HYB4-2-1

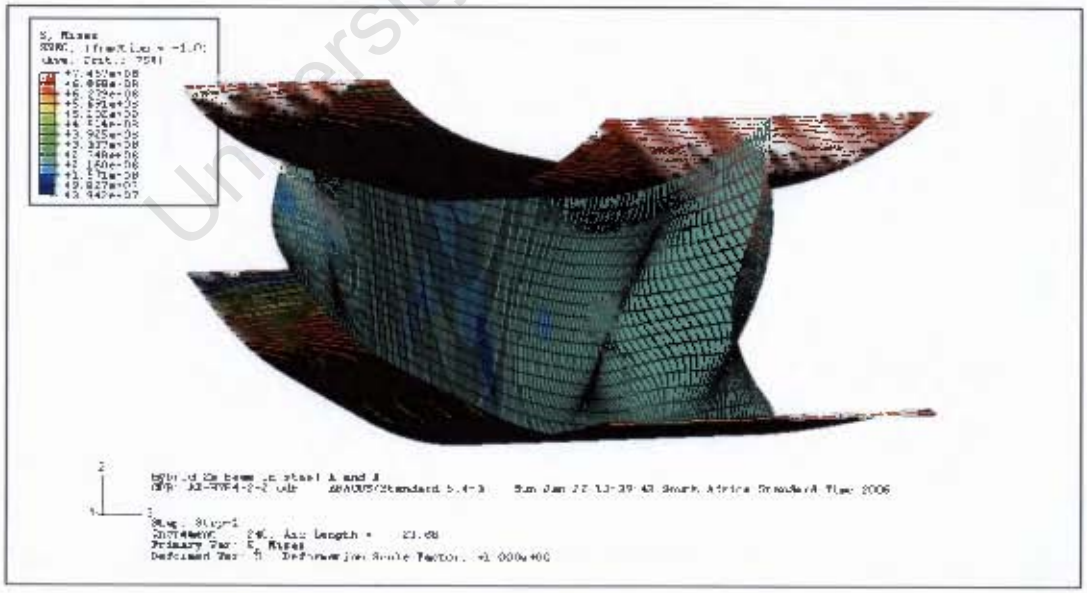

Figure 4.5 Stress Distribution in Hybrid Beam AE-HYB4-2-2

Loss of section height due to shear buckling is demonstrated in Figure 4.6. Flange buckling is not evident in the 2m beams but can be observed in the 4m beams in Figures 4.7 and 4.8.

Figure 4.6 Loss of Section Height in Hybrid Beam AE-HYB4-2-2

Figure 4.7 Buckling in Hybrid Beam AE-HYB4-4-5

Figure 4.8 Flange Buckling in Hybrid Beam AE-HYB4-4-5

4.2.3 Theoretical Numerical Results

The analytical data formed the basis of this portion of the work. Yield, M_y, and plastic, M_p, moments for the homogeneous beams were calculated very simply from elastic theory equations. Values of web yield moment, M_{yw}, flange yield moment, M_{yf}, and theoretic plastic moment, Mp, were calculated for the hybrid beams as described in Section 3.3. The characteristic moments were evaluated at midspan. Spreadsheets were used to carry out the calculations and are included in Table 4.8 below. Curves of moment, M , versus rotation, κ , were then constructed. Moment-curvature, rather than moment-deflection or load-deflection, cures were opted for as the beams were hypothetical and, therefore, had no actual loads or deflections.

Table 4.8 Calculation of Moments for Hybrid Beams of Varying Flange and Web Thickness

analysis	d/2 (m)	*tf*	*tw*	*el. core*	*σf bottom*	*trap. Cent.*	*A1*	*A2*	*A3*
AE-HYB4-2-1	0.1	0.01	0.005	0.035485714	630	0.004912281	2000	272.5714286	177.4285714
AE-HYB4-2-2	0.105	0.015	0.005	0.03726	600	0.007307692	3000	263.7	186.3
AE-HYB4-2-3	0.102	0.012	0.004	0.036195429	617.6470588	0.005875	2400	215.2182857	144.7817143
AE-HYB4-2-4	0.102	0.012	0.008	0.036195429	617.6470588	0.005875	2400	430.4365714	289.5634286
AE-HYB4-2-5	0.102	0.012	0.01	0.036195429	617.6470588	0.005875	2400	538.0457143	361.9542857
AE-HYB4-4-1	0.165	0.015	0.01	0.058551429	636.3636364	0.007380952	3000	914.4857143	585.5142857
AE-HYB4-4-2	0.17	0.02	0.008	0.060325714	617.6470588	0.009791667	4000	717.3942857	482.6057143
AE-HYB4-4-3	0.17	0.02	0.012	0.060325714	617.6470588	0.009791667	4000	1076.091429	723.9085714
AE-HYB4-4-4	0.17	0.02	0.013	0.060325714	617.6470588	0.009791667	4000	1165.765714	784.2342857
AE-HYB4-4-5	0.17	0.02	0.014	0.060325714	617.6470588	0.009791667	4000	1255.44	844.56

(Continued)

y1	*y2*	*y3*	*c1*	*c2*	*c3*	*Myf*	*Mp*	*ρ*	*κ=1/ρ*
0.190175439	0.125485714	0.047314286	1330	67.70674286	22.03662857	262.4722097	276.0602	30	0.033333333
0.195384615	0.12726	0.04968	1950	65.50308	23.13846	390.4854407	419.5602	31.5	0.031746032
0.19225	0.126195429	0.048260571	1581.176471	53.46022217	17.98188891	311.5954284	330.60816	30.6	0.032679739
0.19225	0.126195429	0.048260571	1581.176471	106.9204443	35.96377783	319.2096802	338.65632	30.6	0.032679739
0.19225	0.126195429	0.048260571	1581.176471	133.6505554	44.95472229	323.0168062	342.6804	30.6	0.032679739
0.315238095	0.208551429	0.078068571	2004.545455	227.1582514	72.72087429	684.9604835	717.39	49.5	0.02020202
0.320416667	0.210325714	0.080434286	2635.294118	178.2007406	59.93962971	886.6935562	940.712	51	0.019607843
0.320416667	0.210325714	0.080434286	2635.294118	267.3011109	89.90944457	907.8442559	963.068	51	0.019607843
0.320416667	0.210325714	0.080434286	2635.294118	289.5762034	97.40189829	913.1319308	968.657	51	0.019607843
0.320416667	0.210325714	0.080434286	2635.294118	311.851296	104.894352	918.4196057	974.246	51	0.019607843

(Continued)

ρ	κ=1/ρ	σf top	e. core	trap centre	area 1	area3	lever 1	lever3	ce 1
0.845410628	1.182857143	276	0.09	0.004912281	2000	450	0.190175439	0.12	524.4
0.845410628	1.182857143	289.8	0.09	0.007307692	3000	450	0.195384615	0.12	807.3
0.845410628	1.182857143	281.52	0.09	0.005875	2400	360	0.19225	0.12	635.904
0.845410628	1.182857143	281.52	0.09	0.005875	2400	720	0.19225	0.12	635.904
0.845410628	1.182857143	281.52	0.09	0.005875	2400	900	0.19225	0.12	635.904
0.845410628	1.182857143	273.24	0.15	0.007380952	3000	1500	0.315238095	0.2	782.46
0.845410628	1.182857143	281.52	0.15	0.009791667	4000	1200	0.320416667	0.2	1059.84
0.845410628	1.182857143	281.52	0.15	0.009791667	4000	1800	0.320416667	0.2	1059.84
0.845410628	1.182857143	281.52	0.15	0.009791667	4000	1950	0.320416667	0.2	1059.84
0.845410628	1.182857143	281.52	0.15	0.009791667	4000	2100	0.320416667	0.2	1059.84

(Continued)

ce 3	Myw	ρ	κ=1/ρ
55.89	106.4348	76.0869565	0.01314286
55.89	164.4408	76.0869565	0.01314286
44.712	127.617984	76.0869565	0.01314286
89.424	132.983424	76.0869565	0.01314286
111.78	135.666144	76.0869565	0.01314286
186.3	283.9212	126.811594	0.00788571
149.04	369.3984	126.811594	0.00788571
223.56	384.3024	126.811594	0.00788571
242.19	388.0284	126.811594	0.00788571
260.82	391.7544	126.811594	0.00788571

The spreadsheet data Table 4.8 is further summarised in Table 4.9. Curves for the analytical section were constructed using two reference points for homogeneous beams, and three for hybrids.

Table 4.9 Summary of Analytical Data for Hybrid Beams with Varying Flange and Web Thicknesses

Analysis	M^1_{yw} (kNm)	M^1_{yf} (kNm)	M^1_p (kNm)
AE-HYB4-2-1	106.4	262.5	276.1
AE-HYB4-2-2	164.4	390.5	419.6
AE-HYB4-2-3	127.6	311.6	330.6
AE-HYB4-2-4	133.0	319.2	338.7
AE-HYB4-2-5	135.7	323.0	342.7
AE-HYB4-4-1	283.9	685.0	717.4
AE-HYB4-4-2	369.4	886.7	940.74
AE-HYB4-4-3	384.3	907.8	963.1
AE-HYB4-4-4	388.0	913.1	968.7
AE-HYB4-4-5	391.8	918.4	974.2

[1] All moments calculated at the centre of the span

Figures 4.9 and 4.10 show that web yielding tends not to introduce any high levels of nonlinearity and, to all intents and purposes, the plots are linear up until the flange yield moment. It is also clear that in order for the plastic moment to be attained, very large curvatures are required. Dashed lines are used to indicate that areas of the plot have been truncated in order to accommodate the large curvatures.

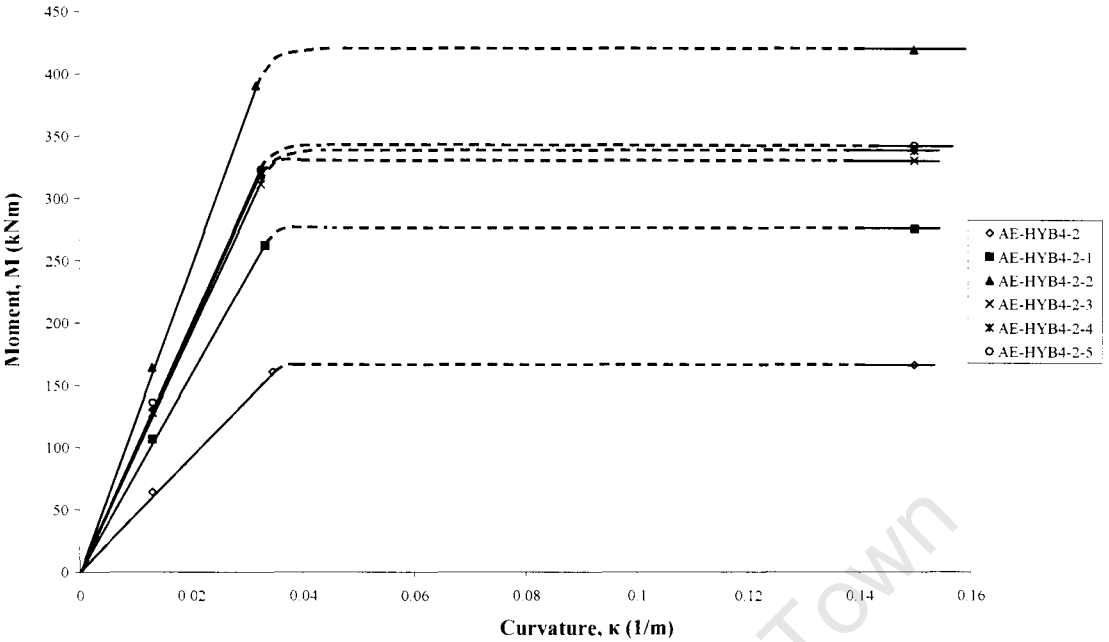

Figure 4.9 Comparison of Analytical Results for the Moment-Curvature Response of 2m Hybrid Beams with Varying Flange and Web Thickness

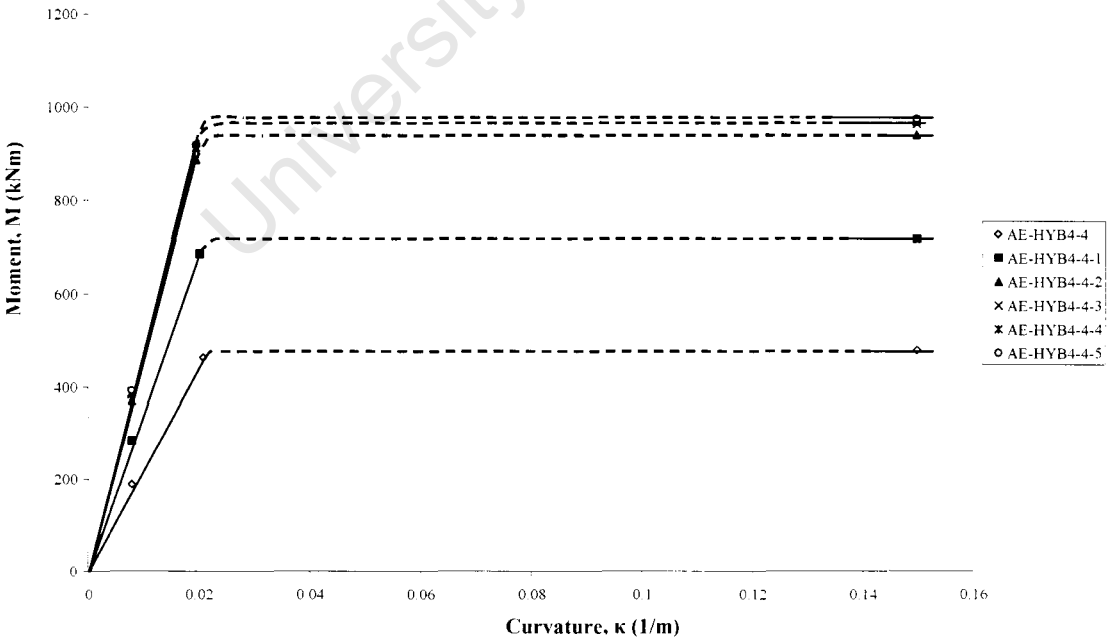

Figure 4.10 Comparison of Analytical Results for the Moment-Curvature Response of 4m Hybrid Beams with Varying Flange and Web Thickness

Analytical results indicated that AE-HYB4-2-2, with the least slender flanges, would be able to sustain larger moments. AE-HYB4-2, with the most slender flanges, would carry the least moment. AE-HYB4-4-5 and AE-HYB4-4 would achieve the greatest and least moments, respectively.

4.2.4 Summary of Results

All curves generated using the ABAQUS data are nonlinear in nature and, even within the elastic range, tended to overestimate the deflections of the members when compared to those deflections calculated from elastic theory equations. While there were no difficulties associated with the homogeneous members, the hybrid beam analyses tended to stop quite abruptly, possibly due to convergence problems.

Focussing only on the beams with the highest and lowest carrying capacities gives the impression that the ABAQUS and analytical results are contradictory. However, when beams of equal length are ranked in order of decreasing load carrying capacity, it becomes clear that both sets of results show relatively similar trends.

Closer inspection of the beams with identical web width to thickness ratios showed that beams with less slender flanges could sustain greater loads and moments in both the ABAQUS and analytical results. This was true for both beam lengths. The opposite was also true i.e. for the same flange width to thickness ratio; beams with less slender webs could carry greater loads. Again, this was true for both sets of results.

4.3 Influence of Length on Bending Behaviour

4.3.1 Introduction

A total of fifteen Hybrid 4 (HYB4) beams can be generated when all the steel grades, A to F, are paired in different flange and web combinations. When both 2m and 4m lengths are considered, thirty Hybrid 4 beams are then realised. This part of the study was specifically aimed at finding any changes in the bending behaviour of the hybrids as length increased.

4.3.1.1 Model Data

Dimensional properties of the beams are given in Table 4.10.

Table 4.10 Flange and Web Dimensions for Hybrid Beams to be Investigated for the Influence of Length on Bending Behaviour

Beam Length	b_f (mm)	t_f (mm)	h_w (mm)	t_w (mm)	Depth of Section, d
2m	200	6	180	5	192
4m	200	10	300	8	320

4.3.2 ABAQUS Results

4.3.2.1 Two Metre Beams with 350MPa Flanges

The curves were presented in such a fashion that the behaviour of each hybrid was plotted on the same axes as the homogeneous beams made up of the web and flange material. For example, beam AF-HYB4-2 was plotted against A-HOM-2 and F-HOM-2.

The load-deflection curves for all 2m beams are highly non-linear and essentially all have the same basic shape. Each hybrid beam could sustain a load greater than that which causes flange yielding but most of the analyses did not run to completion because of convergence problems. Only the hybrid beams CD-HYB4-2 (Figure 4.26) and DE-HYB4-2 (Figure 4.35) began to unload since the constituent steels had yield strengths which were close and, On the other hand, all the homogeneous beams reached their ultimate load and, thereafter, unloaded abruptly.

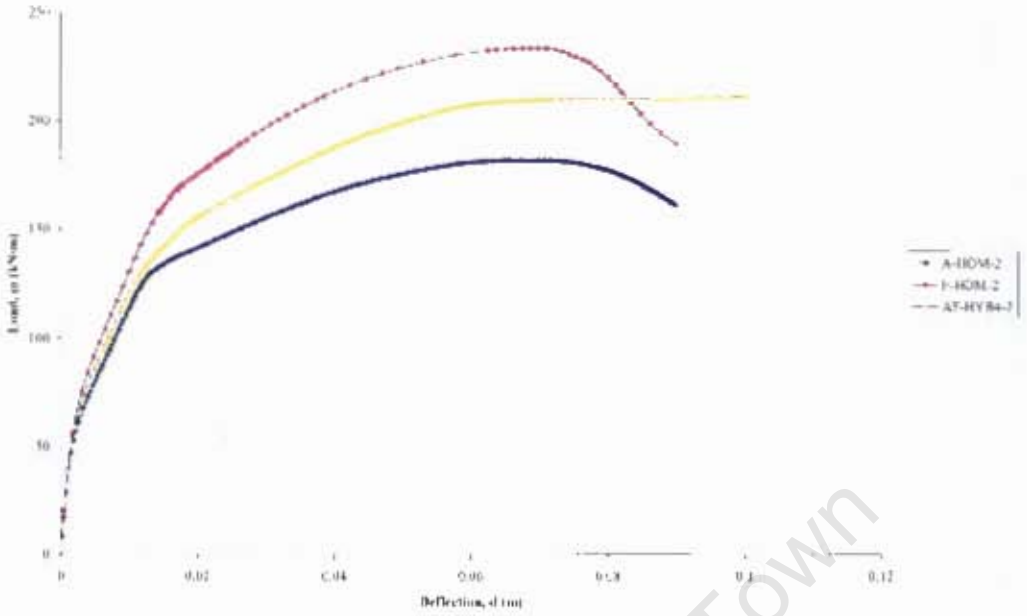

Figure 4.11 Comparison of the Load-Deflection Response between AF-HYB4-2 and Equivalent Homogeneous Sections A-HOM-2 and F-HOM-2

4.3.2.2 Two Metre Beams with 460MPa Flanges

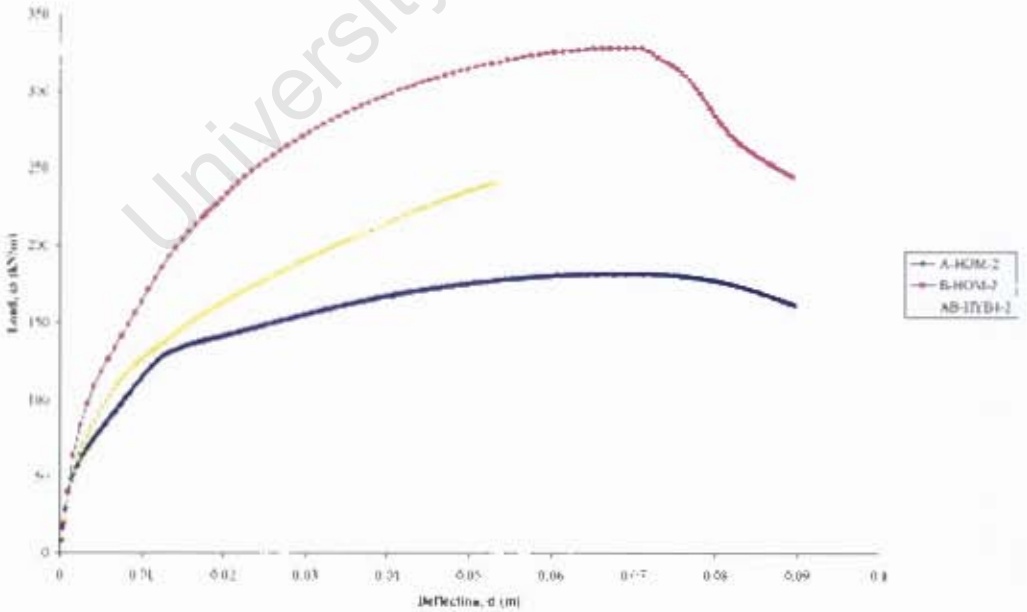

Figure 4.12 Comparison of the Load-Deflection Response between AB-HYB4-2 and Equivalent Homogeneous Sections A-HOM-2 and B-HOM-2

Figure 4.13 Stress Distribution in Hybrid Beam AB-HYB4-2

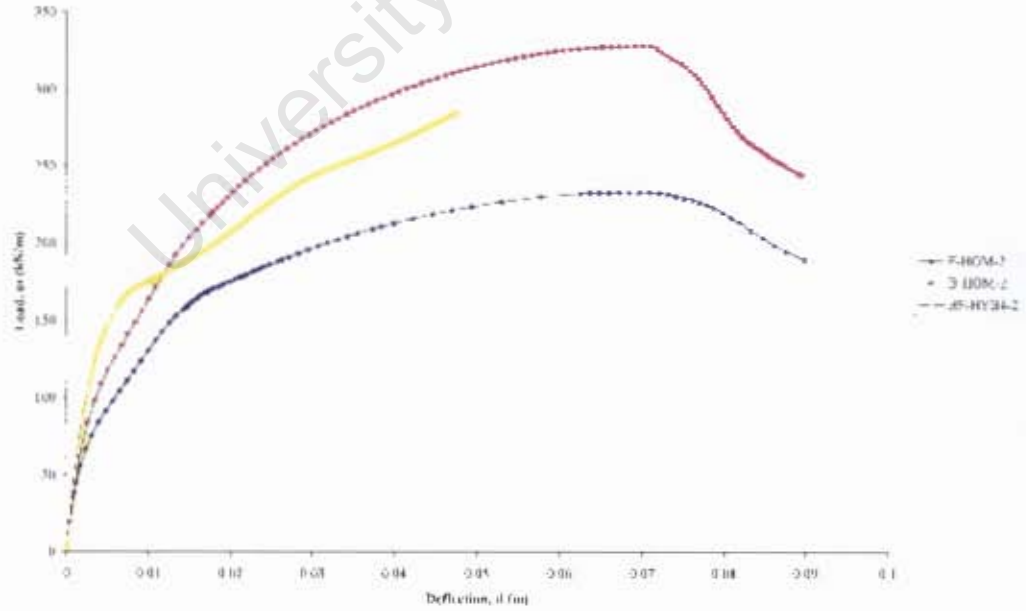

Figure 4.14 Comparison of the Load-Deflection Response between BF-HYB4-2 and Equivalent Homogeneous Sections B-HOM-2 and F-HOM-2

4.3.2.3 Two Metre Beams with 550MPa Flanges

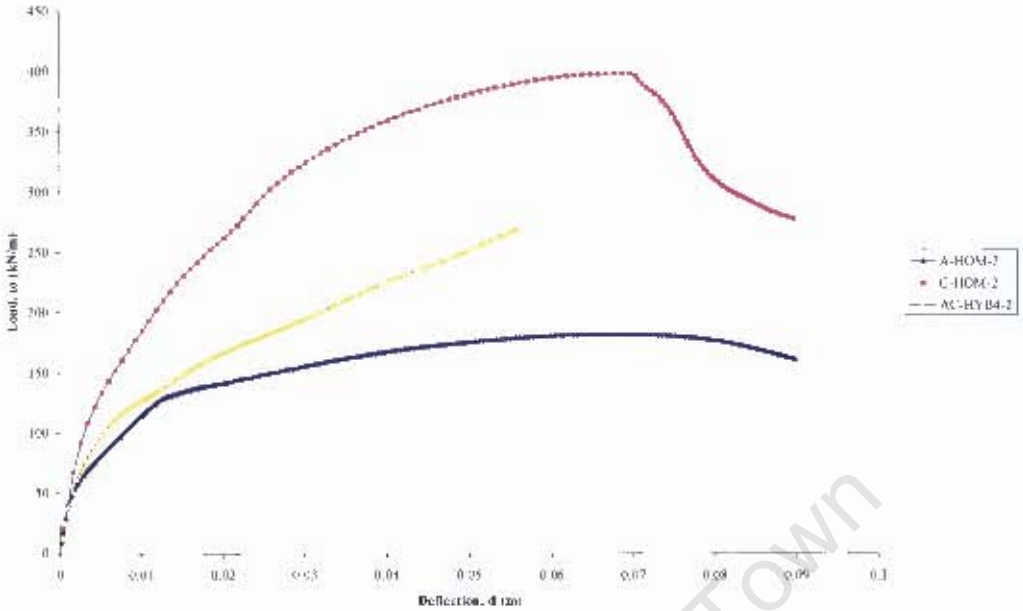

Figure 4.15 Comparison of the Load-Deflection Response between AC-HYB4-2 and Equivalent Homogeneous Sections A-HOM-2 and C-HOM-2

In the typical hybrid beams, material yielding starts at the centre of the span, in the portion of the web that is in tension. This zone of yielding then progresses towards the web centre while, simultaneously, the tension flange material starts yielding. The compression flanges have much lower stresses during most of the loading stage.

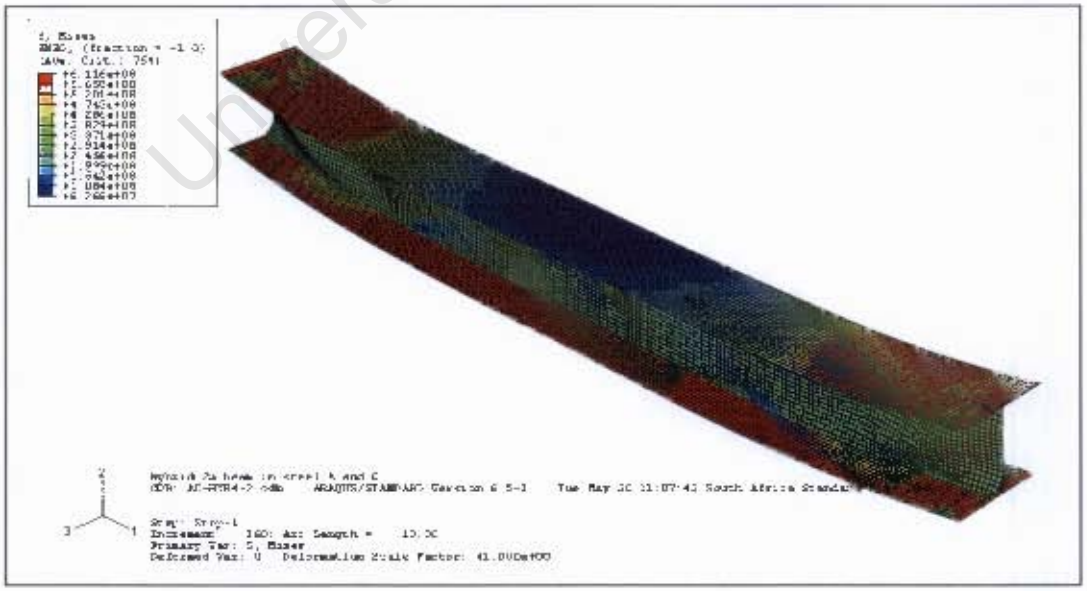

Figure 4.16 Stress Distribution in Hybrid Beam AC-HYB4-2

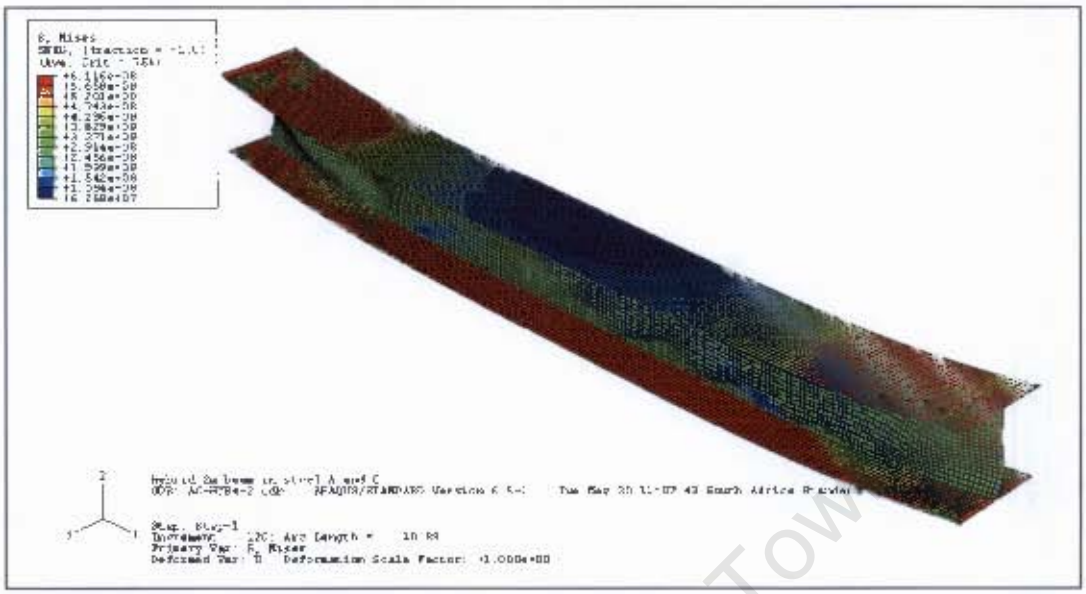

Figure 4.17 Stress Distribution in Hybrid Beam AC-HYB4-2

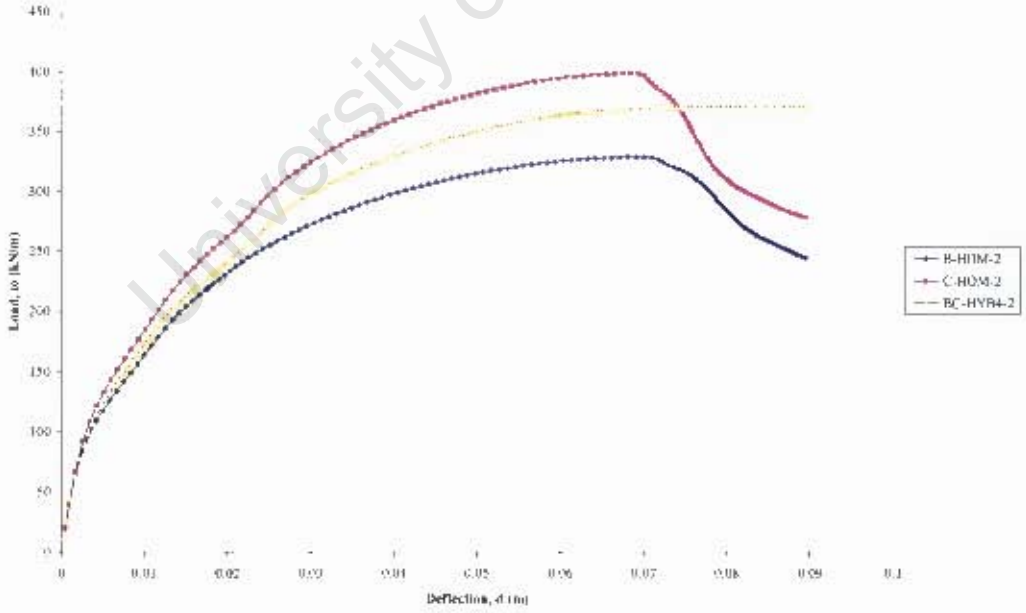

Figure 4.18 Comparison of the Load-Deflection Response between BC-HYB4-2 and Equivalent Homogeneous Sections B-HOM-2 and C-HOM-2

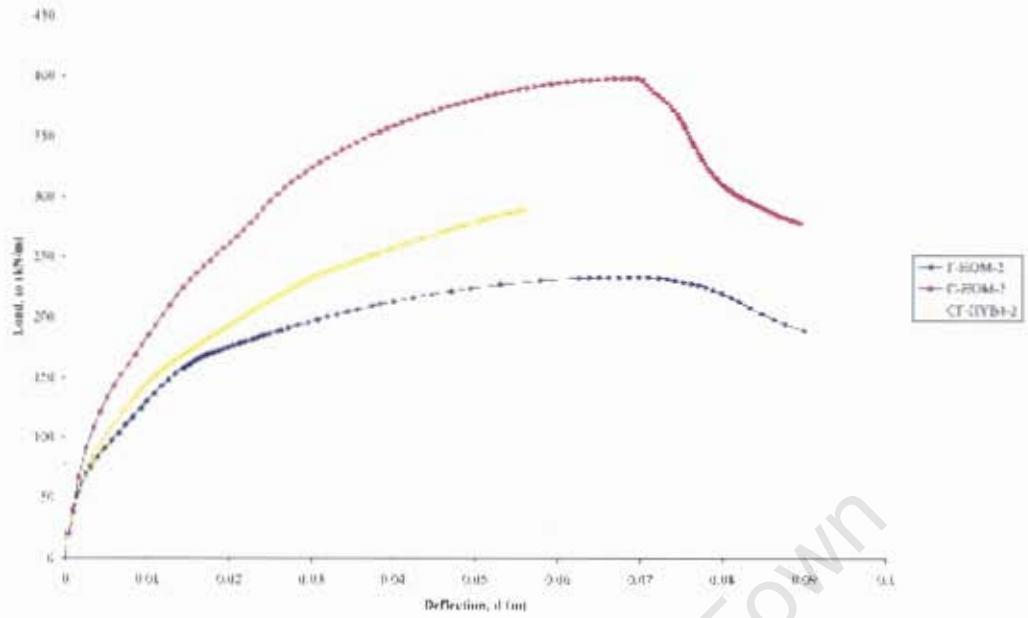

Figure 4.19 Comparison of the Load-Deflection Response between CF-HYB4-2 and Equivalent Homogeneous Sections C-HOM-2 and F-HOM-2

4.3.2.4 Two Metre Beams with 690MPa Flanges

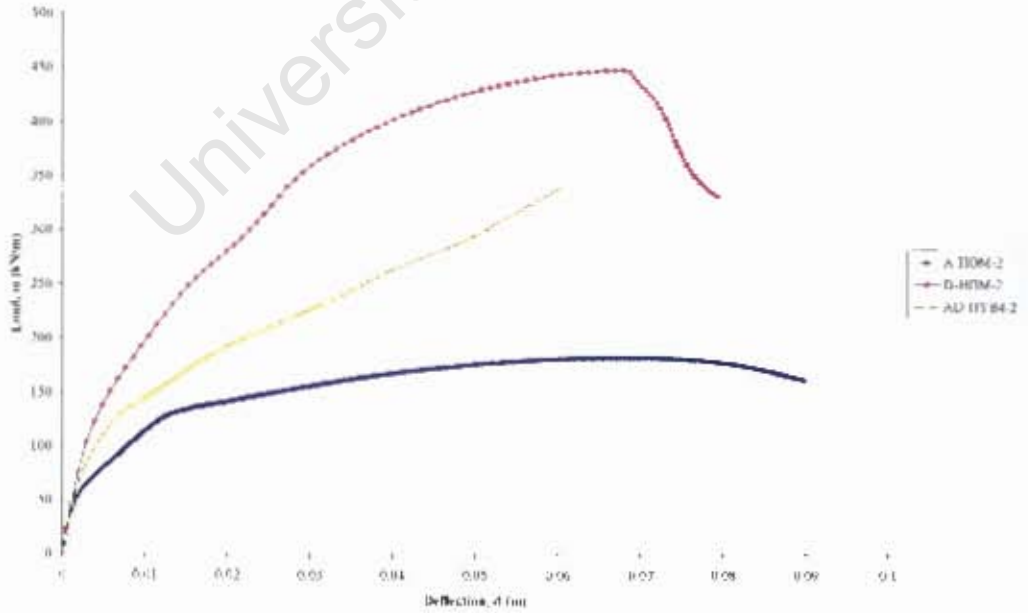

Figure 4.20 Comparison of the Load-Deflection Response between AD-HYB4-2 and Equivalent Homogeneous Sections A-HOM-2 and D-HOM-2

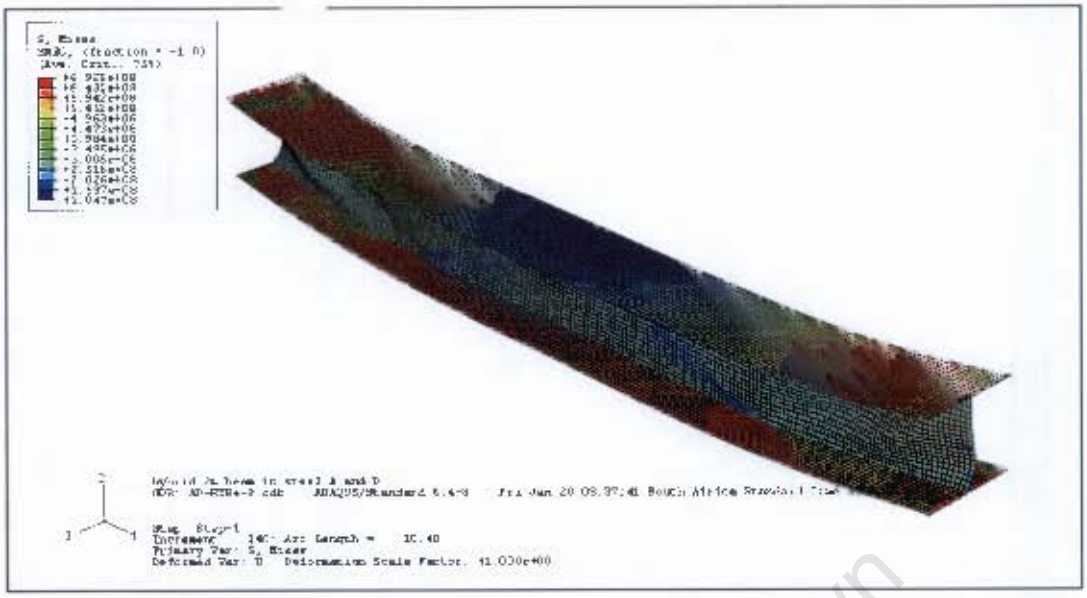

Figure 4.21 Stress Distribution in Hybrid Beam AD-HYB4-2

Buckles appear at the edges of the webs and these gradually become diagonal; resembling those buckles which occur when there is tension field action in the web. Figures 4.22 and 4.30 show material yielding in the tension flange where these diagonal buckles end. Usually tension field action is taken into account where there are stiffeners but it may be that the higher strength steel in the flanges plays a similar role to stiffeners in stiffened beams.

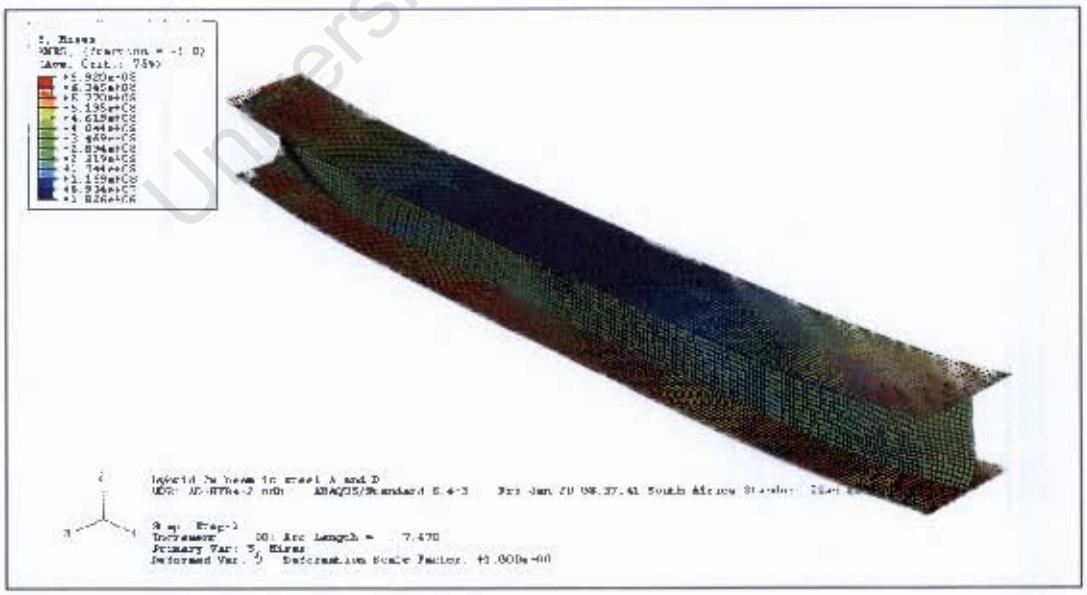

Figure 4.22 Stress Distribution in Hybrid Beam AD-HYB4-2

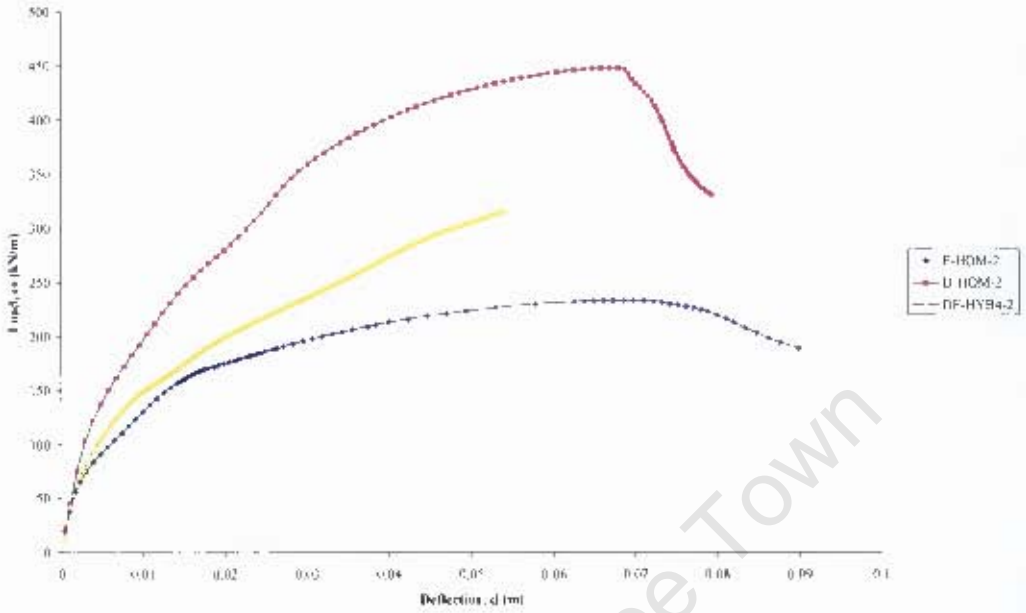

Figure 4.23 Comparison of the Load-Deflection Response between DF-HYB4-2 and Equivalent Homogeneous Sections D-HOM-2 and F-HOM-2

Figure 4.24 Stress Distribution in Hybrid Beam DF-HYB4-2

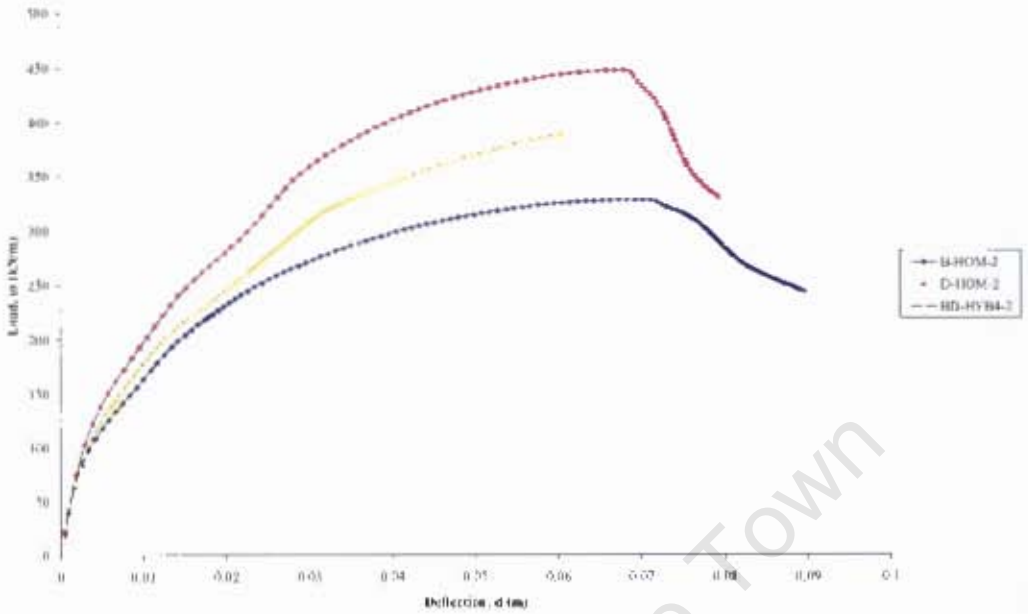

Figure 4.25 Comparison of the Load-Deflection Response between BD-HYB4-2 and Equivalent Homogeneous Sections B-HOM-2 and D-HOM-2

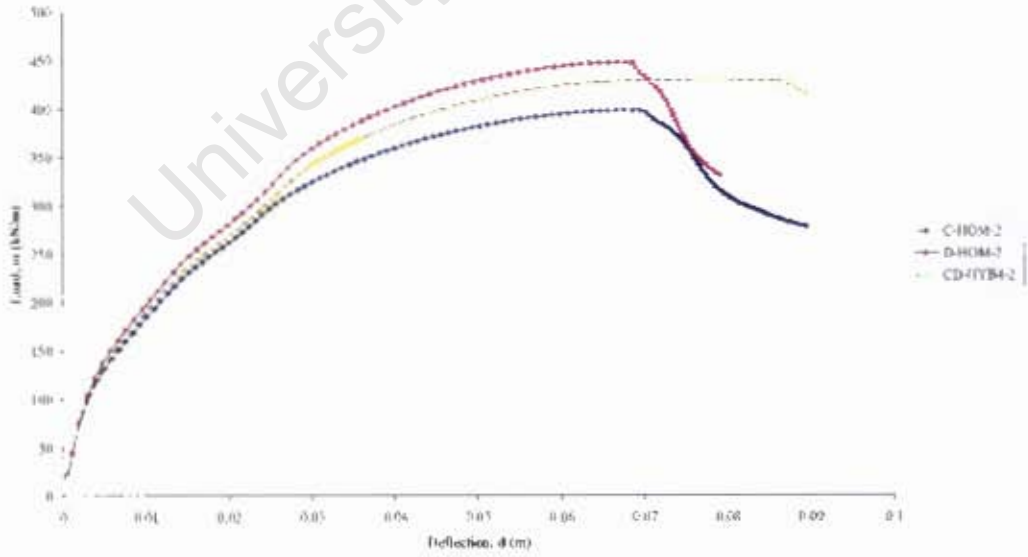

Figure 4.26 Comparison of the Load-Deflection Response between CD-HYB4-2 and Equivalent Homogeneous Sections C-HOM-2 and D-HOM-2

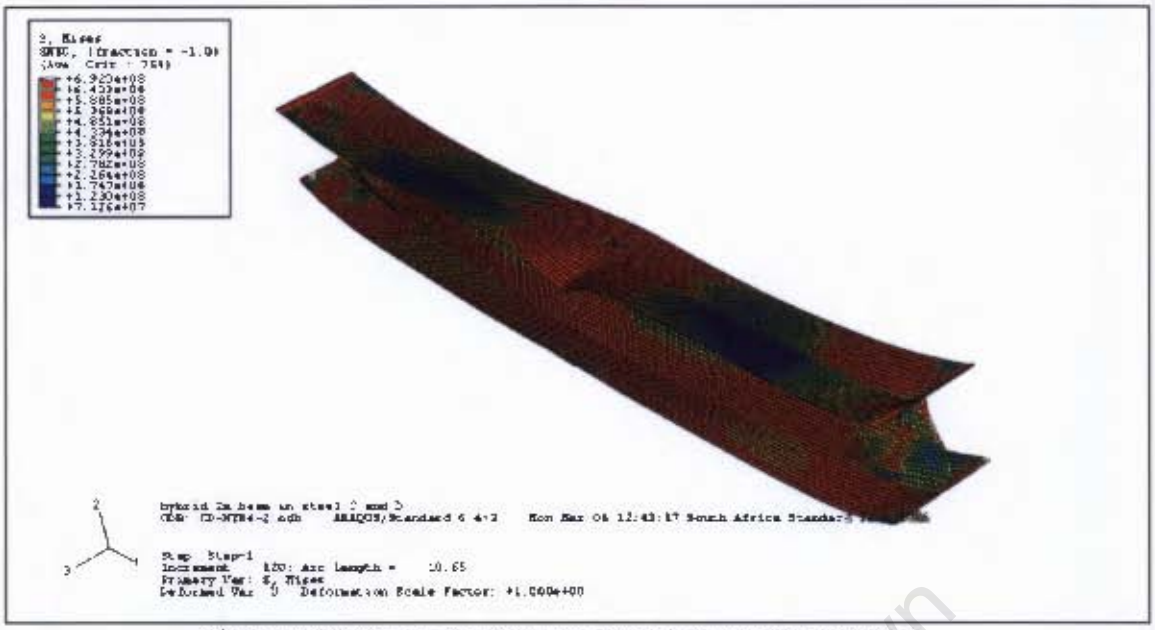

Figure 4.27 Flange Buckling in Hybrid Beam CD-HYB4-2

At the end of loading, hybrid beams whose constituent metals have yield stresses which are fairly close as in beams CD-HYB4-2 (Figures 4.27and 4.28), CE-HYB4-2 (Figure 4.34) and DE-HYB4-2 (Figure 4.36) exhibit asymmetrical flange buckling. Although lateral torsional buckling was not considered, out-of-plane movements of the flange was observed n some beams. This is accompanied by widespread yielding of flanges and web. This pattern of stress distribution and instability is also evident in all homogeneous 2 beams (Figures 4.37 and 4.38).

Figure 4.28 Lateral Flange Displacement in Hybrid Beam CD-HYB4-2

4.3.2.5 Two Metre Beams with 700MPa Flanges

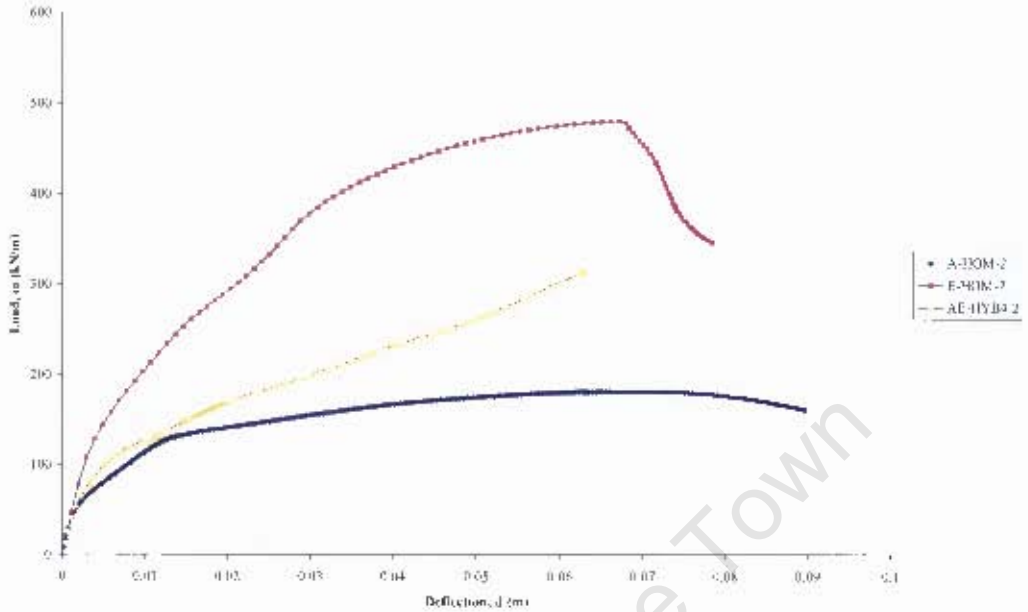

Figure 4.29 Comparison of the Load-Deflection Response between AE-HYB4-2 and Equivalent Homogeneous Sections A-HOM-2 and E-HOM-2

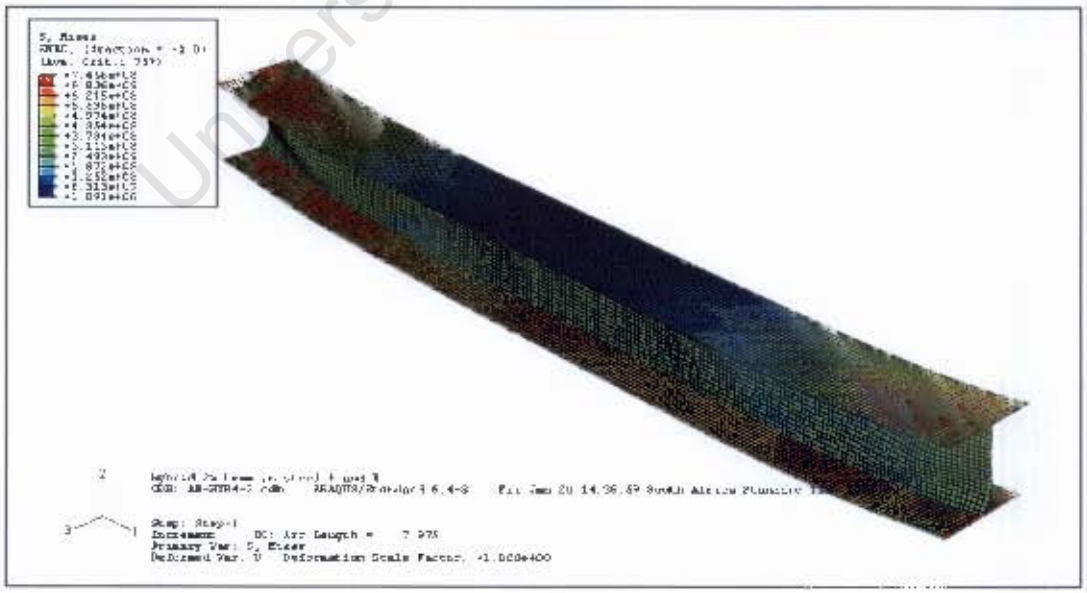

Figure 4.30 Stress Distribution in Hybrid Beam AE-HYB4-2

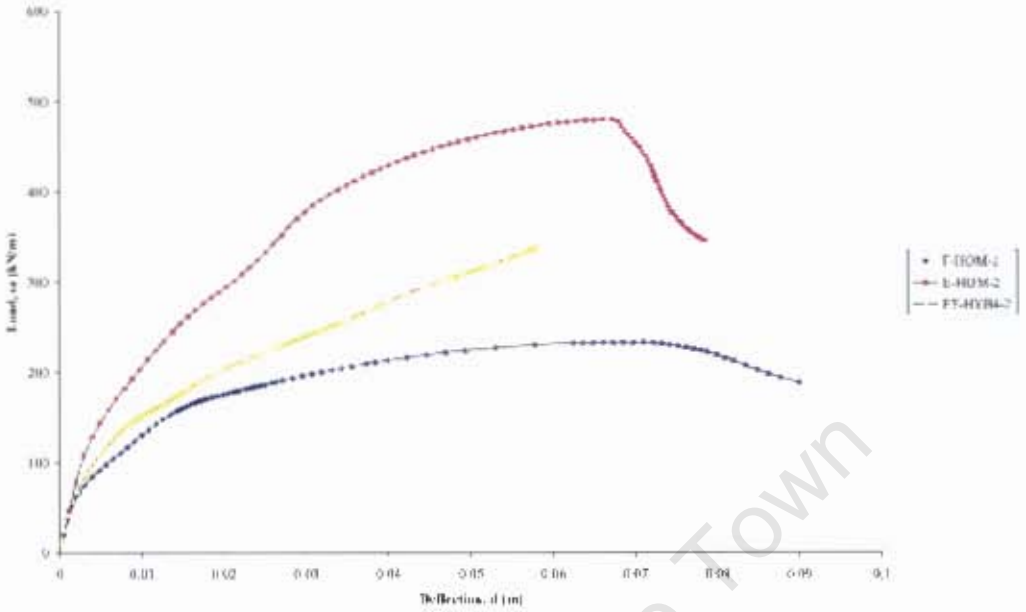

Figure 4.31 Comparison of the Load-Deflection Response between FF-HYB4-2 and Equivalent Homogeneous Sections E-HOM-2 and F-HOM-2

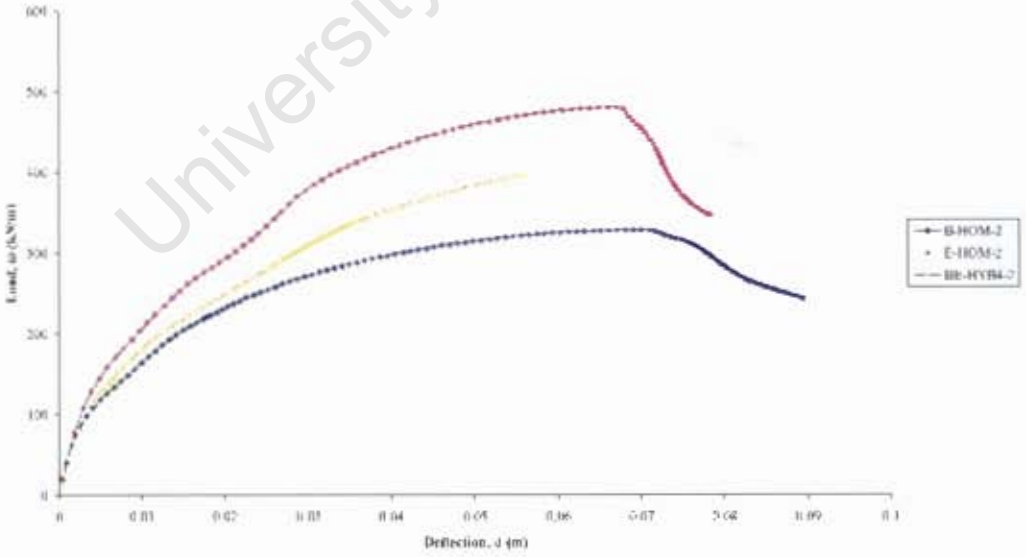

Figure 4.32 Comparison of the Load-Deflection Response between BE-HYB4-2 and Equivalent Homogeneous Sections B-HOM-2 and E-HOM-2

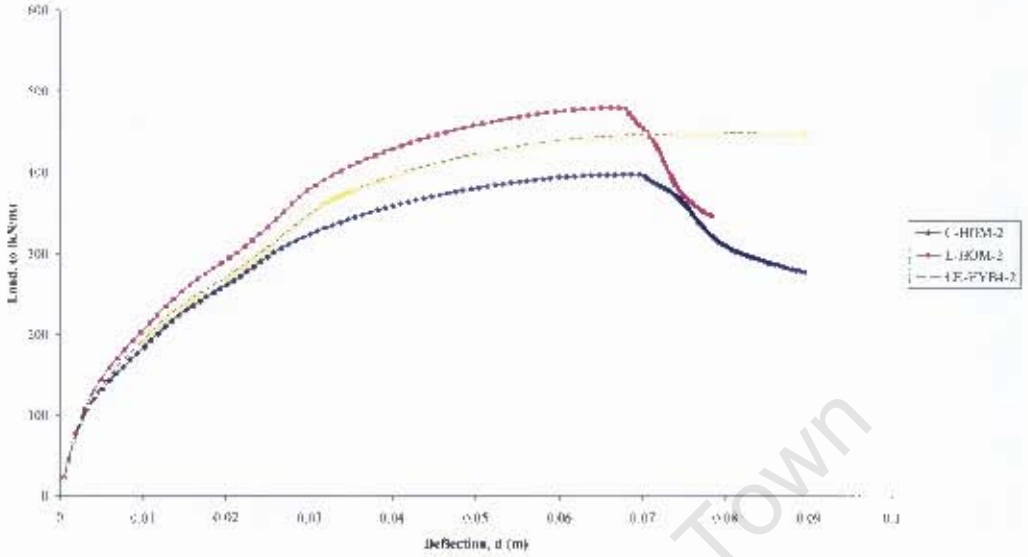

Figure 4.33 Comparison of the Load-Deflection Response between CE-HYB4-2 and Equivalent Homogeneous Sections C-HOM-2 and E-HOM-2

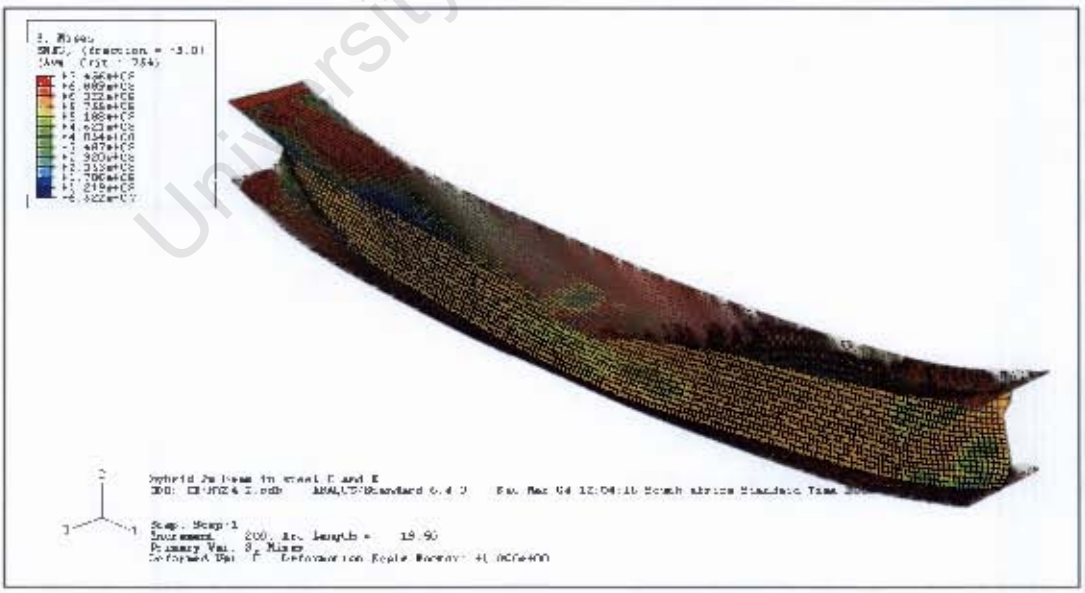

Figure 4.34 Stress Distribution in Hybrid Beam CE-HYB4-2

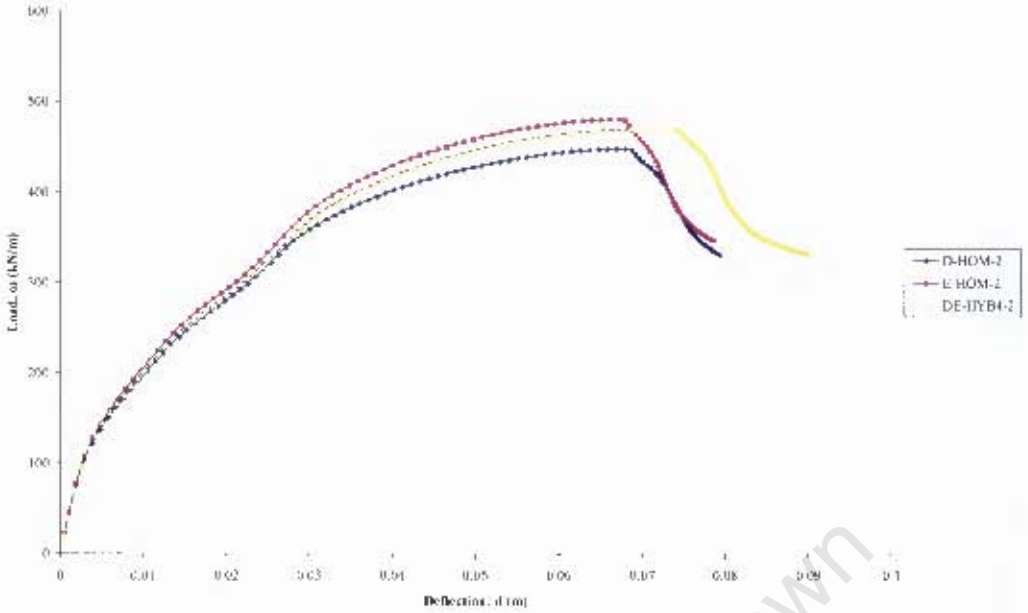

Figure 4.35 Comparison of the Load-Deflection Response between DE-HYB4-2 and Equivalent Homogeneous Sections D-HOM-2 and E-HOM-2

With the higher strength steel in the flanges, the webs of the hybrid beams commenced yielding first and this was evident in all but one of the specimens. The hybrid in question, DE-HYB4-2 (Figures 4.35 and 4.36), is composed of 700MPa flanges and a 690MPa web and behaves more a like homogeneous beam than a hybrid because the steel grades were nearly equivalent. The development of stresses across the beam cross-section was similar to that of a homogeneous member, with initial flange yielding.

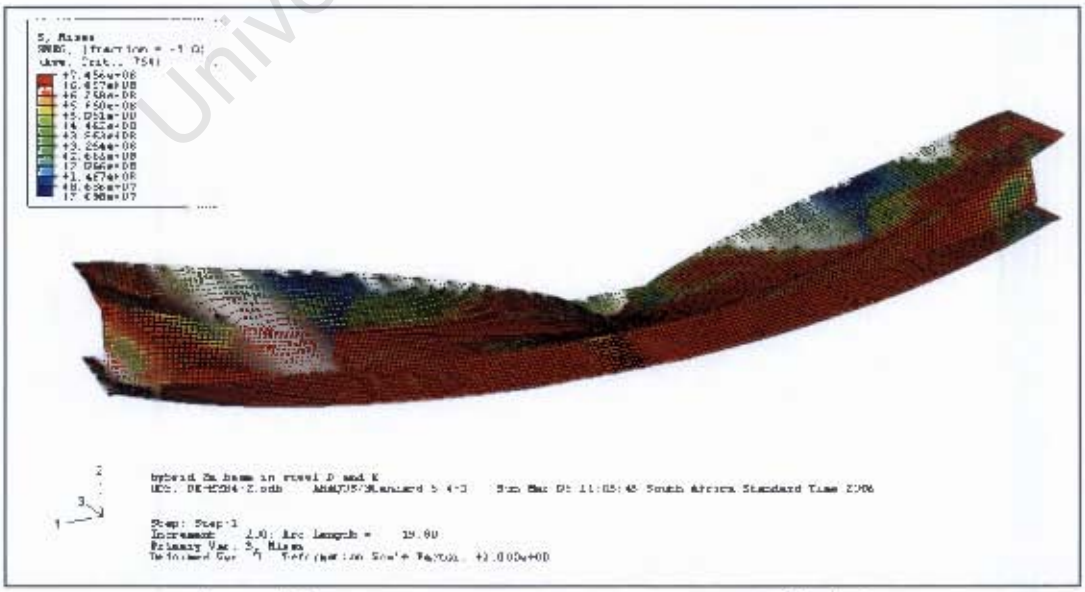

Figure 4.36 Flange Buckling in Hybrid Beam DE-HYB4-2

Figure 4.37 Flange Buckling in Beam A-HOM-2

Figure 4.38 Lateral Flange Displacement in A-HOM-2

4.3.2.6 Four Metre Beams with 350MPa Flanges

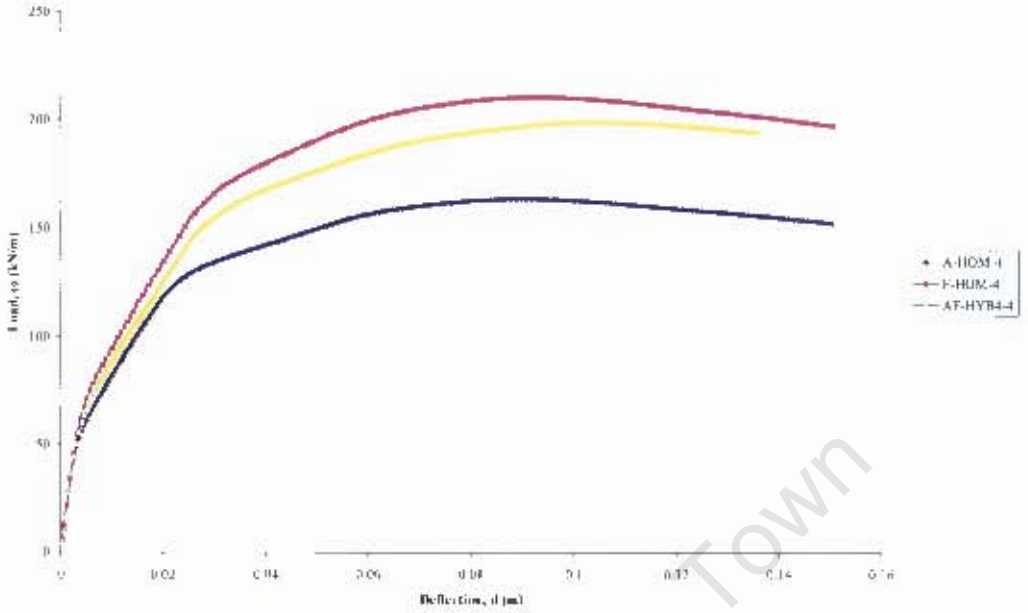

Figure 4.39 Comparison of the Load-Deflection Response between AF-HYB4-4 and Equivalent Homogeneous Sections A-HOM-4 and F-HOM-4

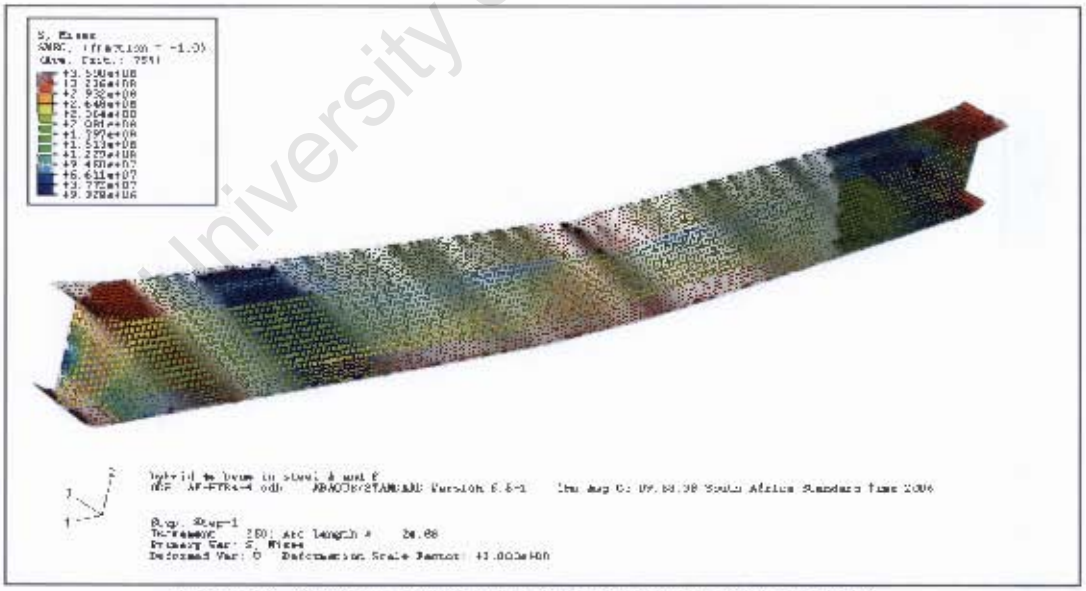

Figure 4.40 Stress Distribution in Hybrid Beam AF-HYB4-4

4.3.2.7 Four Metre Beams with 460MPa Flanges

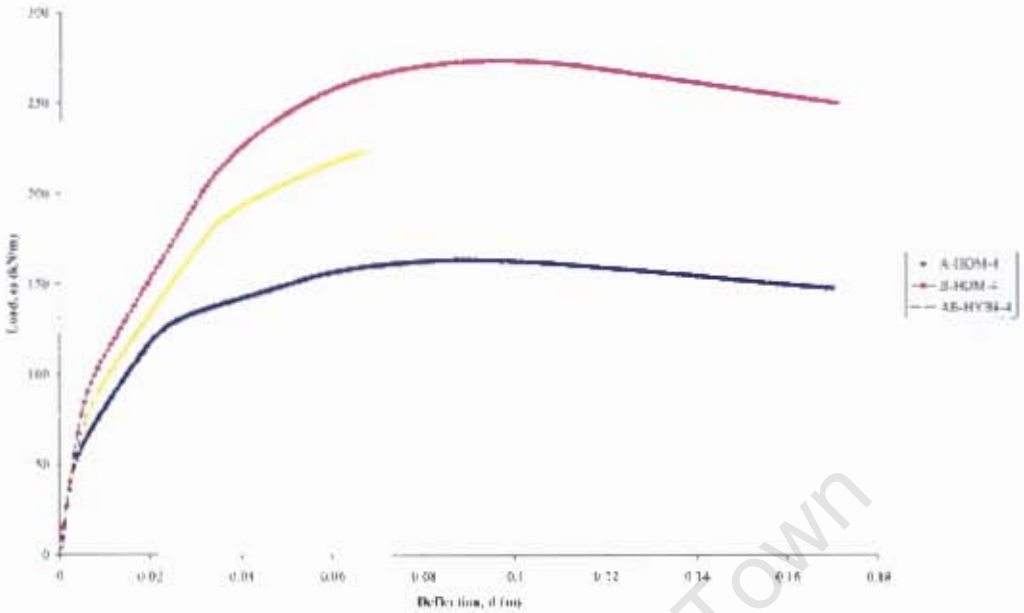

Figure 4.41 Comparison of the Load-Deflection Response between AB-HYB4-4 and Equivalent Homogeneous Sections A-HOM-4 and B-HOM-4

The load-deflection curves for the 4m beams are more rounded in shape. The load decreases gradually with no sudden change in gradient, unlike the typical 2m beam load-deflection curve.

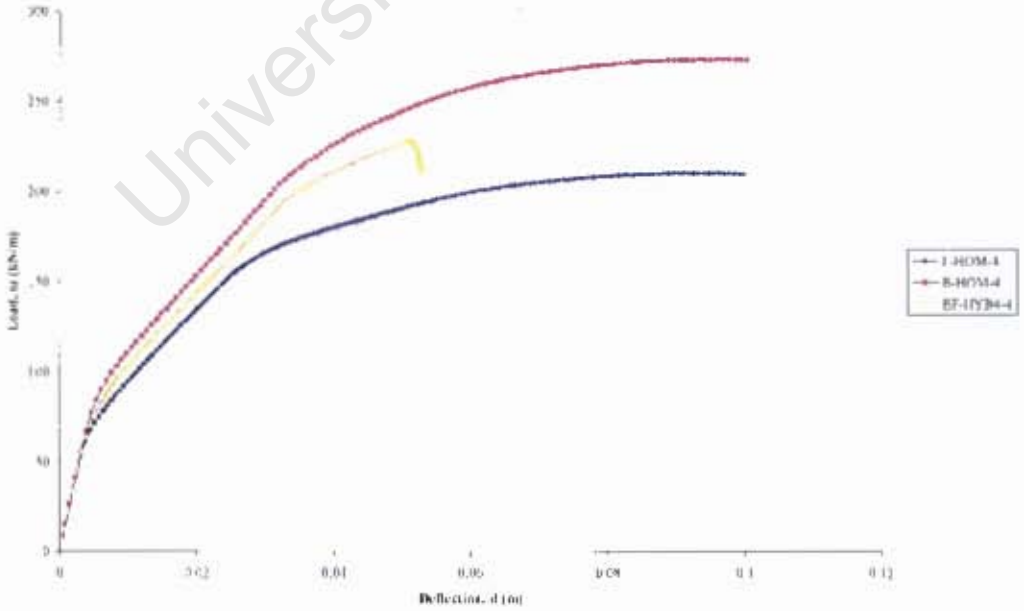

Figure 4.42 Comparison of the Load-Deflection Response between BF-HYB4-4 and Equivalent Homogeneous Sections B-HOM-4 and F-HOM-4

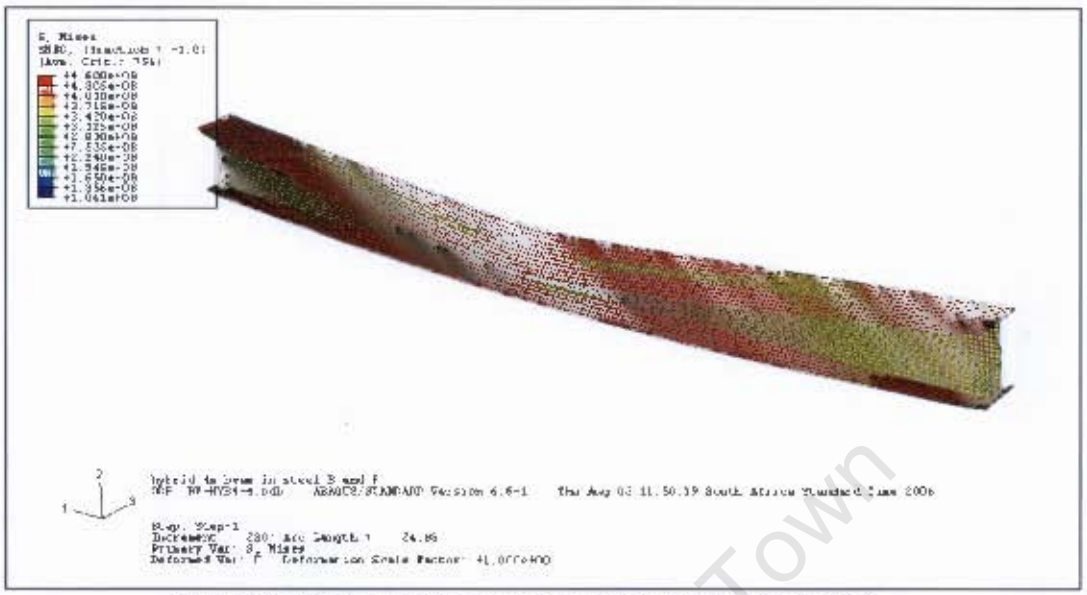

Figure 4.43 Stress Distribution in Hybrid Beam BF-HYB4-4

4.3.2.8 Four Metre Beams with 550MPa Flanges

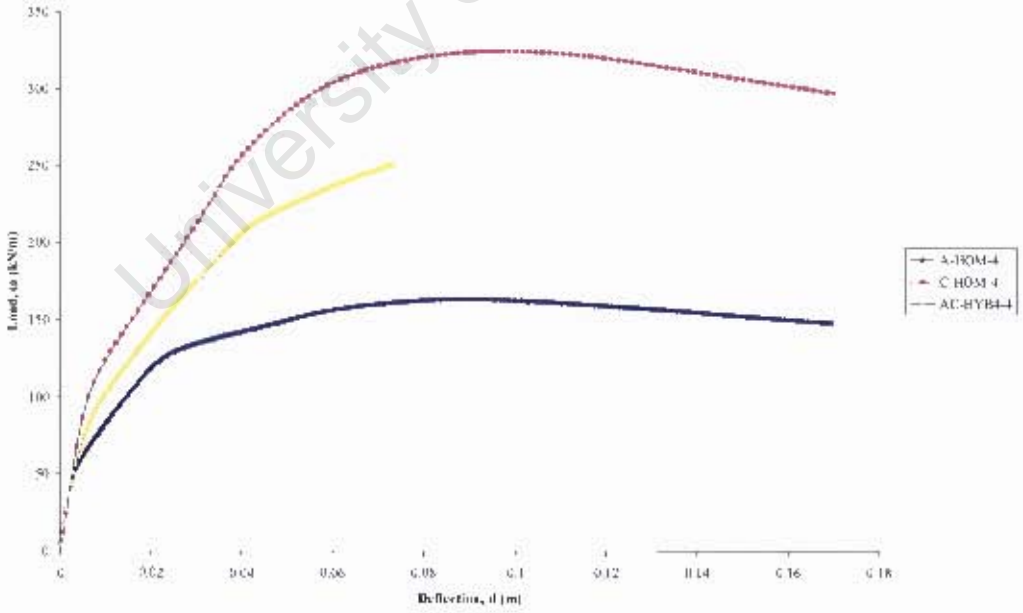

Figure 4.44 Comparison of the Load-Deflection Response between AC-HYB4-4 and Equivalent Homogeneous Sections A-HOM-4 and C-HOM-4

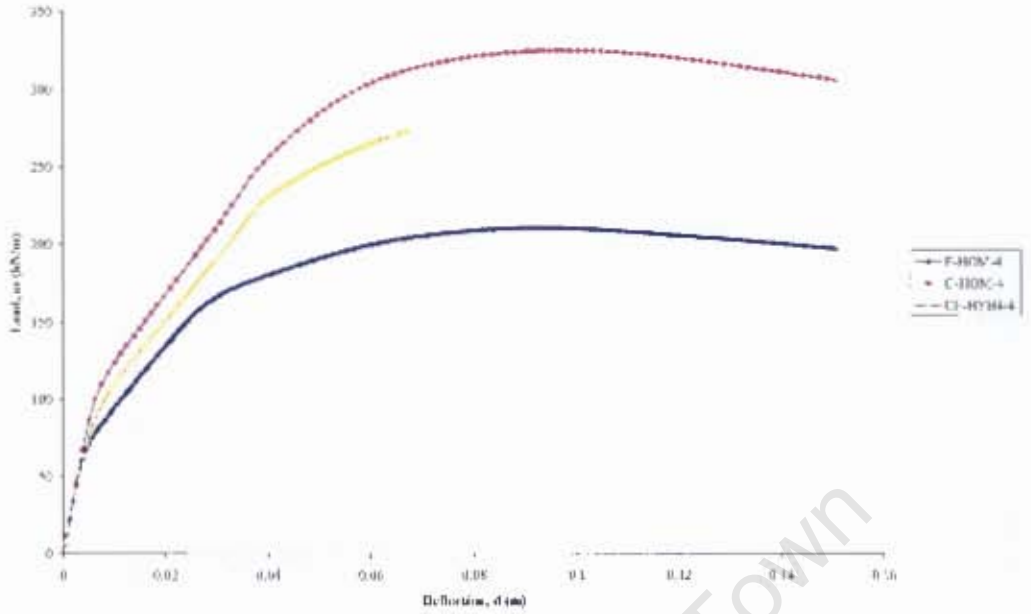

Figure 4.45 Comparison of the Load-Deflection Response between CF-HYB4-4 and Equivalent Homogeneous Sections C-HOM-4 and F-HOM-4

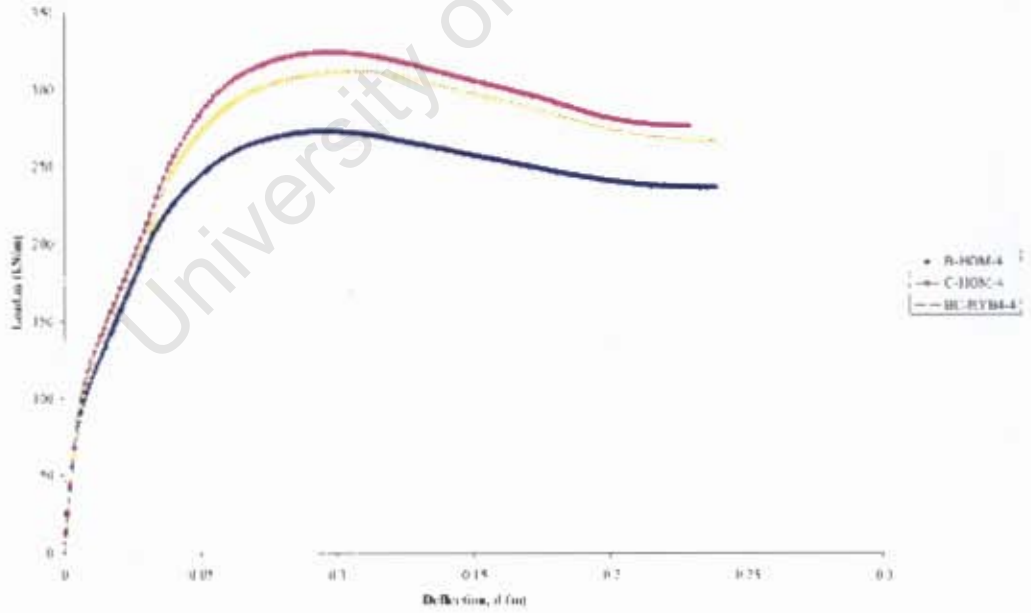

Figure 4.46 Comparison of the Load-Deflection Response between BC-HYB4-4 and Equivalent Homogeneous Sections B-HOM-4 and C-HOM-4

4.3.2.9 Four Metre Beams with 690MPa Flanges

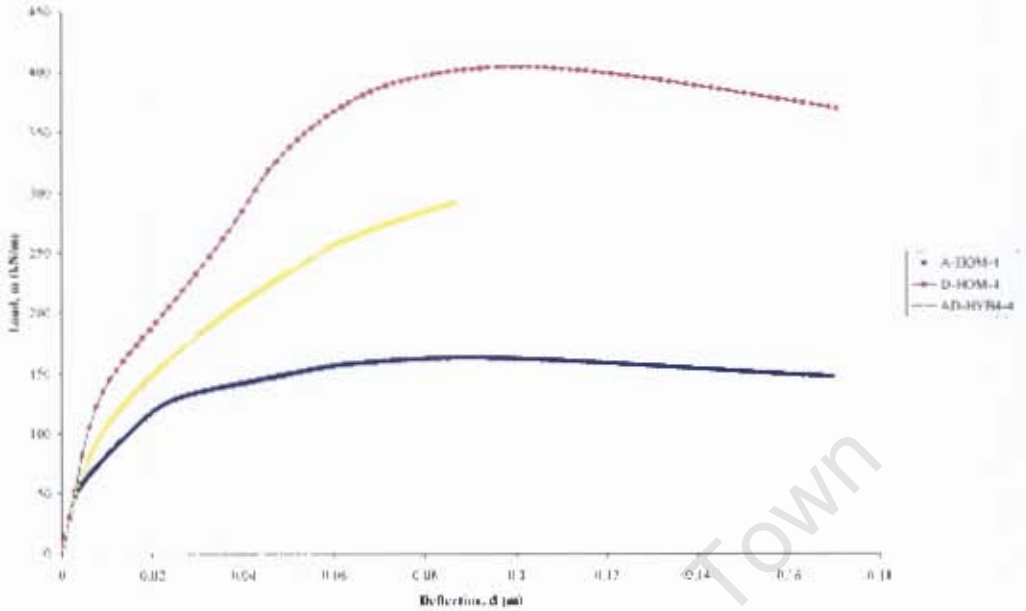

Figure 4.47 Comparison of the Load-Deflection Response between AD-HYB4-4 and Equivalent Homogeneous Sections A-HOM-4 and D-HOM-4

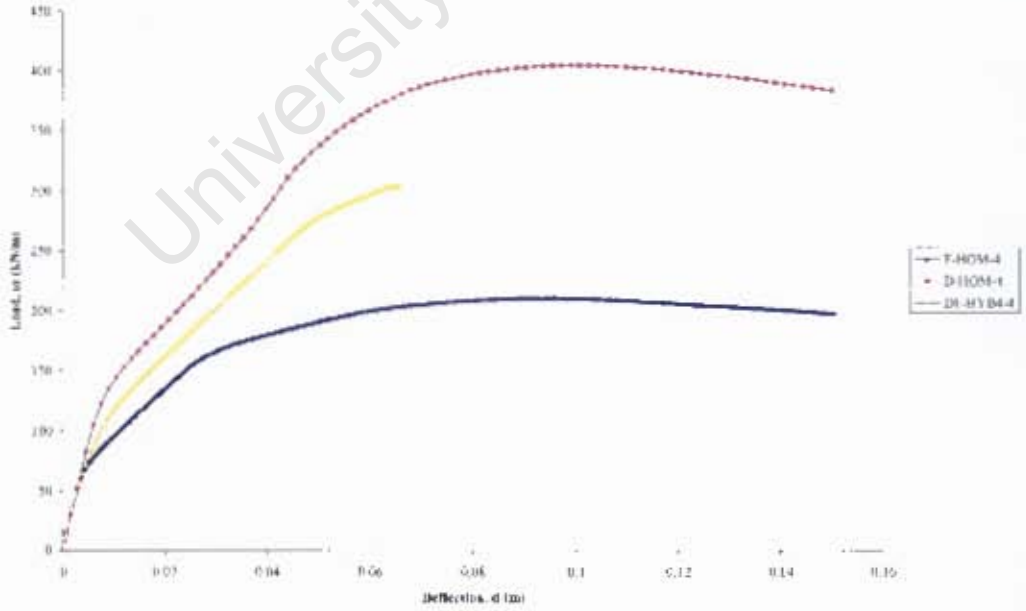

Figure 4.48 Comparison of the Load-Deflection Response between DF-HYB4-4 and Equivalent Homogeneous Sections D-HOM-4 and F-HOM-4

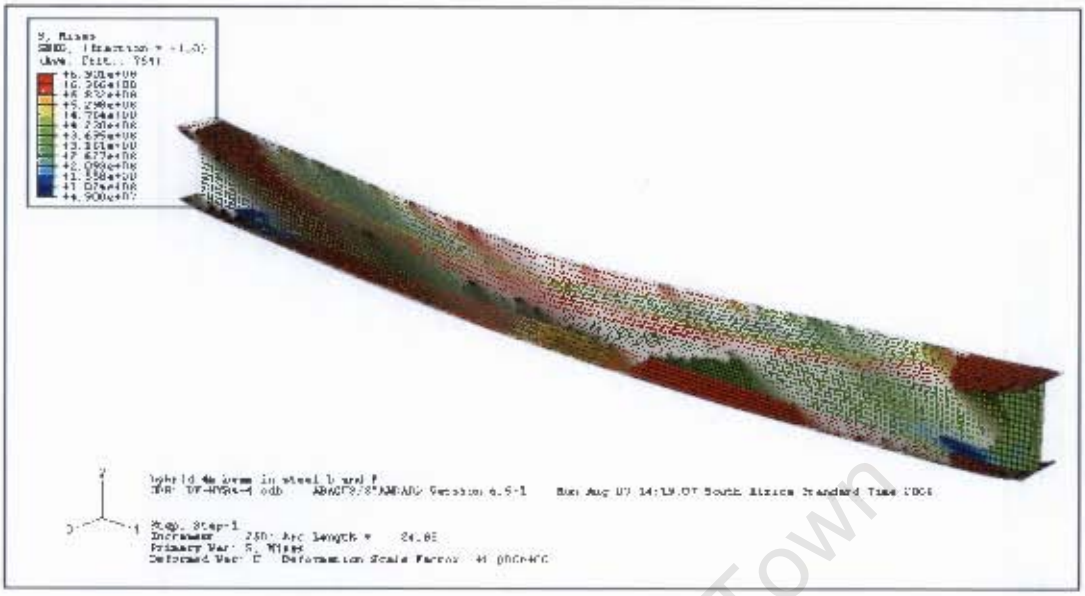

Figure 4.49 Stress Distribution in Hybrid Beam DF-HYB4-4

Beams BF-HYB4-4 and DF-HYB4-4 (Figures 4.43 and 4.49) show a lateral movement of the flange which is atypical of the rest of the beams. Perhaps this may be an indication of some peculiarity in the material data for steel F.

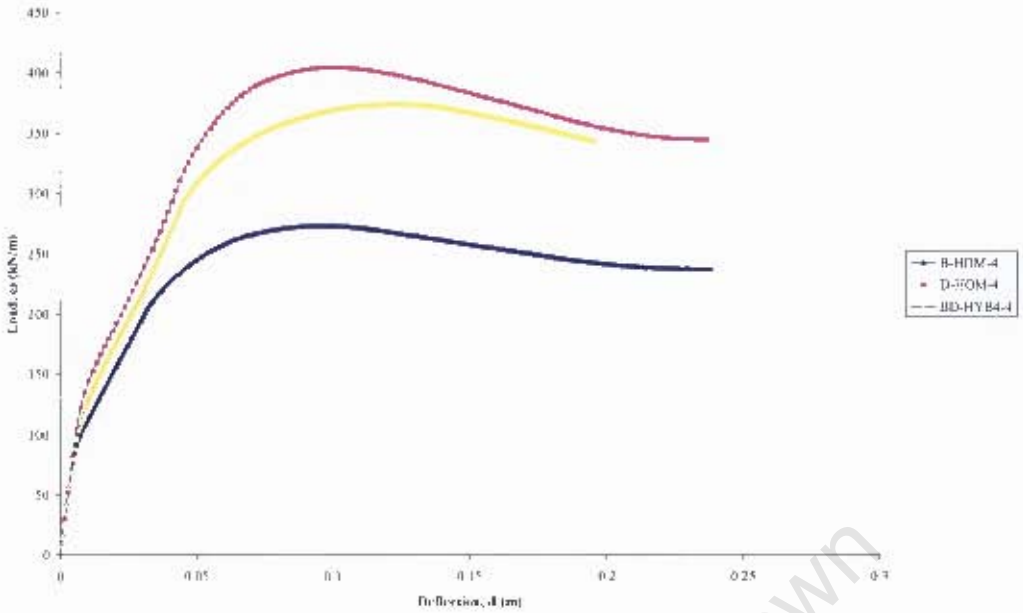

Figure 4.50 Comparison of the Load-Deflection Response between BD-HYB4-4 and Equivalent Homogeneous Sections B-HOM-4 and D-HOM-4

Figure 4.51 Stress Distribution in Hybrid Beam BD-HYB4-4

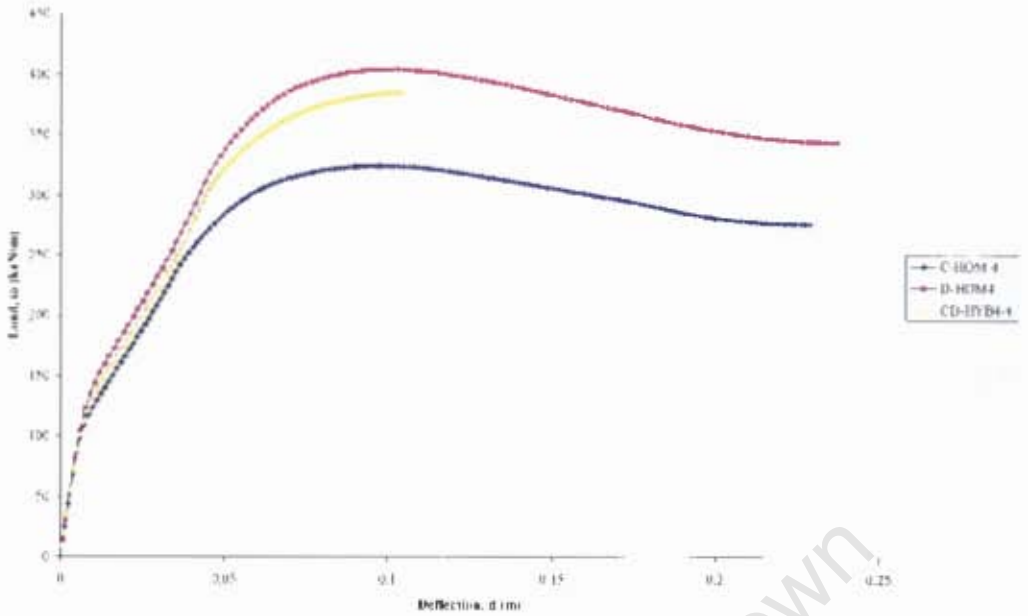

Figure 4.52 Comparison of the Load-Deflection Response between CD-HYB4-4 and Equivalent Homogeneous Sections C-HOM-4 and D-HOM-4

4.3.2.10 Four Metre Beams with 700MPa Flanges

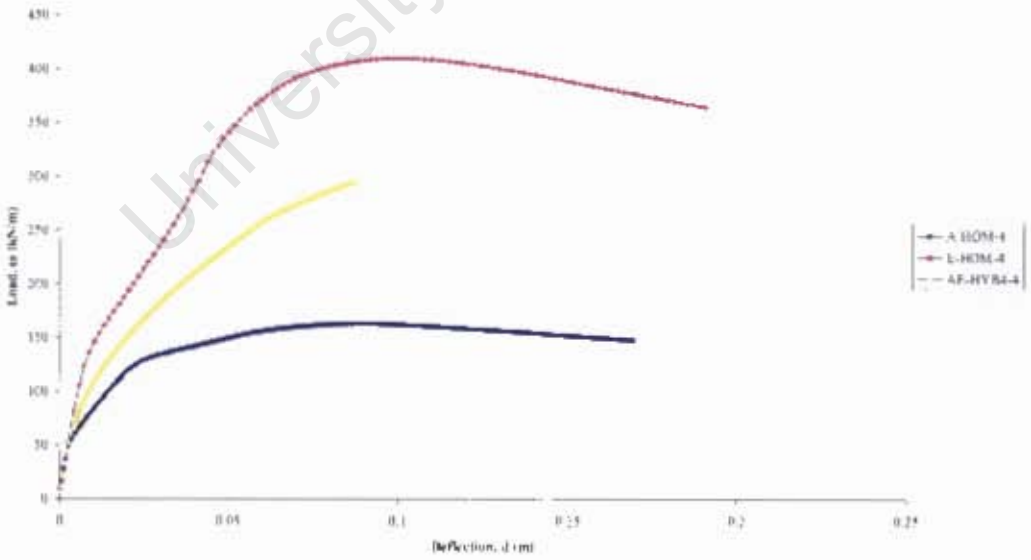

Figure 4.53 Comparison of the Load-Deflection Response between AE-HYB4-4 and Equivalent Homogeneous Sections A-HOM-4 and E-HOM-4

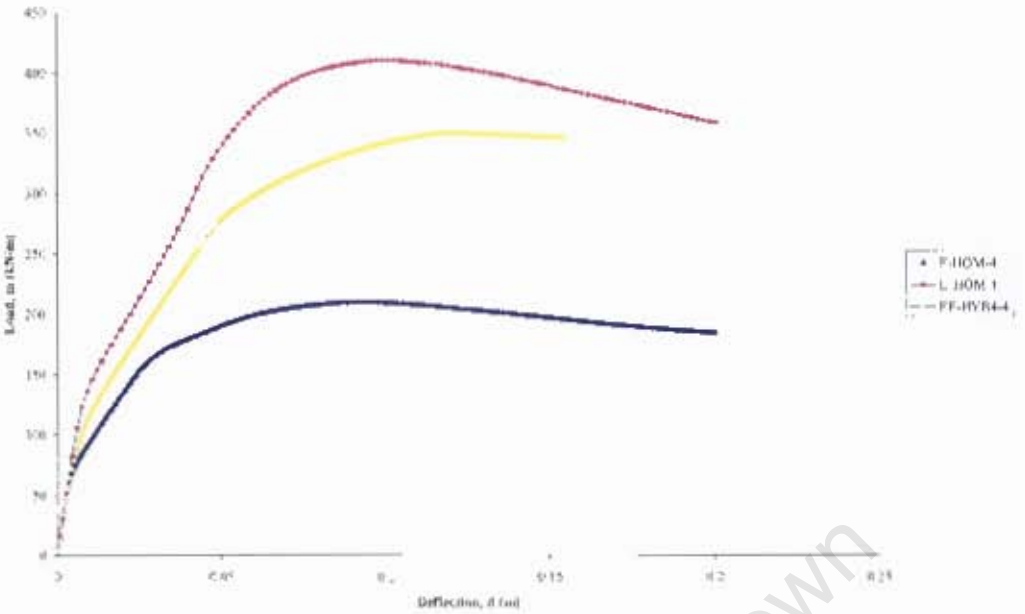

Figure 4.54 Comparison of the Load-Deflection Response between EF-HYB4-4 and Equivalent Homogeneous Sections E-HOM-4 and F-HOM-4

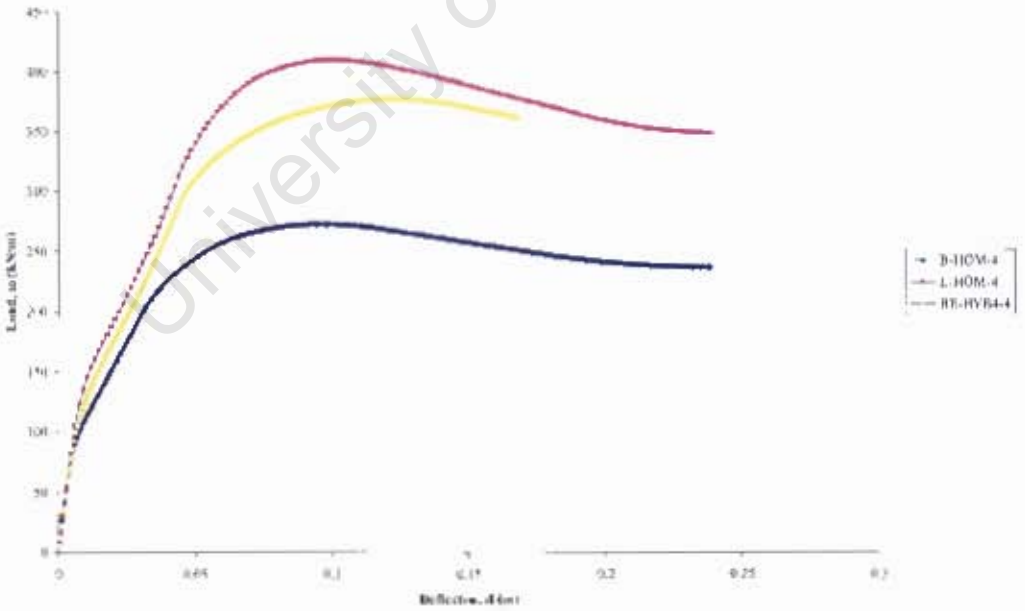

Figure 4.55 Comparison of the Load-Deflection Response between BF-HYB4-4 and Equivalent Homogeneous Sections B-HOM-4 and E-HOM-4

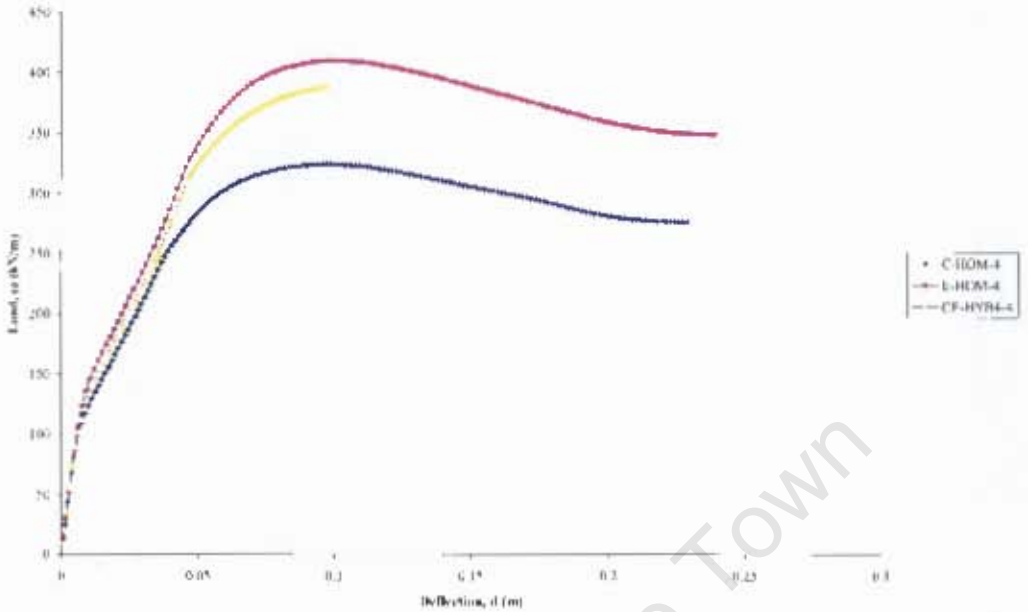

Figure 4.56 Comparison of the Load-Deflection Response between CE-HYB4-4 and Equivalent Homogeneous Sections C-HOM-4 and E-HOM-4

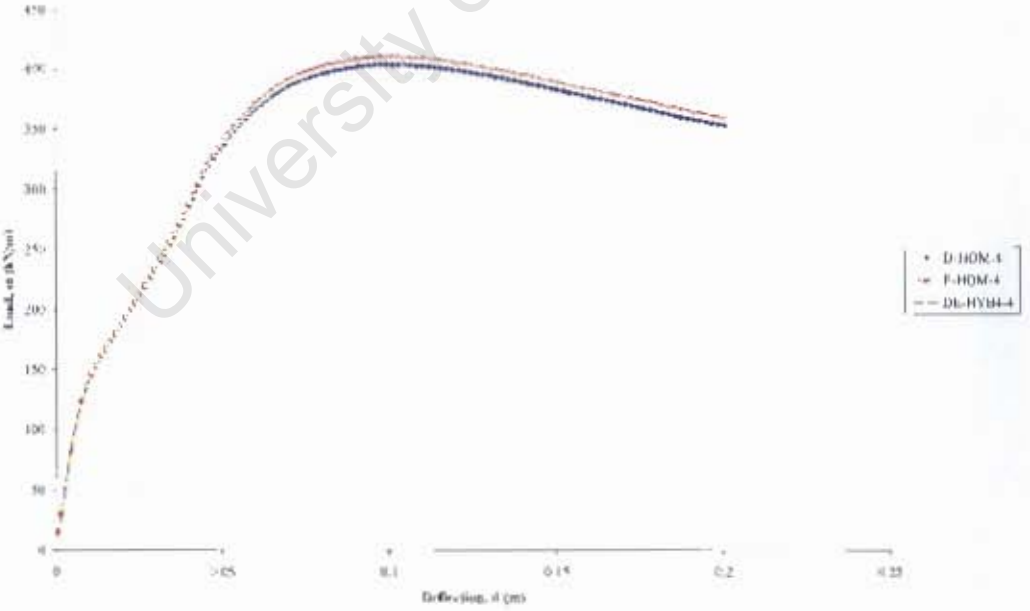

Figure 4.57 Comparison of the Load-Deflection Response between DE-HYB4-4 and Equivalent Homogeneous Sections D-HOM-4 and E-HOM-4

DE-HYB4-4 (Figures 4.57 to 4.59) again does not behave like the usual hybrid beams as yielding begins in the flanges.

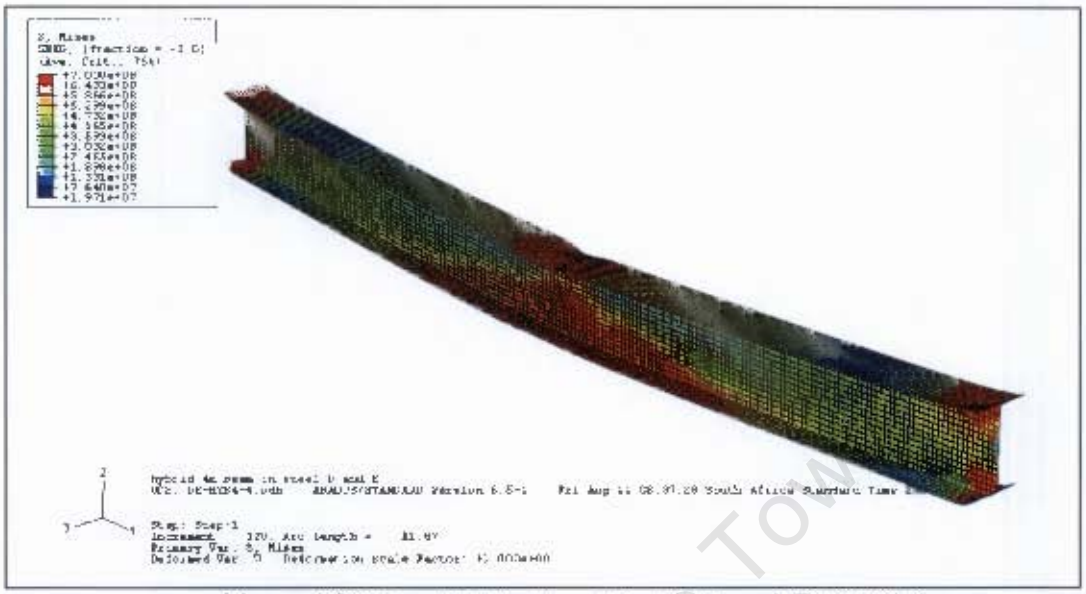

Figure 4.58 Stress Distribution in Hybrid Beam DE-HYB4-4

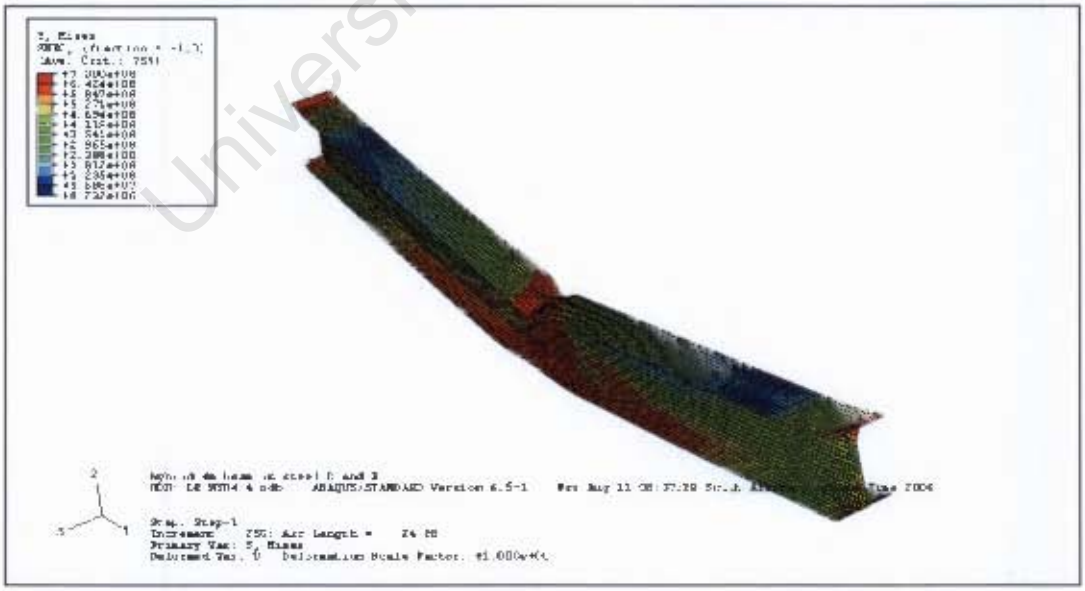

Figure 4.59 Flange Buckling in Hybrid Beam DE-HYB4-4

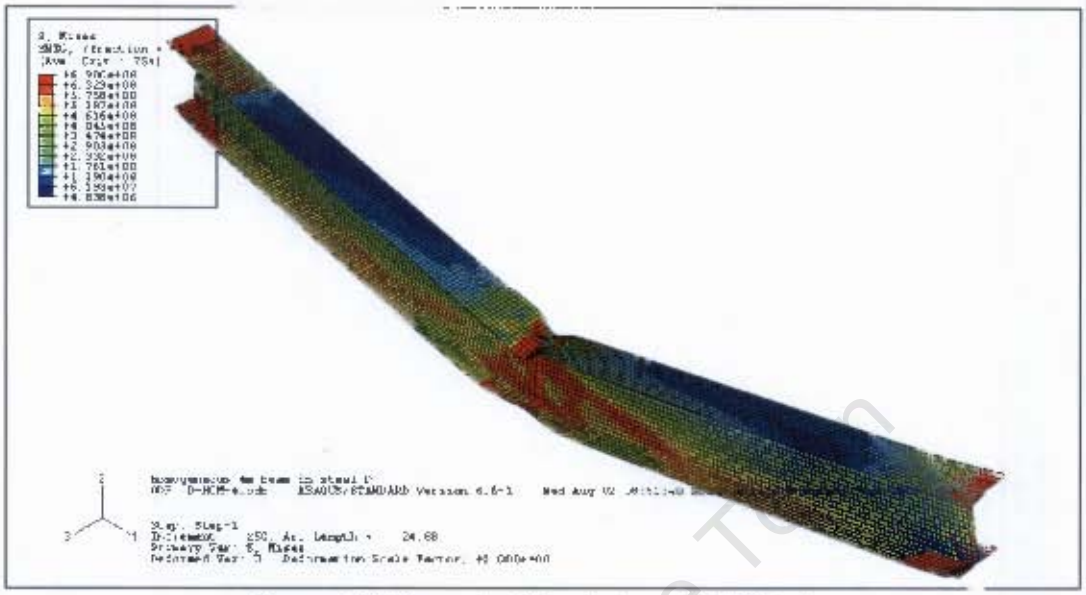

Figure 4.60 Flange Buckling in Beam D-HOM-4

Figure 4.61 Vertical Flange Buckling in Hybrid Beam BC-HYB4-4

At the end of loading, the beams had a distinct V-shape. The formation of the plastic hinges at midspan is facilitated by tension flange yielding over a wide area and buckling of the compression flange.

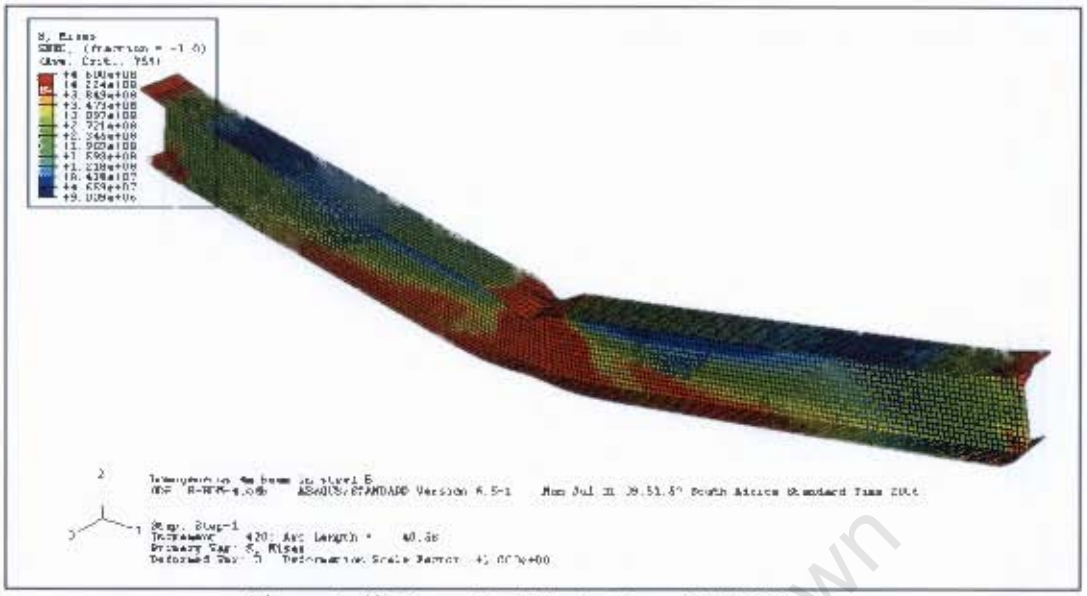

Figure 4.62 Flange Buckling in Beam B-HOM-4

While the 2m beams have widespread yielding of flanges and web over the entire beam, the homogeneous 4m beams have localised regions of material yielding at the centre of the span as shown in Figure 4.60. Vertical flange buckling is also evident. Most of the 4m hybrids have a stress distribution and instability reminiscent of that in the homogeneous 4m beam (e.g. Figure 4.58 and 4.61).

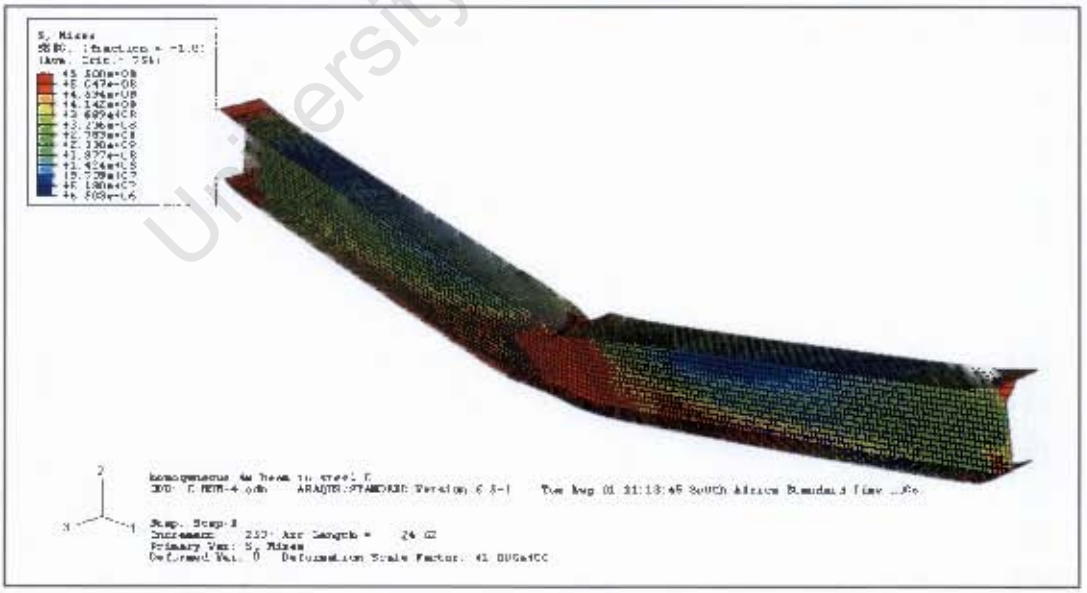

Figure 4.63 Flange Buckling in Beam C-HOM-4

4.3.3 Summary of ABAQUS Results

When the load-deflection response of an unstiffened hybrid beam is plotted against the load-deflection responses of the two parent steels, it is seen that, although the hybrids are not able to carry the same loads as the homogeneous higher strength member, they can still carry far more loading than the homogeneous lower strength member.

One generalisation would be that for the same load, the hybrid will experience larger midspan deflections than the homogeneous beam of the higher strength material. As the web commences to and continues yielding, the effective moment of inertia to resist bending decreases.

While the 2m beams tend to fail by yielding, the 4m beams buckle. In both beam lengths, hybrids with flange and web steels that are close in value show Mises stress distributions and instability resembling those appearing in homogeneous members.

All 2m beams had imperfection seeds introduced into the model in the form of initial displacements of element nodes. These imperfections influenced the progress of the analysis and the subsequent failure of the beams. This is particularly evident in the asymmetrical Mises stress distributions and flange/web displacements of the 2m beams. The 4m beams showed more symmetrical Mises stress distributions as no imperfection seeds were introduced.

4.3.4 Theoretical Numerical Results

The spreadsheets containing calculations of the homogeneous and hybrid yield and plastic moments can be found in Tables 4.11 to 4.13. This information, summarised in Tables 4.14 and 4.15, was then used to construct the moment-curvature plots in Figures 4.64 to 4.93.

Tables 4.14 and 4.15 illustrate the fact that all beams with identical webs, i.e. the same web steel, will have equal web yield moments. In the same token, for all hybrids with the same flange material, the contribution that the flange steel makes at M_{yf} is constant. The remainder of the strength is, therefore, contributed by the web which means M_{yf} increases with increasing web yield stress.

Confirmation that the flange yield moment is a suitable characteristic strength for hybrid beams is given by the fact that the difference (in kNm) between the flange yield moment, M_{yf}, and the plastic moment, M_p, is very small(Tables 4.14 and 4.15). this is especially true for the 2m beams. At the plastic moment the gain in strength from the flange yield is only 3.2% for AE-HYB4-2 and a maximum of 6.5% for BC-HYB4-2. DE-HYB4-2 experiences a strength gain of 8.3% while the homogeneous beams would gain approximately 9.1% more strength at the plastic moment.

Table 4.11 Calculation of Yield and Plastic Moments for Homogeneous Beams

analysis	σ	*bf (m)*	*tf*	*hw*	*tw*	*d*	*I (mm4)*	*Z (mm3)*	*My*
A-HOM-2	248.4	0.2	0.006	0.18	0.005	0.192	23194800	263700	60.016545
F-HOM-2	350	0.2	0.006	0.18	0.005	0.192	23194800	263700	84.564375
B-HOM-2	460	0.2	0.006	0.18	0.005	0.192	23194800	263700	111.14175
C-HOM-2	550	0.2	0.006	0.18	0.005	0.192	23194800	263700	132.886875
D-HOM-2	690	0.2	0.006	0.18	0.005	0.192	23194800	263700	166.712625
E-HOM-2	700	0.2	0.006	0.18	0.005	0.192	23194800	263700	169.12875
A-HOM-4	248.4	0.2	0.01	0.3	0.008	0.32	114133333.3	800000	177.192
F-HOM-4	350	0.2	0.01	0.3	0.008	0.32	114133333.3	800000	249.6666667
B-HOM-4	460	0.2	0.01	0.3	0.008	0.32	114133333.3	800000	328.1333333
C-HOM-4	550	0.2	0.01	0.3	0.008	0.32	114133333.3	800000	392.3333333
D-HOM-4	690	0.2	0.01	0.3	0.008	0.32	114133333.3	800000	492.2
E-HOM-4	700	0.2	0.01	0.3	0.008	0.32	114133333.3	800000	499.3333333

(Continued)

Mp	ρ (at My)	*κ=1/ρ*	ρ (at Mp)	*κ=1/ρ*
65.50308	81.15942029	0.012321429	0.845410628	1.182857143
92.295	57.6	0.017361111	0.6	1.666666667
121.302	43.82608696	0.02281746	0.456521739	2.19047619
145.035	36.65454545	0.027281746	0.381818182	2.619047619
181.953	29.2173913	0.03422619	0.304347826	3.285714286
184.59	28.8	0.034722222	0.3	3.333333333
198.72	135.2657005	0.007392857	0.845410628	1.182857143
280	96	0.010416667	0.6	1.666666667
368	73.04347826	0.013690476	0.456521739	2.19047619
440	61.09090909	0.016369048	0.381818182	2.619047619
552	48.69565217	0.020535714	0.304347826	3.285714286
560	48	0.020833333	0.3	3.333333333

Table 4.12 Calculation of Flange Yield and Plastic Moments for 2m Hybrid Beams

analysis	*σf (Mpa)*	*σf bottom*	*σw*	*el. Core*	*trap. Cent.*	*A1*	*A2*	*A3*	*y1*
AE-HYB4-2	700	656.25	248.4	0.034066286	0.002967742	1200	279.6685714	170.3314286	0.186064516
EF-HYB4-2	700	656.25	350	0.048	0.002967742	1200	210	240	0.186064516
BE-HYB4-2	700	656.25	460	0.063085714	0.002967742	1200	134.5714286	315.4285714	0.186064516
CE-HYB4-2	700	656.25	550	0.075428571	0.002967742	1200	72.85714286	377.1428571	0.186064516
AD-HYB4-2	690	646.875	248.4	0.03456	0.002967742	1200	277.2	172.8	0.186064516
DF-HYB4-2	690	646.875	350	0.048695652	0.002967742	1200	206.5217391	243.4782609	0.186064516
BD-HYB4-2	690	646.875	460	0.064	0.002967742	1200	130	320	0.186064516
CD-HYB4-2	690	646.875	550	0.076521739	0.002967742	1200	67.39130435	382.6086957	0.186064516
AC-HYB4-2	550	515.625	248.4	0.043357091	0.002967742	1200	233.2145455	216.7854545	0.186064516
CF-HYB4-2	550	515.625	350	0.061090909	0.002967742	1200	144.5454545	305.4545455	0.186064516
BC-HYB4-2	550	515.625	460	0.080290909	0.002967742	1200	48.54545455	401.4545455	0.186064516
AB-HYB4-2	460	431.25	248.4	0.05184	0.002967742	1200	190.8	259.2	0.186064516
BF-HYB4-2	460	431.25	350	0.073043478	0.002967742	1200	84.7826087	365.2173913	0.186064516
AF-HYB4-2	350	328.125	248.4	0.068132571	0.002967742	1200	109.3371429	340.6628571	0.186064516

(Continued)

y2	*y3*	*c1*	*c2*	*c3*	*Myf*	*Mp*	ρ (at Myf)	*κ=1/ρ*	ρ (at Mp)
0.124066286	0.045421714	813.75	69.46967314	21.15516343	160.9897481	166.3002	28.8	0.034722222	0.845410628
0.138	0.064	813.75	73.5	42	164.241	170.415	28.8	0.034722222	0.6
0.153085714	0.084114286	813.75	61.90285714	72.54857143	166.9888144	174.87	28.8	0.034722222	0.456521739
0.165428571	0.100571429	813.75	40.07142857	103.7142857	168.4696531	178.515	28.8	0.034722222	0.381818182
0.12456	0.04608	802.125	68.85648	21.46176	158.812721	164.0682	29.2173913	0.03422619	0.845410628
0.138695652	0.064927536	802.125	72.2826087	42.60869565	162.0387612	168.183	29.2173913	0.03422619	0.6
0.154	0.085333333	802.125	59.8	73.6	164.7367333	172.638	29.2173913	0.03422619	0.456521739
0.166521739	0.102028986	802.125	37.06521739	105.2173913	166.1543882	176.283	29.2173913	0.03422619	0.381818182
0.133357091	0.057809455	639.375	57.93049309	26.92475345	128.2469473	132.8202	36.65454545	0.027281746	0.845410628
0.151090909	0.081454545	639.375	50.59090909	53.45454545	130.9629421	136.935	36.65454545	0.027281746	0.6
0.170290909	0.107054545	639.375	22.33090909	92.33454545	132.6525836	141.39	36.65454545	0.027281746	0.456521739
0.14184	0.06912	534.75	47.39472	32.19264	108.4456224	112.7322	43.82608696	0.02281746	0.845410628
0.163043478	0.097391304	534.75	29.67391304	63.91304348	110.5607127	116.847	43.82608696	0.02281746	0.6
0.158132571	0.090843429	406.875	27.15934629	42.31032686	83.84339242	88.1802	57.6	0.017361111	0.845410628

(Continued)

κ=1/ρ	σf top	e. core	trap centre	area 1	area3	lever 1	lever3	ce 1	ce 3
1.182857143	264.96	0.09	0.002967742	1200	450	0.186064516	0.12	308.016	55.89
1.666666667	373.3333333	0.09	0.002967742	1200	450	0.186064516	0.12	434	78.75
2.19047619	490.6666667	0.09	0.002967742	1200	450	0.186064516	0.12	570.4	103.5
2.619047619	586.6666667	0.09	0.002967742	1200	450	0.186064516	0.12	682	123.75
1.182857143	264.96	0.09	0.002967742	1200	450	0.186064516	0.12	308.016	55.89
1.666666667	373.3333333	0.09	0.002967742	1200	450	0.186064516	0.12	434	78.75
2.19047619	490.6666667	0.09	0.002967742	1200	450	0.186064516	0.12	570.4	103.5
2.619047619	586.6666667	0.09	0.002967742	1200	450	0.186064516	0.12	682	123.75
1.182857143	264.96	0.09	0.002967742	1200	450	0.186064516	0.12	308.016	55.89
1.666666667	373.3333333	0.09	0.002967742	1200	450	0.186064516	0.12	434	78.75
2.19047619	490.6666667	0.09	0.002967742	1200	450	0.186064516	0.12	570.4	103.5
1.182857143	264.96	0.09	0.002967742	1200	450	0.186064516	0.12	308.016	55.89
1.666666667	373.3333333	0.09	0.002967742	1200	450	0.186064516	0.12	434	78.75
1.182857143	264.96	0.09	0.002967742	1200	450	0.186064516	0.12	308.016	55.89

(Continued)

Myw	ρ (at Myw)	κ=1/ρ
64.017648	76.0869565	0.01314286
90.202	54	0.01851852
118.5512	41.0869565	0.02433862
141.746	34.3636364	0.02910053
64.017648	76.0869565	0.01314286
90.202	54	0.01851852
118.5512	41.0869565	0.02433862
141.746	34.3636364	0.02910053
64.017648	76.0869565	0.01314286
90.202	54	0.01851852
118.5512	41.0869565	0.02433862
64.017648	76.0869565	0.01314286
90.202	54	0.01851852
64.017648	76.0869565	0.01314286

Table 4.13 Calculation of Flange Yield and Plastic Moments for 4m Hybrid Beams

analysis	*σf (Mpa)*	*σf bottom*	*σw*	*el. Core*	*trap. Cent.*	*A1*	*A2*	*A3*	*y1*
AE-HYB4-4	700	656.25	248.4	0.056777143	0.004946237	2000	745.7828571	454.2171429	0.310107527
EF-HYB4-4	700	656.25	350	0.08	0.004946237	2000	560	640	0.310107527
BE-HYB4-4	700	656.25	460	0.105142857	0.004946237	2000	358.8571429	841.1428571	0.310107527
CE-HYB4-4	700	656.25	550	0.125714286	0.004946237	2000	194.2857143	1005.714286	0.310107527
AD-HYB4-4	690	646.875	248.4	0.0576	0.004946237	2000	739.2	460.8	0.310107527
DF-HYB4-4	690	646.875	350	0.08115942	0.004946237	2000	550.7246377	649.2753623	0.310107527
BD-HYB4-4	690	646.875	460	0.106666667	0.004946237	2000	346.6666667	853.3333333	0.310107527
CD-HYB4-4	690	646.875	550	0.127536232	0.004946237	2000	179.7101449	1020.289855	0.310107527
AC-HYB4-4	550	515.625	248.4	0.072261818	0.004946237	2000	621.9054545	578.0945455	0.310107527
CF-HYB4-4	550	515.625	350	0.101818182	0.004946237	2000	385.4545455	814.5454545	0.310107527
BC-HYB4-4	550	515.625	460	0.133818182	0.004946237	2000	129.4545455	1070.545455	0.310107527
AB-HYB4-4	460	431.25	248.4	0.0864	0.004946237	2000	508.8	691.2	0.310107527
BF-HYB4-4	460	431.25	350	0.12173913	0.004946237	2000	226.0869565	973.9130435	0.310107527
AF-HYB4-4	350	328.125	248.4	0.113554286	0.004946237	2000	291.5657143	908.4342857	0.310107527

(Continued)

y2	*y3*	*c1*	*c2*	*c3*	*Myf*	*Mp*	ρ (at Myf)	*κ=1/ρ*	ρ (at Mp)
0.206777143	0.075702857	1356.25	185.2524617	56.41376914	463.1599916	478.712	48	0.020833333	0.845410628
0.23	0.106666667	1356.25	196	112	477.61	497	48	0.020833333	0.6
0.255142857	0.140190476	1356.25	165.0742857	193.4628571	489.8225083	516.8	48	0.020833333	0.456521739
0.275714286	0.167619048	1356.25	106.8571429	276.5714286	496.4040136	533	48	0.020833333	0.381818182
0.2076	0.0768	1336.875	183.61728	57.23136	457.0893158	472.512	48.69565217	0.020535714	0.845410628
0.23115942	0.10821256	1336.875	192.7536232	113.6231884	471.4272719	490.8	48.69565217	0.020535714	0.6
0.256666667	0.142222222	1336.875	159.4666667	196.2666667	483.4182593	510.6	48.69565217	0.020535714	0.456521739
0.277536232	0.170048309	1336.875	98.84057971	280.5797101	489.7189473	526.8	48.69565217	0.020535714	0.381818182
0.222261818	0.096349091	1065.625	154.4813149	71.79934255	371.7114326	385.712	61.09090909	0.016369048	0.845410628
0.251818182	0.135757576	1065.625	134.9090909	142.5454545	383.7825207	404	61.09090909	0.016369048	0.6
0.283818182	0.178424242	1065.625	59.54909091	246.2254545	391.2920382	423.8	61.09090909	0.016369048	0.456521739
0.2364	0.1152	891.25	126.38592	85.84704	316.1505438	329.912	73.04347826	0.013690476	0.845410628
0.27173913	0.162318841	891.25	79.13043478	170.4347826	325.5509452	348.2	73.04347826	0.013690476	0.6
0.263554286	0.151405714	678.125	72.42492343	112.8275383	246.4622997	261.712	96	0.010416667	0.845410628

(Continued)

κ=1/ρ	σf top	e. core	trap centre	area 1	area3	lever 1	lever3	ce 1	ce 3
1.182857143	264.96	0.15	0.004946237	2000	1200	0.310107527	0.2	513.36	149.04
1.666666667	373.3333333	0.15	0.004946237	2000	1200	0.310107527	0.2	723.3333333	210
2.19047619	490.6666667	0.15	0.004946237	2000	1200	0.310107527	0.2	950.6666667	276
2.619047619	586.6666667	0.15	0.004946237	2000	1200	0.310107527	0.2	1136.666667	330
1.182857143	264.96	0.15	0.004946237	2000	1200	0.310107527	0.2	513.36	149.04
1.666666667	373.3333333	0.15	0.004946237	2000	1200	0.310107527	0.2	723.3333333	210
2.19047619	490.6666667	0.15	0.004946237	2000	1200	0.310107527	0.2	950.6666667	276
2.619047619	586.6666667	0.15	0.004946237	2000	1200	0.310107527	0.2	1136.666667	330
1.182857143	264.96	0.15	0.004946237	2000	1200	0.310107527	0.2	513.36	149.04
1.666666667	373.3333333	0.15	0.004946237	2000	1200	0.310107527	0.2	723.3333333	210
2.19047619	490.6666667	0.15	0.004946237	2000	1200	0.310107527	0.2	950.6666667	276
1.182857143	264.96	0.15	0.004946237	2000	1200	0.310107527	0.2	513.36	149.04
1.666666667	373.3333333	0.15	0.004946237	2000	1200	0.310107527	0.2	723.3333333	210
1.182857143	264.96	0.15	0.004946237	2000	1200	0.310107527	0.2	513.36	149.04

(Continued)

Myw	ρ (at Myw)	κ=1/ρ
189.0048	126.811594	0.00788571
266.3111111	90	0.01111111
350.0088889	68.4782609	0.01460317
418.4888889	57.2727273	0.01746032
189.0048	126.811594	0.00788571
266.3111111	90	0.01111111
350.0088889	68.4782609	0.01460317
418.4888889	57.2727273	0.01746032
189.0048	126.811594	0.00788571
266.3111111	90	0.01111111
350.0088889	68.4782609	0.01460317
189.0048	126.811594	0.00788571
266.3111111	90	0.01111111
189.0048	126.811594	0.00788571

Table 4.14 Summary of Analytical Hybrid Moments for 2m Beams

Analysis	M^{I}_{yw} (kNm)	M^{I}_{yf} (kNm)	M^{I}_{p} (kNm)
AE-HYB4-2	64.0	161.0	166.3
EF-HYB4-2	90.2	164.2	170.4
BE-HYB4-2	118.6	167.0	174.9
CE-HYB4-2	141.7	168.5	178.5
AD-HYB4-2	64.0	158.8	164.1
DF-HYB4-2	90.2	162.0	168.2
BD-HYB4-2	118.6	164.7	172.6
CD-HYB4-2	141.7	166.2	176.3
AC-HYB4-2	64.0	128.2	132.8
CF-HYB4-2	90.2	131.0	136.9
BC-HYB4-2	118.6	132.7	141.4
AB-HYB4-2	64.0	108.4	112.7
BF-HYB4-2	90.2	110.6	116.8
AF-HYB4-2	64.0	83.8	88.2
DE-HYB4-2	-	170.0	184.2

[1] All moments calculated at the centre of the span

Table 4.15 Summary of Analytical Hybrid Moments for 4m Beams

Analysis	M^{I}_{yw} (kNm)	M^{I}_{yf} (kNm)	M^{I}_{p} (kNm)
AE-HYB4-4	189.0	463.2	478.7
EF-HYB4-4	266.3	477.6	497.0
BE-HYB4-4	350.0	489.8	516.8
CE-HYB4-4	418.5	496.4	533.0
AD-HYB4-4	189.0	457.1	472.5
DF-HYB4-4	266.3	471.49	490.8
BD-HYB4-4	350.0	483.4	510.6
CD-HYB4-4	418.5	489.73	526.8
AC-HYB4-4	189.0	371.7	385.7
CF-HYB4-4	266.3	383.8	404.0
BC-HYB4-4	350.0	391.3	423.8
AB-HYB4-4	189.0	316.2	329.9
BF-HYB4-4	266.3	325.6	348.2
AF-HYB4-4	189.0	246.5	261.7
DE-HYB4-4	-	503.4	558.2

[1] All moments calculated at the centre of the span

4.3.4.1 Two Metre Beams with 350MPa Flanges

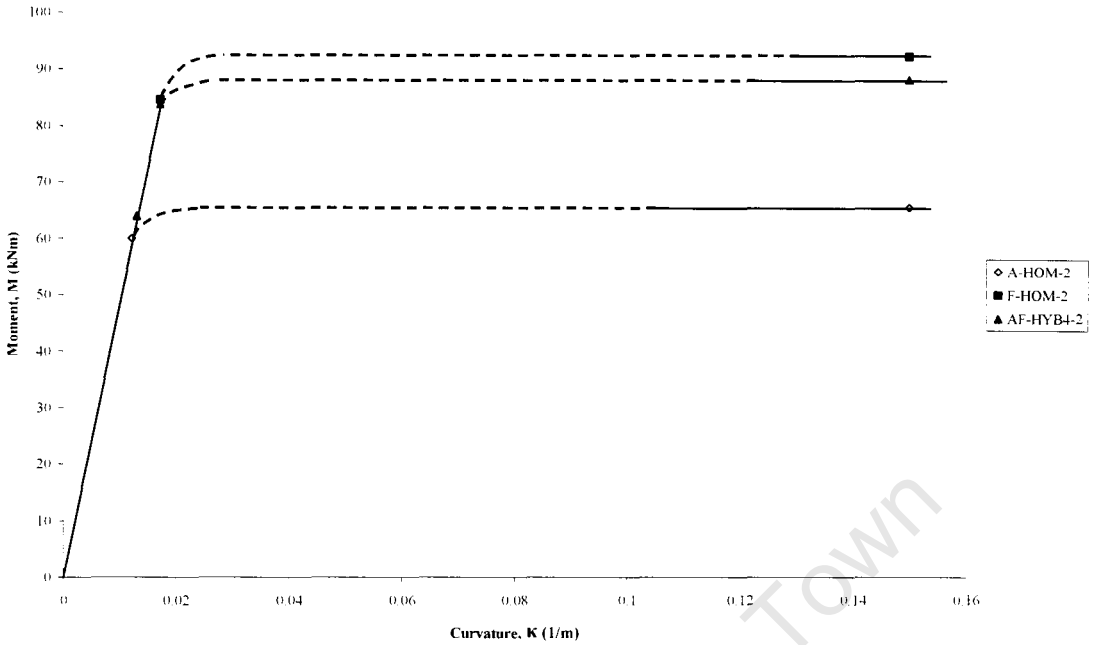

Figure 4.64 Comparison of Analytical Results for the Moment-Curvature Response of AF-HYB4-2 and Equivalent Homogeneous Sections A-HOM-2 and F-HOM-2

4.3.4.2 Two Metre Beams with 460MPa Flanges

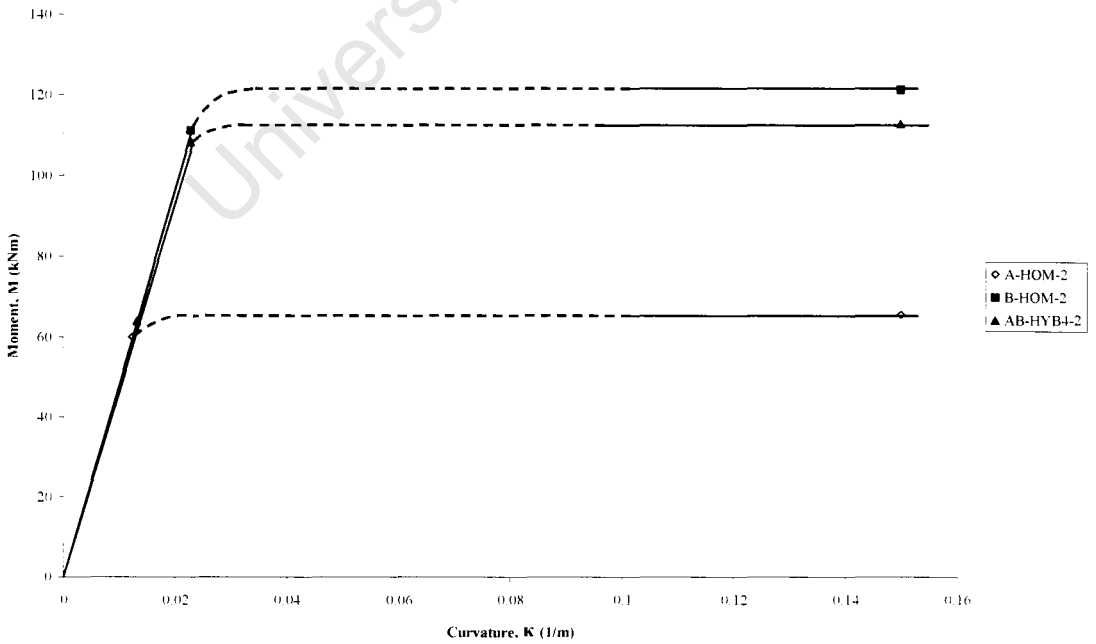

Figure 4.65 Comparison of Analytical Results for the Moment-Curvature Response of AB-HYB4-2 and Equivalent Homogeneous Sections A-HOM-2 and B-HOM-2

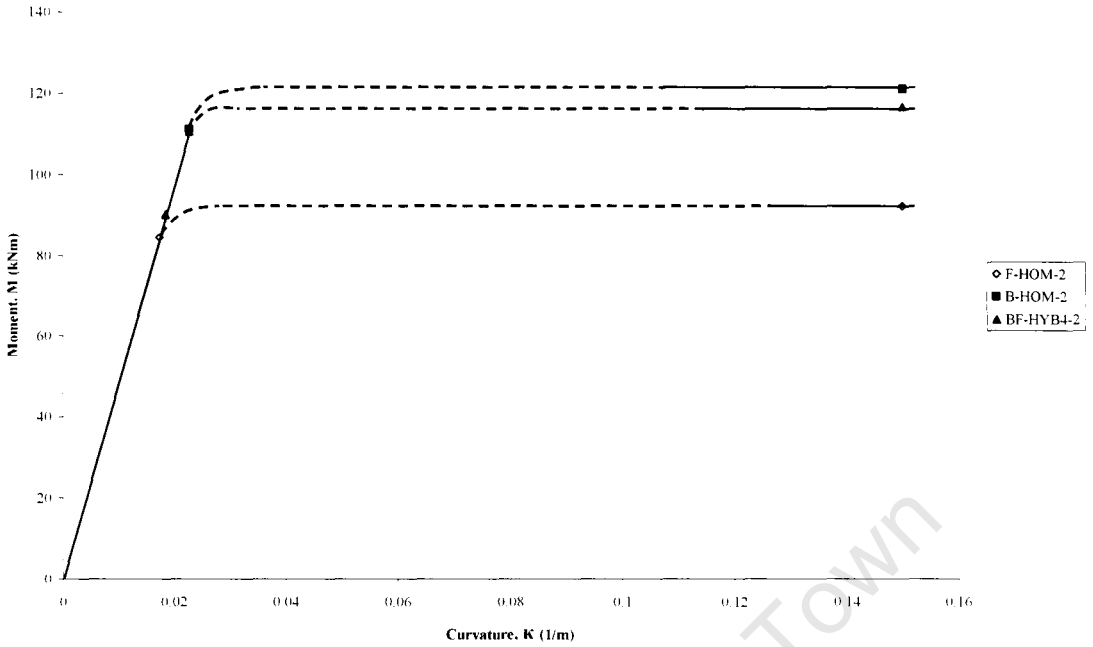

Figure 4.66 Comparison of Analytical Results for the Moment-Curvature Response of BF-HYB4-2 and Equivalent Homogeneous Sections B-HOM-2 and F-HOM-2

4.3.4.3 Two Metre Beams with 550MPa Flanges

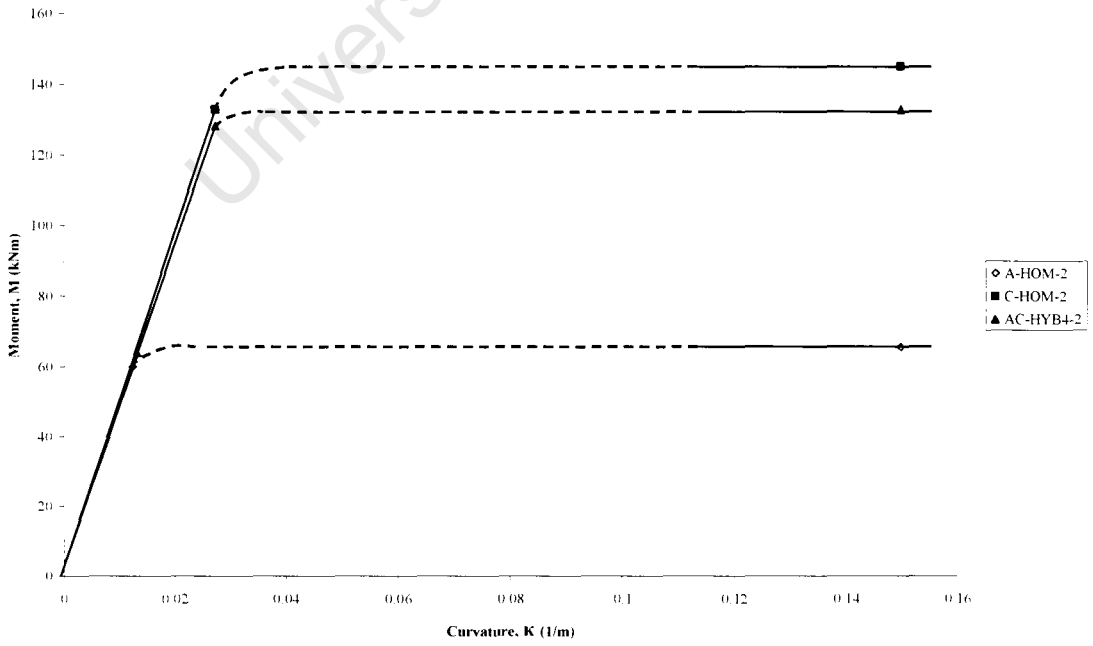

Figure 4.67 Comparison of Analytical Results for the Moment-Curvature Response of AC-HYB4-2 and Equivalent Homogeneous Sections A-HOM-2 and C-HOM-2

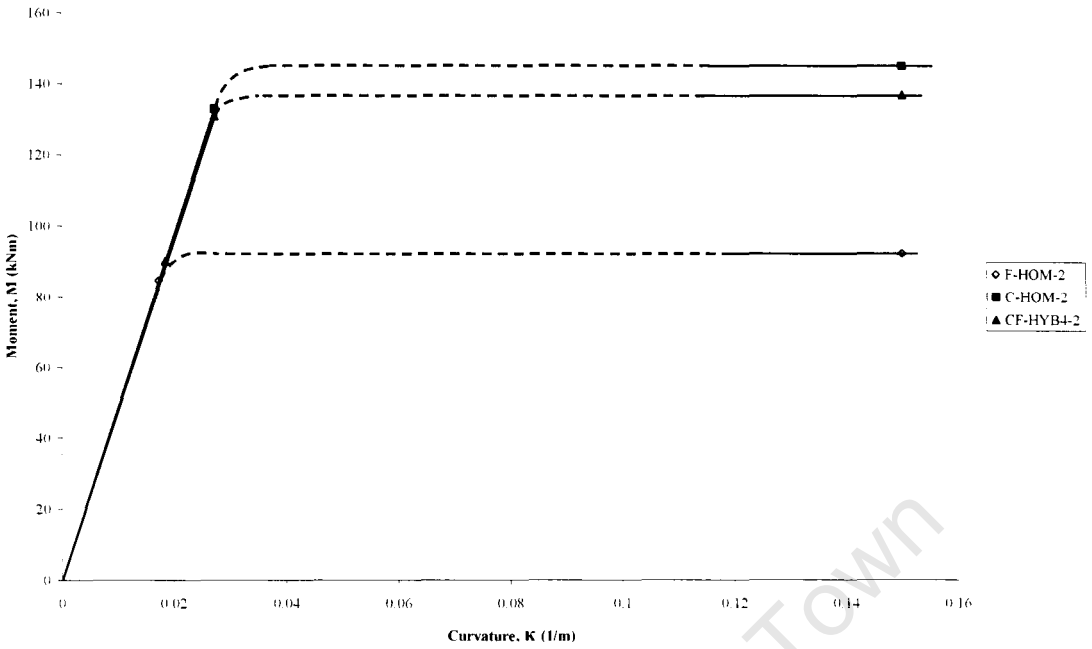

Figure 4.68 Comparison of Analytical Results for the Moment-Curvature Response of CF-HYB4-2 and Equivalent Homogeneous Sections C-HOM-2 and F-HOM-2

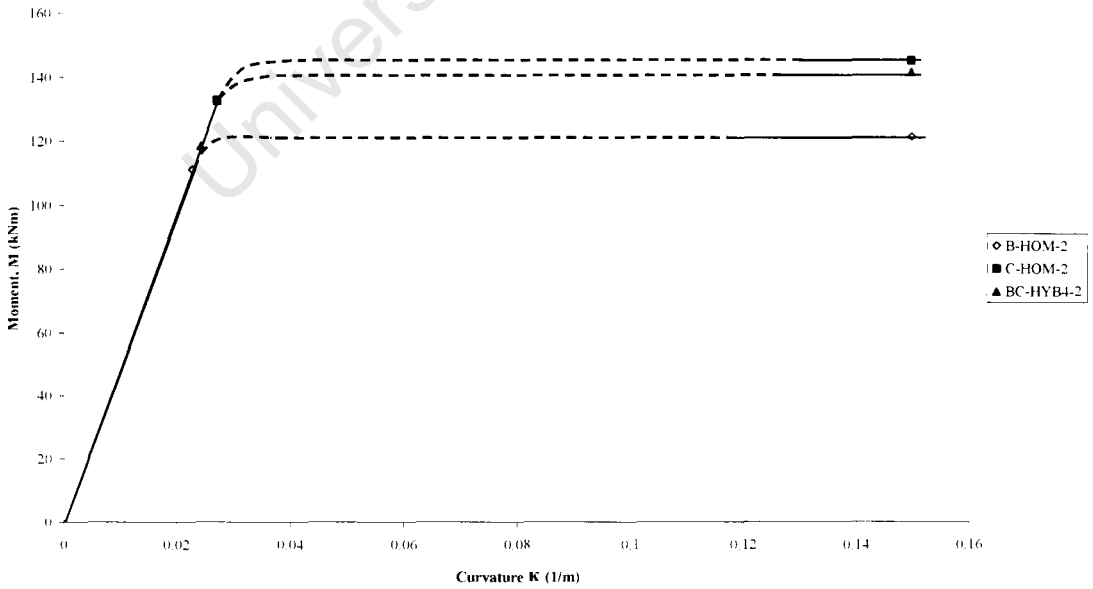

Figure 4.69 Comparison of Analytical Results for the Moment-Curvature Response of BC-HYB4-2 and Equivalent Homogeneous Sections B-HOM-2 and C-HOM-2

4.3.4.4 Two Metre Beams with 690MPa Flanges

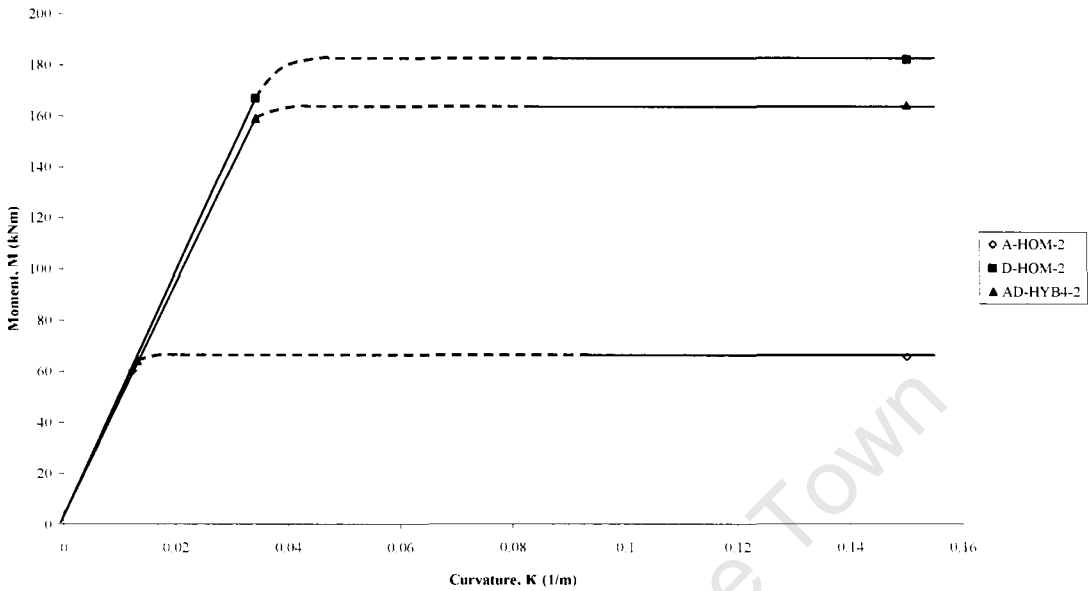

Figure 4.70 Comparison of Analytical Results for the Moment-Curvature Response of AD-HYB4-2 and Equivalent Homogeneous Sections A-HOM-2 and D-HOM-2

In many of the beams investigated the flange yield moment corresponded quite closely with the yield moment of the higher strength homogeneous beam. This may imply that in some cases, instead of using rigorous methods of calculating the characteristic strength of the hybrid, the yield moment of an identically proportioned homogeneous member may be used instead. Examples of this phenomenon can be found in beams with steel combinations BF, BC, CD, CE, and DE. The difference in yield stress of the flange and web steels ranged from 10MPa in DE to 150MPa in CE so perhaps the condition under which the flange yield moment for a hybrid can be approximated by the homogeneous yield moment is that the ratio of the material yield stress of the web to that of the flange should be less than 4:5. This would need to be verified for other beam dimensions.

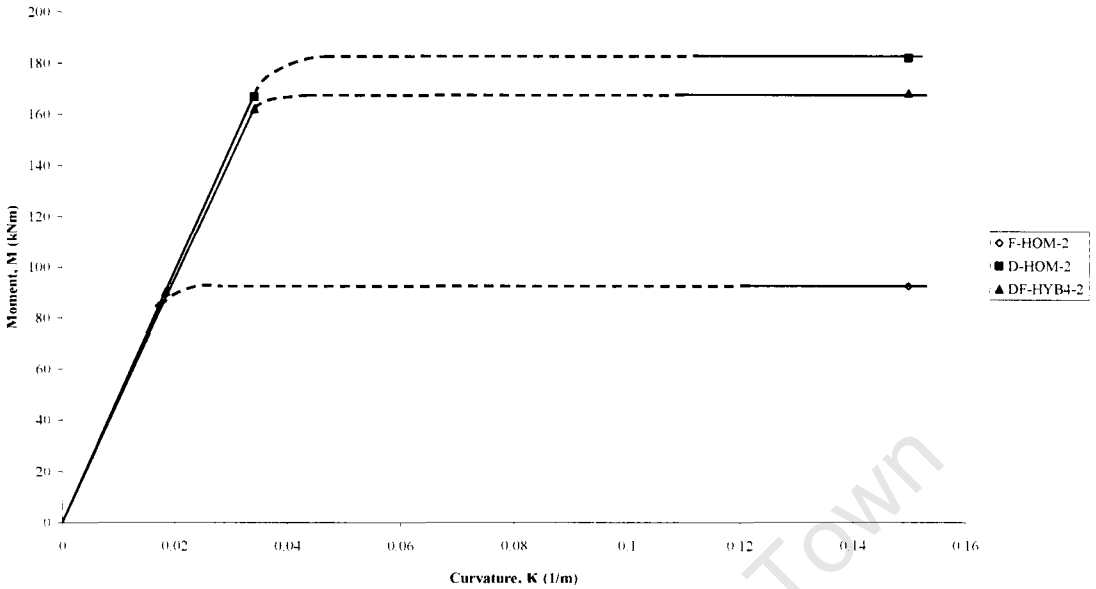

Figure 4.71 Comparison of Analytical Results for the Moment-Curvature Response of DF-HYB4-2 and Equivalent Homogeneous Sections D-HOM-2 and F-HOM-2

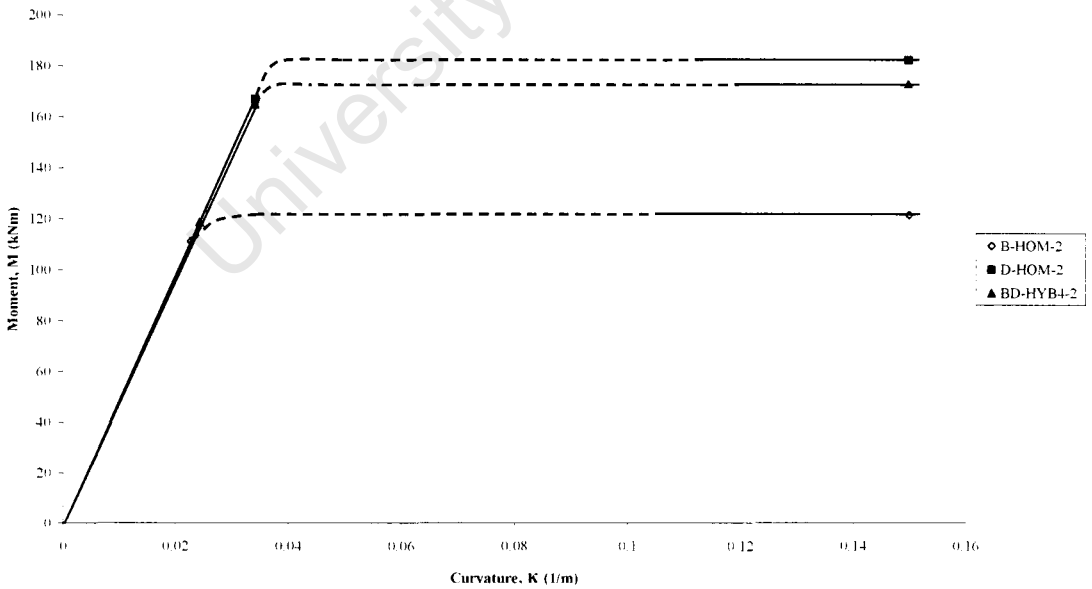

Figure 4.72 Comparison of Analytical Results for the Moment-Curvature Response of BD-HYB4-2 and Equivalent Homogeneous Sections B-HOM-2 and D-HOM-2

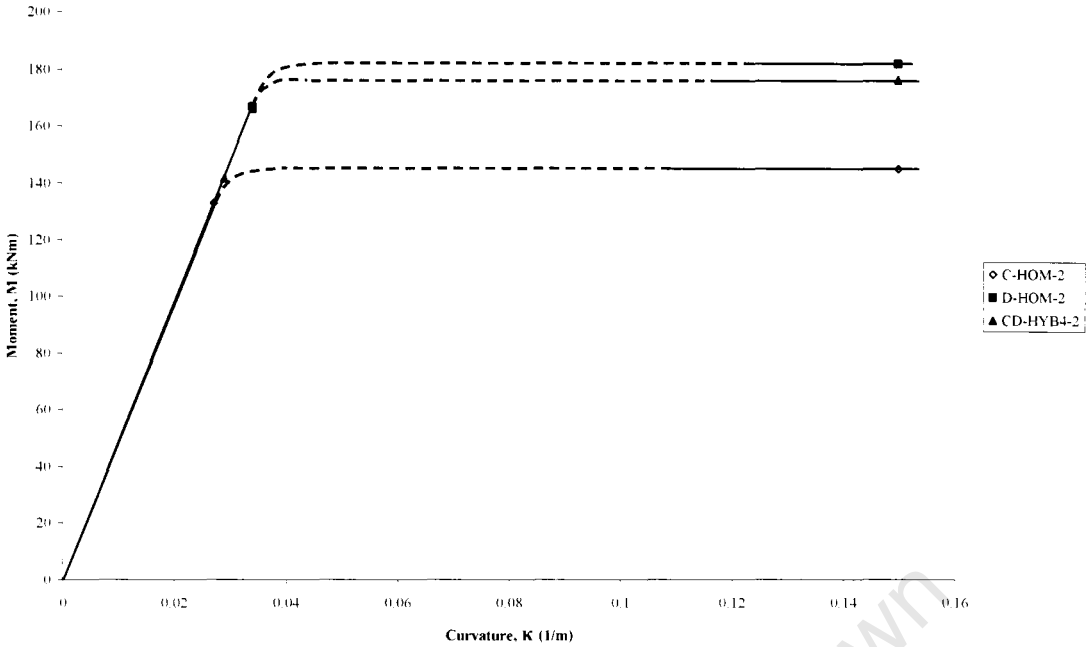

Figure 4.73 Comparison of Analytical Results for the Moment-Curvature Response of CD-HYB4-2 and Equivalent Homogeneous Sections C-HOM-2 and D-HOM-2

4.3.4.5 Two Metre Beams with 700MPa Flanges

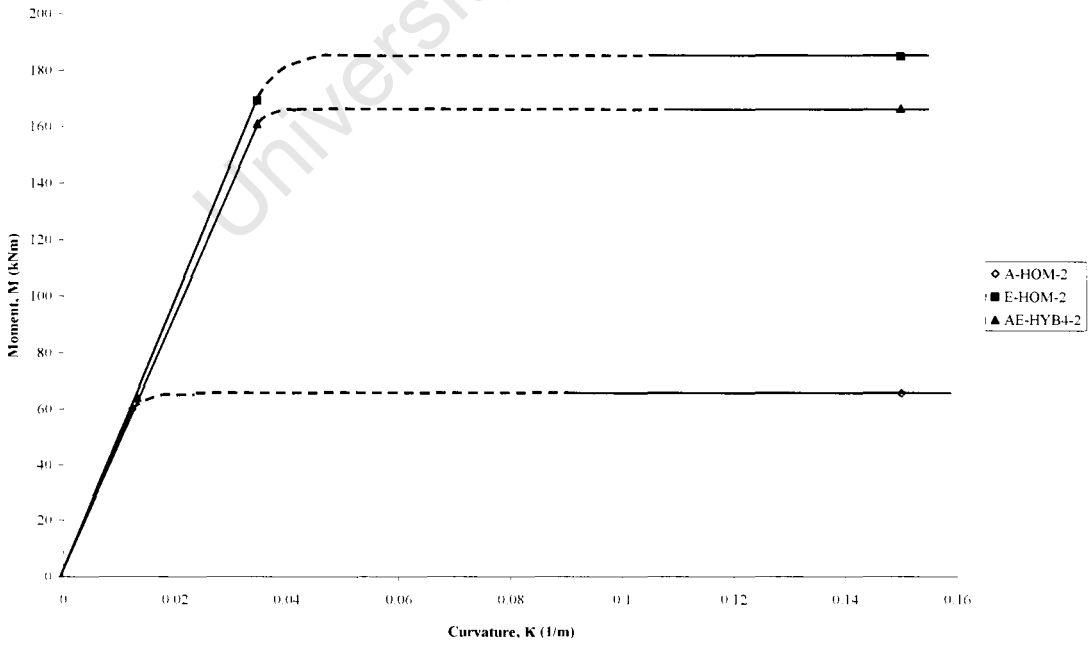

Figure 4.74 Comparison of Analytical Results for the Moment-Curvature Response of AE-HYB4-2 and Equivalent Homogeneous Sections A-HOM-2 and E-HOM-2

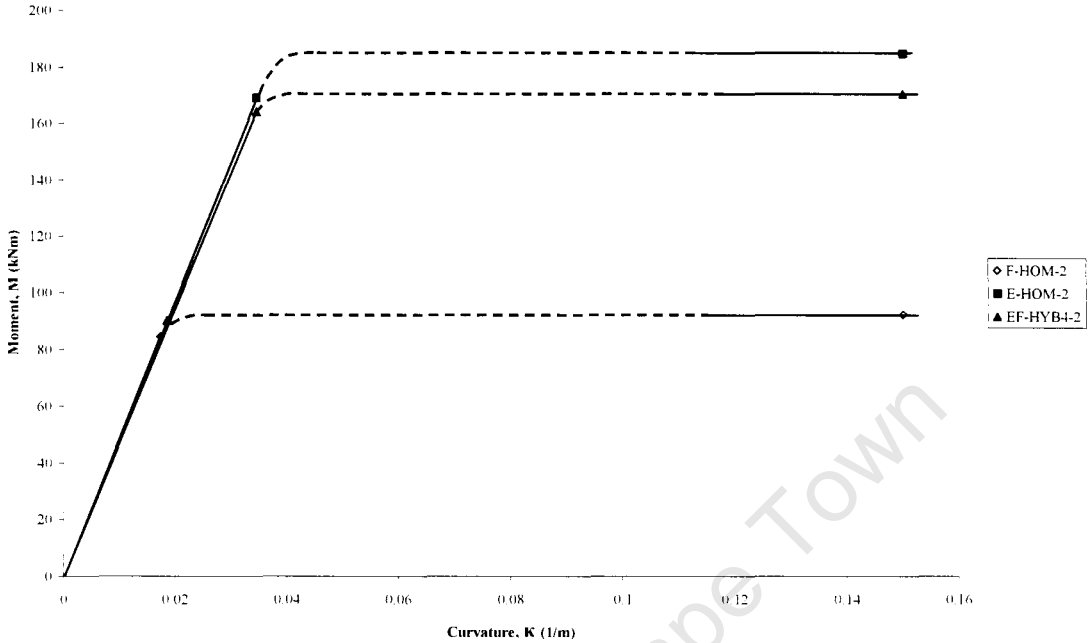

Figure 4.75 Comparison of Analytical Results for the Moment-Curvature Response of EF-HYB4-2 and Equivalent Homogeneous Sections E-HOM-2 and F-HOM-2

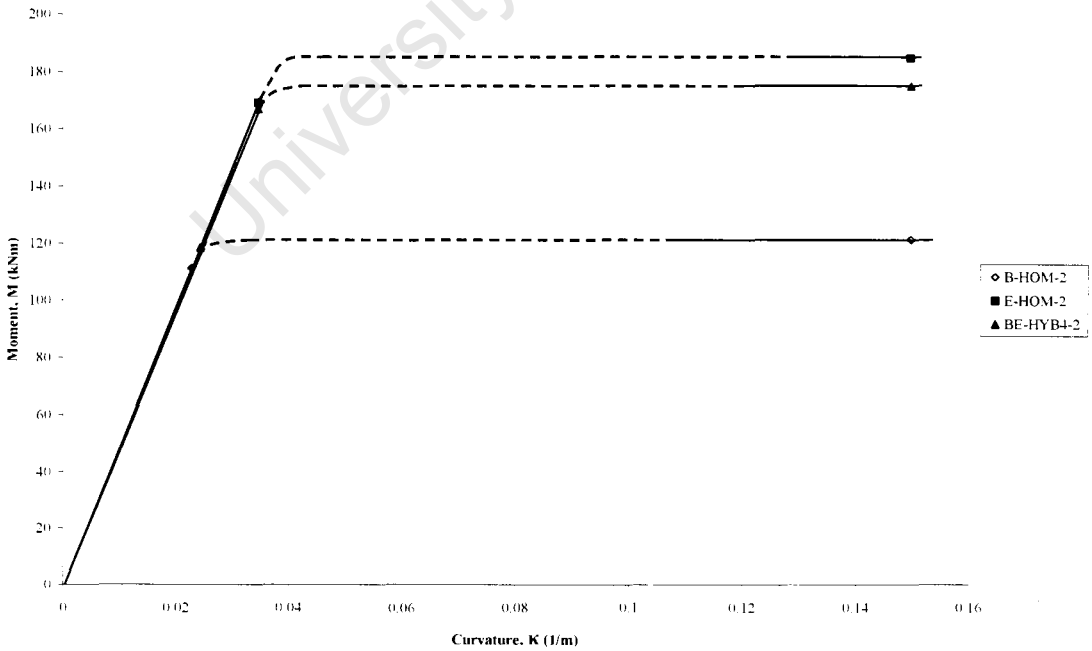

Figure 4.76 Comparison of Analytical Results for the Moment-Curvature Response of BE-HYB4-2 and Equivalent Homogeneous Sections B-HOM-2 and E-HOM-2

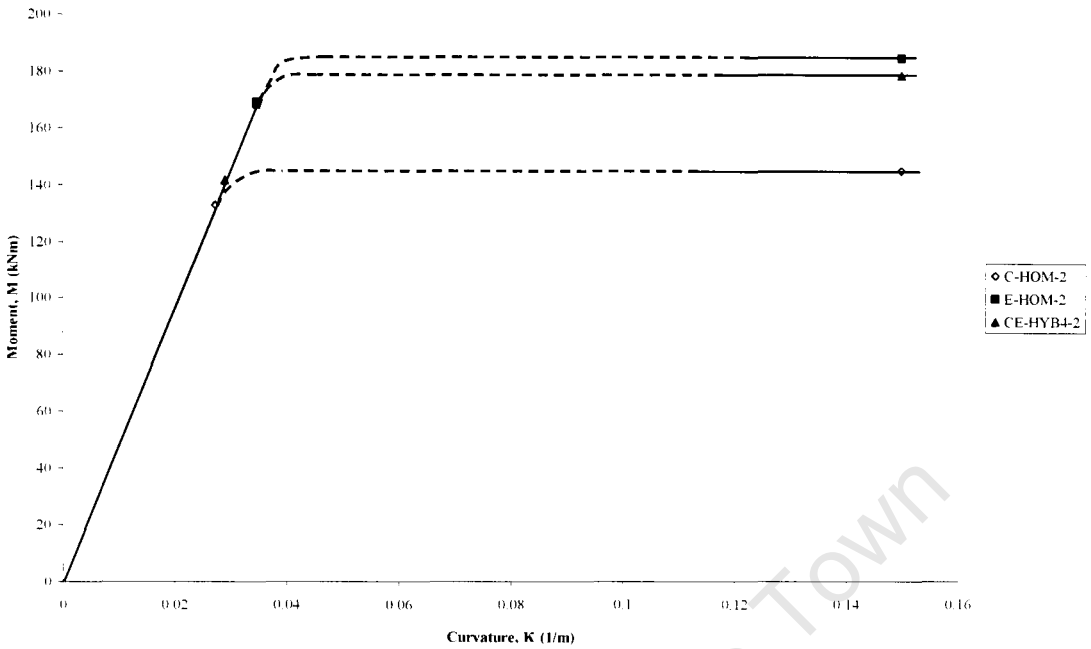

Figure 4.77 Comparison of Analytical Results for the Moment-Curvature Response of CE-HYB4-2 and Equivalent Homogeneous Sections C-HOM-2 and E-HOM-2

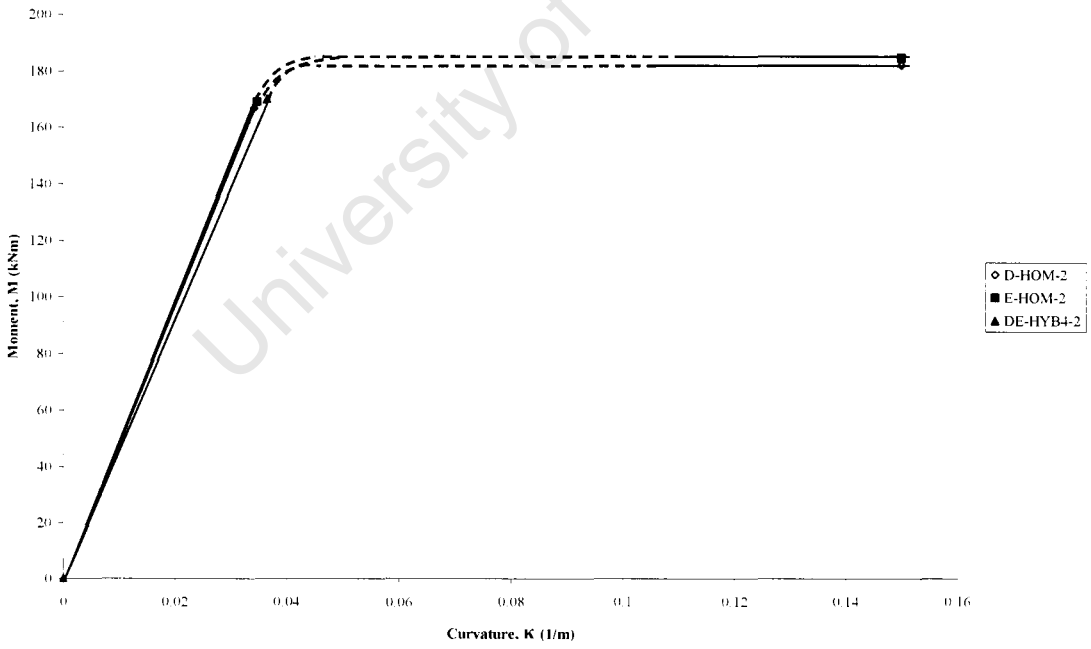

Figure 4.78 Comparison of Analytical Results for the Moment-Curvature Response of DE-HYB4-2 and Equivalent Homogeneous Sections D-HOM-2 and E-HOM-2

The flange yield moment of DE-HYB4-2 is almost equal to the homogeneous yield moment as shown in Figure 4.78.

4.3.4.6 Four Metre Beams with 350MPa Flanges

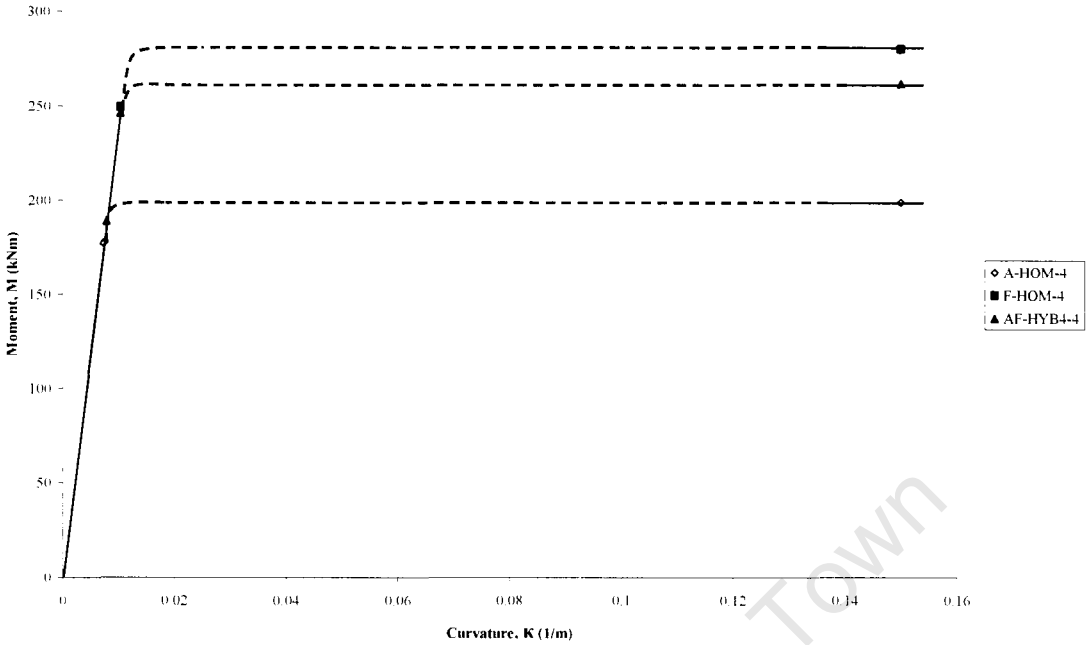

Figure 4.79 Comparison of Analytical Results for the Moment-Curvature Response of AF-HYB4-4 and Equivalent Homogeneous Sections A-HOM-4 and F-HOM-4

4.3.4.7 Four Metre Beams with 460MPa Flanges

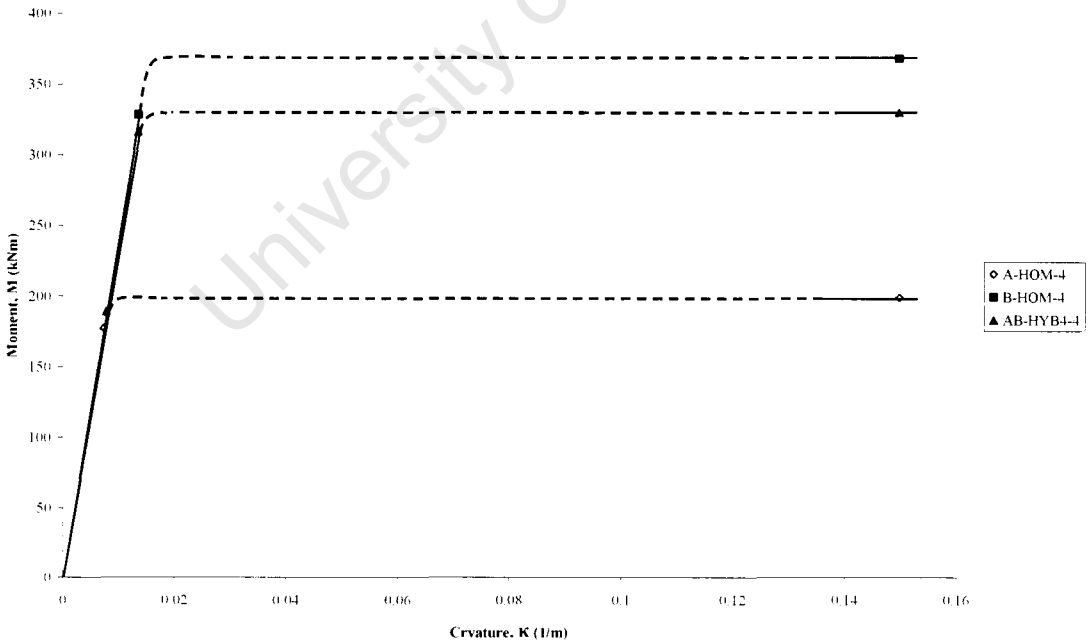

Figure 4.80 Comparison of Analytical Results for the Moment-Curvature Response of AB-HYB4-4 and Equivalent Homogeneous Sections A-HOM-4 and B-HOM-4

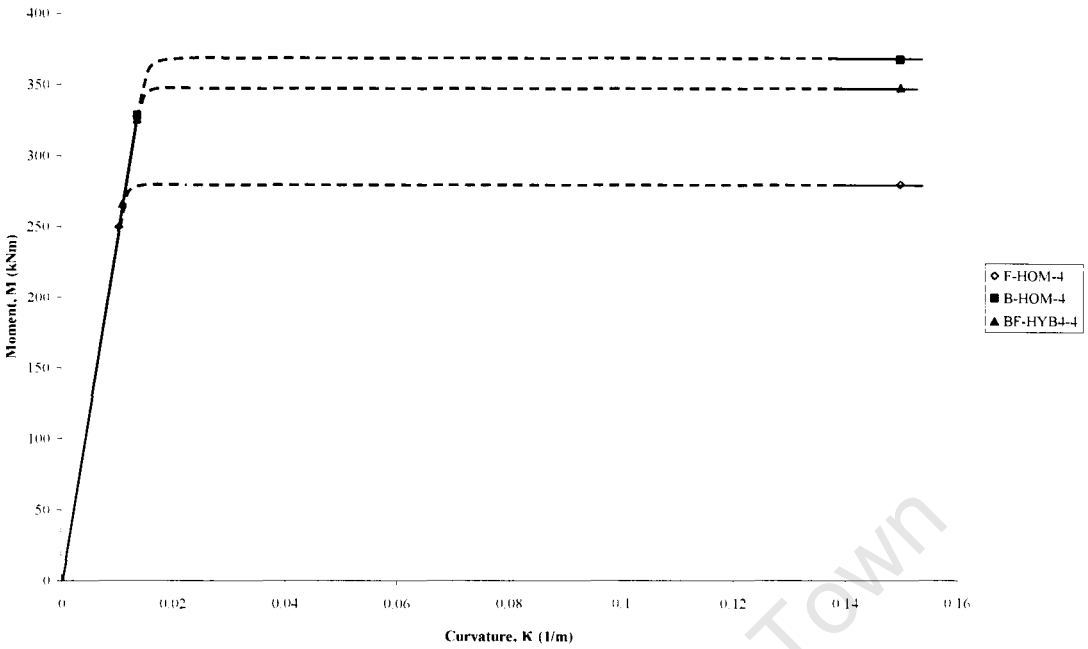

Figure 4.81 Comparison of Analytical Results for the Moment-Curvature Response of BF-HYB4-4 and Equivalent Homogeneous Sections B-HOM-4 and F-HOM-4

4.3.4.8 Four Metre Beams with 550MPa Flanges

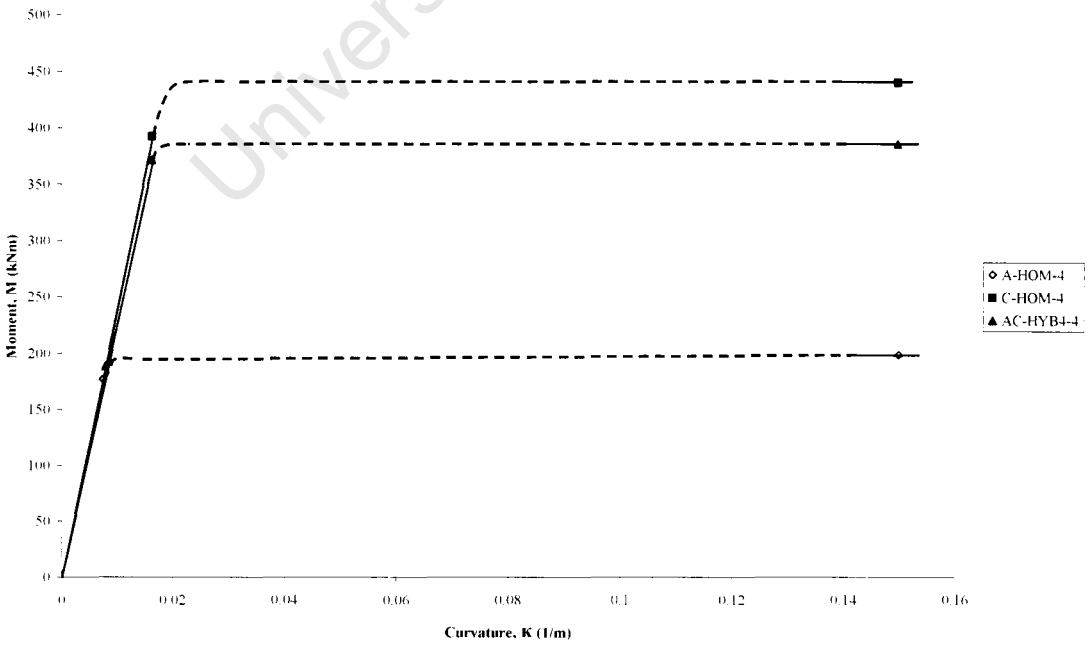

Figure 4.82 Comparison of Analytical Results for the Moment-Curvature Response of AC-HYB4-4 and Equivalent Homogeneous Sections A-HOM-4 and C-HOM-4

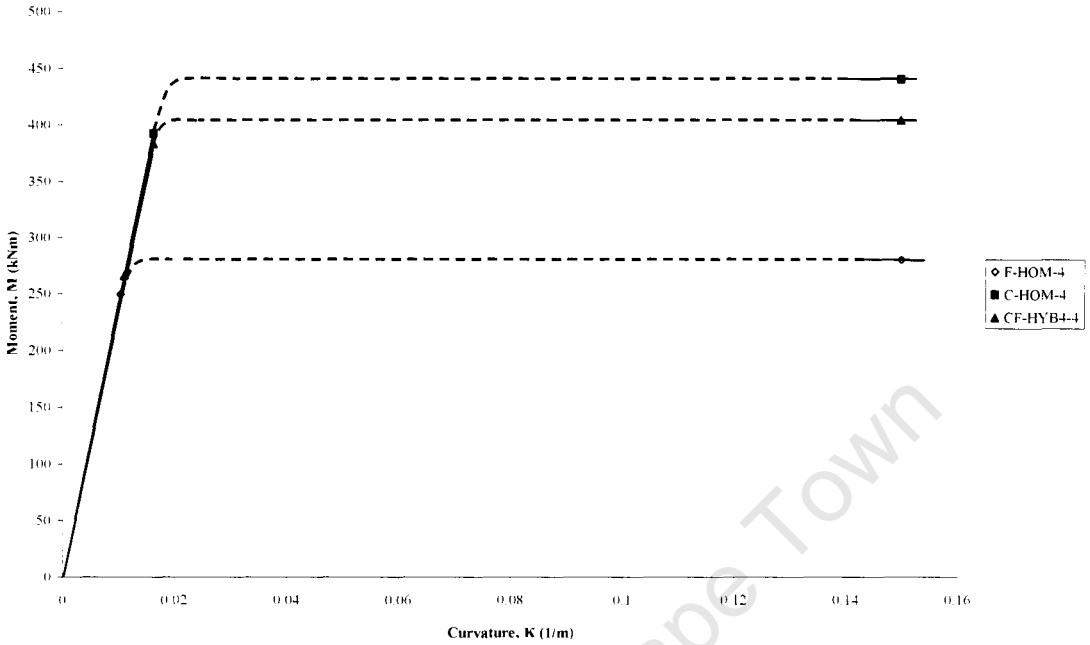

Figure 4.83 Comparison of Analytical Results for the Moment-Curvature Response of CF-HYB4-4 and Equivalent Homogeneous Sections C-HOM-4 and F-HOM-4

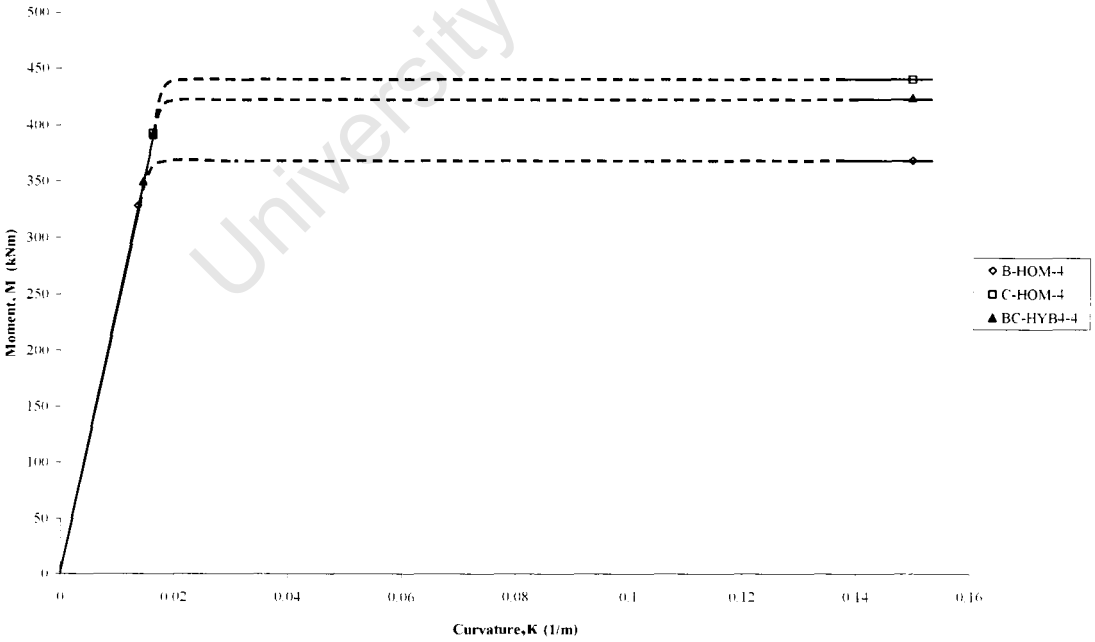

Figure 4.84 Comparison of Analytical Results for the Moment-Curvature Response of BC-HYB4-4 and Equivalent Homogeneous Sections B-HOM-4 and C-HOM-4

4.3.4.9 Four Metre Beams with 690MPa Flanges

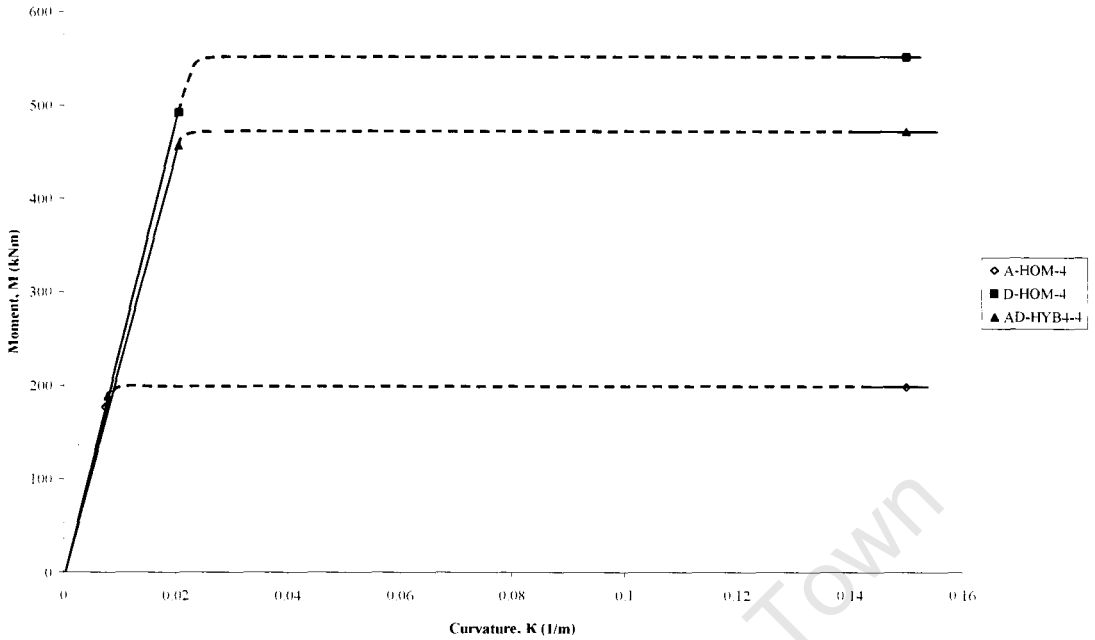

Figure 4.85 Comparison of Analytical Results for the Moment-Curvature Response of AD-HYB4-4 and Equivalent Homogeneous Sections A-HOM-4 and D-HOM-4

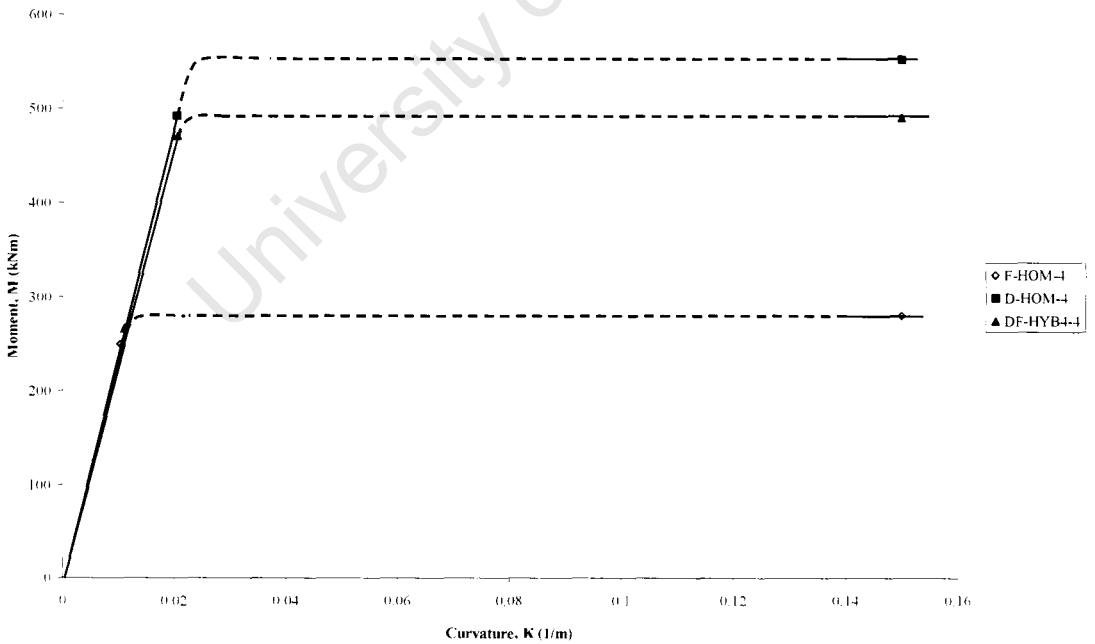

Figure 4.86 Comparison of Analytical Results for the Moment-Curvature Response of DF-HYB4-4 and Equivalent Homogeneous Sections D-HOM-4 and F-HOM-4

As in the short beams, the yielding of the web in the 4m beams did not introduce any great significant changes in the linear portion of the analytical curves. The difference in bending strength (in MPa) between the flange yield moment and the plastic moment is slightly higher. AE-HYB4-4 experiences a gain of 3.4% compared to 3.2% for the two metre beam. That of BC-HYB4-4 increases from 6.5% to 8.3%. DE-HYB4-4 has a 10% gain in strength. The gain in strength for the four metre homogeneous beams is 12.4%. Even though the gain in strength is marginally higher, it again appears that the flange yield moment is a safer strength to design for.

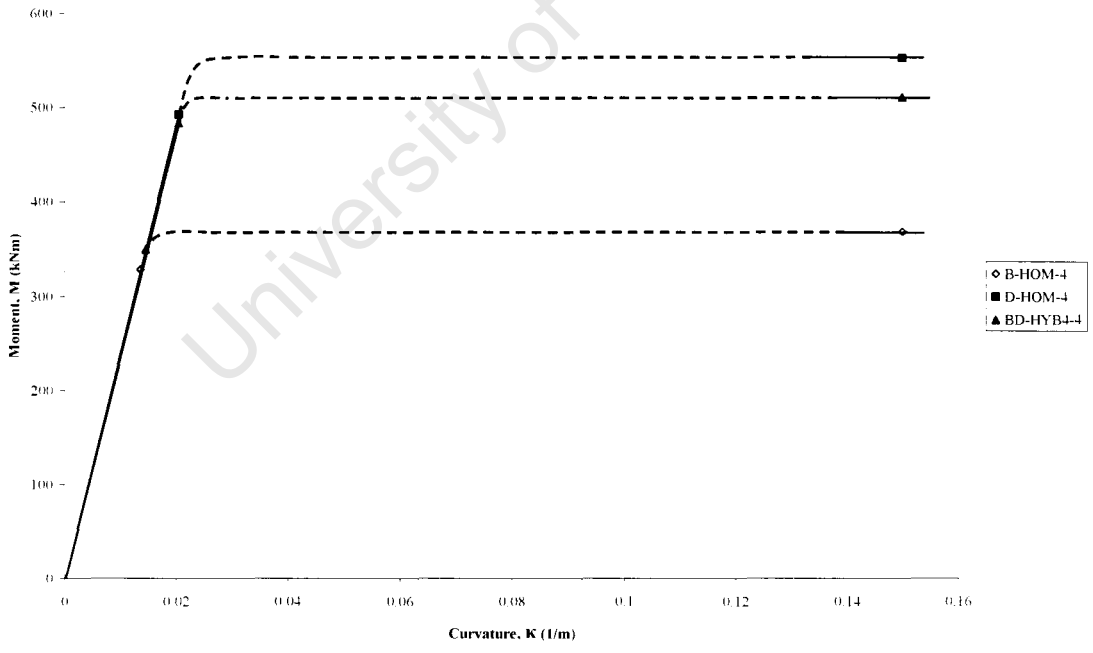

Figure 4.87 Comparison of Analytical Results for the Moment-Curvature Response of BD-HYB4-4 and Equivalent Homogeneous Sections B-HOM-4 and D-HOM-4

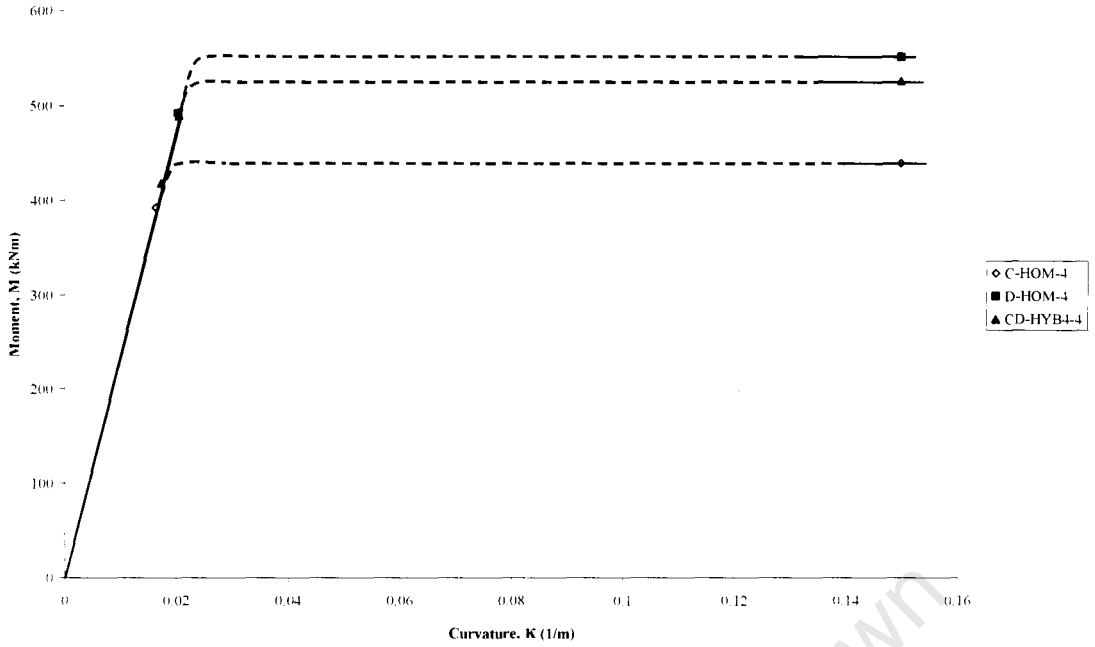

Figure 4.88 Comparison of Analytical Results for the Moment-Curvature Response of CD-HYB4-4 and Equivalent Homogeneous Sections C-HOM-4 and D-HOM-4

4.3.4.10 For Metre Beams with 700MPa Flanges

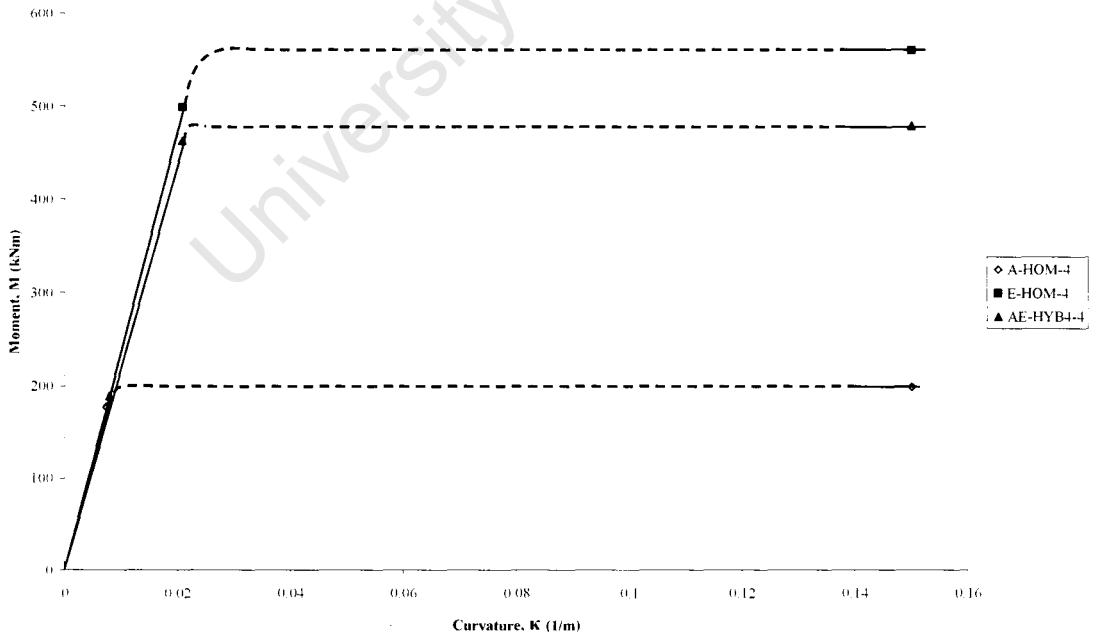

Figure 4.89 Comparison of Analytical Results for the Moment-Curvature Response of AE-HYB4-4 and Equivalent Homogeneous Sections A-HOM-4 and E-HOM-4

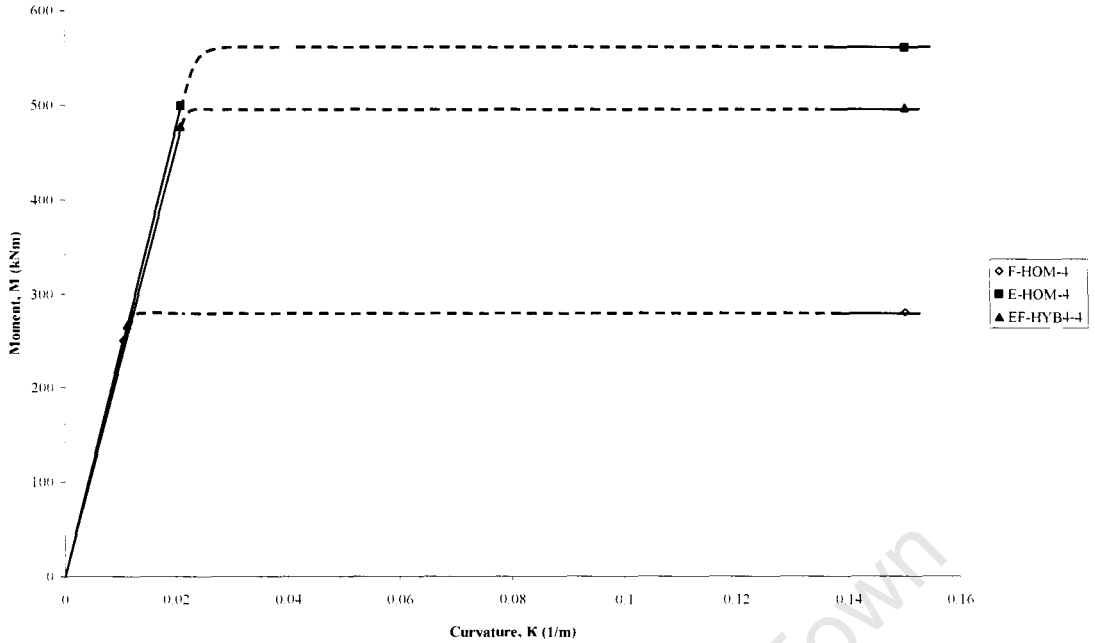

Figure 4.90 Comparison of Analytical Results for the Moment-Curvature Response of EF-HYB4-4 and Equivalent Homogeneous Sections E-HOM-4 and F-HOM-4

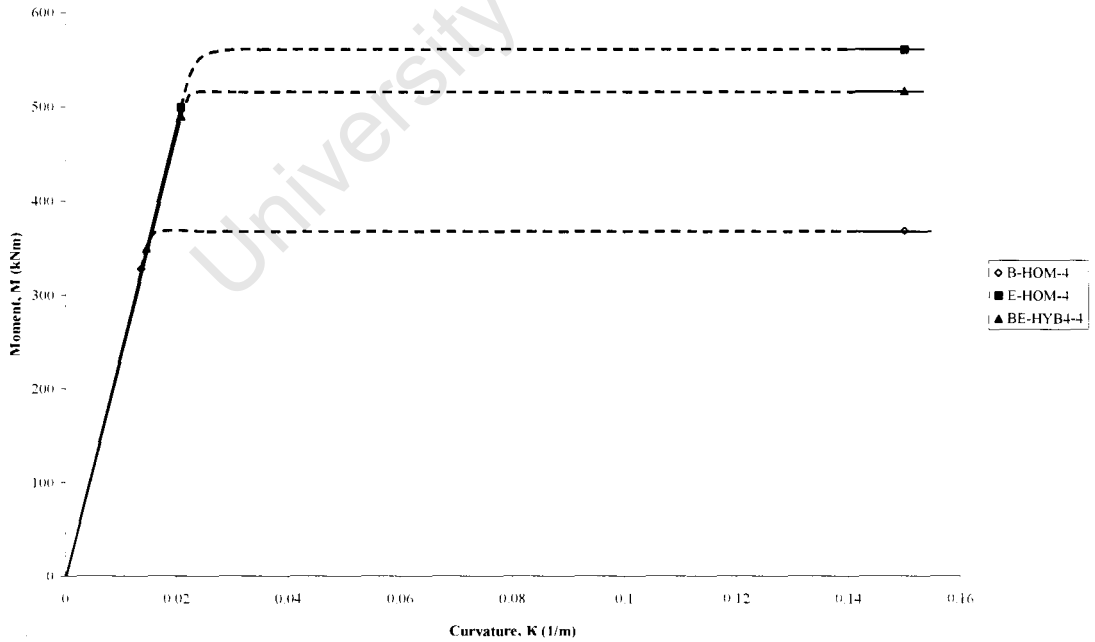

Figure 4.91 Comparison of Analytical Results for the Moment-Curvature Response of BE-HYB4-4 and Equivalent Homogeneous Sections B-HOM-4 and E-HOM-4

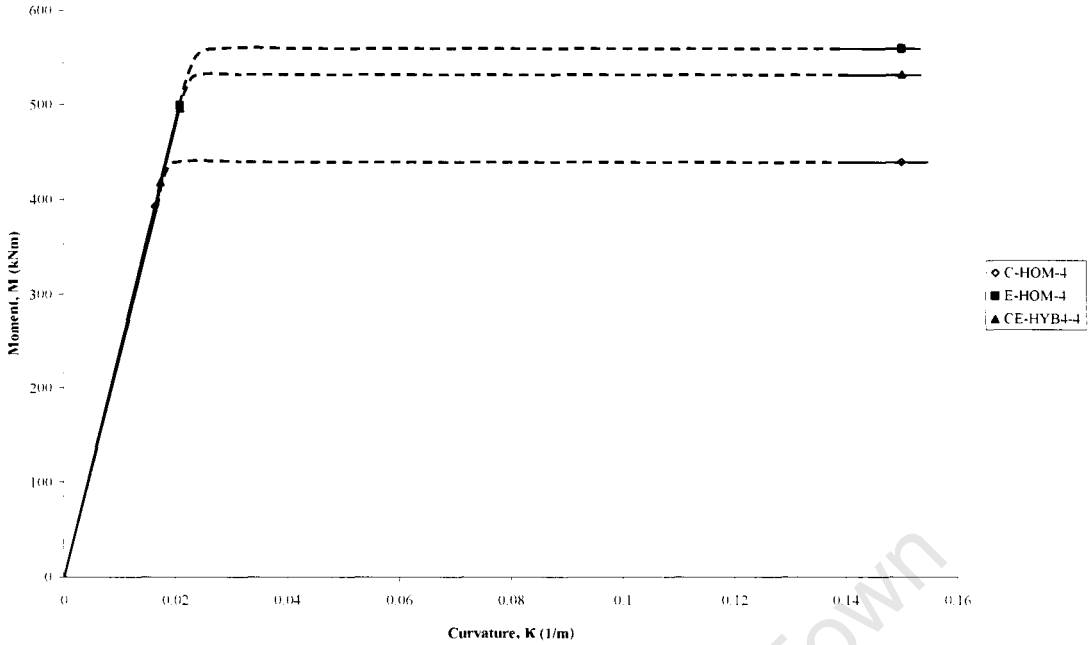

Figure 4.92 Comparison of Analytical Results for the Moment-Curvature Response of CE-HYB4-4 and Equivalent Homogeneous Sections C-HOM-4 and E-HOM-4

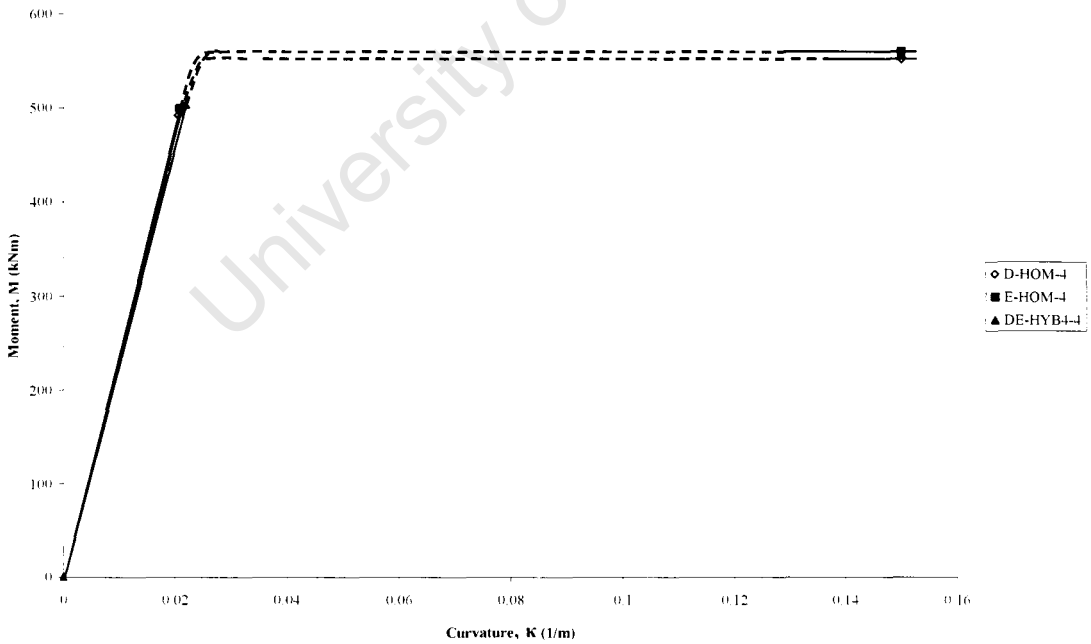

Figure 4.93 Comparison of Analytical Results for the Moment-Curvature Response of DE-HYB4-4 and Equivalent Homogeneous Sections D-HOM-4 and E-HOM-4

4.3.5 Summary of Theoretical Numerical Results

The theoretical results again show that all hybrids, except for DE-HYB4-2 and DE-HYB4-4, will experience web yielding prior to flange yielding. Despite this fact, it is clear that the web yielding does not cause significant non-linearity of the moment-curvature plots. The plots change shape, and plateau immediately after the flange yields and this confirms that the flange yield moment should be the characteristic strength of a hybrid beam. The relatively small difference between the flange yield and plastic moment suggests that taking the plastic moment as the characteristic hybrid beam strength may not be conservative.

4.4 Influence of Hybrid Configuration on Bending Behaviour

4.4.1 Introduction

Six different hybrid beams were generated by varying the position of the high strength steel in the member cross-section. In Figure 4.94 hatched regions indicate the location of the higher strength material. Although some of these configurations are unlikely in practice (e.g. Hybrid 2) others are widely reported in literature (e.g. Hybrid 4), and yet others have been recommended as providing a more cost effect alternative to Hybrid 4 in specific regions. Hybrid 5 was thought to be more effective at negative moment regions while Hybrid 6 was recommended for positive moment regions (Wasserman et al, 1998). In order to represent the most severe case, only Steel A (248.4MPa) and Steel E (700MPa) were used. The chosen beam length was 2m.

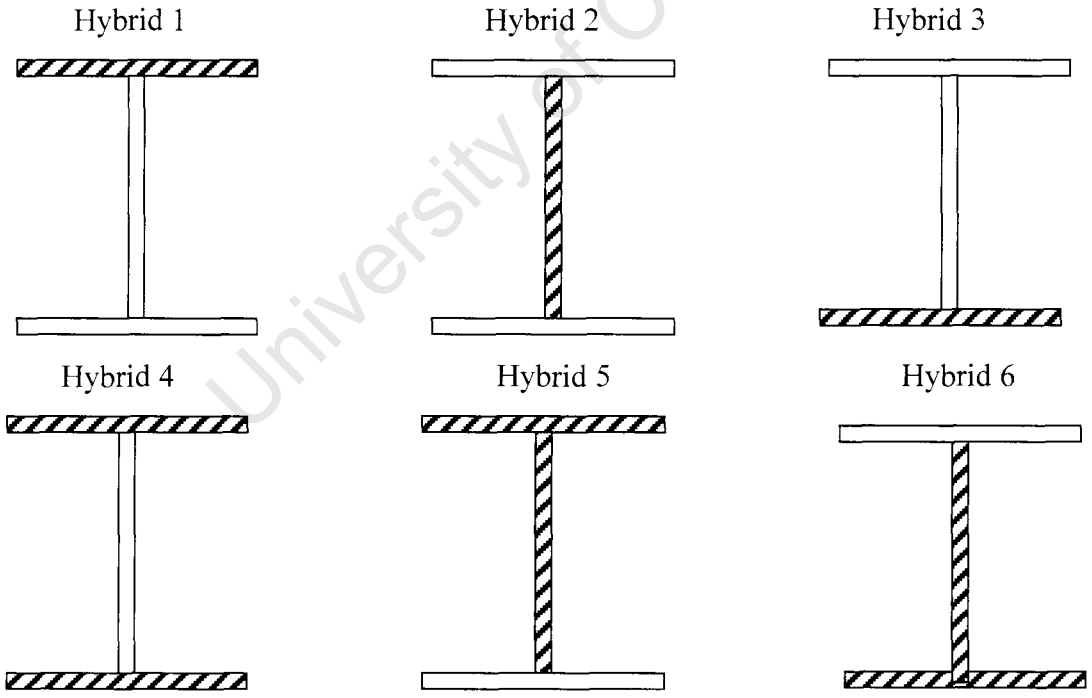

Figure 4.94 Cross-Sections used in the Analysis of Hybrid Configurations

4.4.1.1 Model Data

Table 4.16 gives the dimensional properties of the hybrid beams that were investigated. The 2m beams were simply supported and subjected to a uniformly distributed load.

Table 4.16 Flange and Web Dimensions of Various Hybrid Configurations

Flange Width b_f (mm)	Flange Thickness t_f (mm)	Web Height h_w (mm)	Web Thickness t_w (mm)	Depth of Section d (mm)
200	6	180	5	192

4.4.2 ABAQUS Results

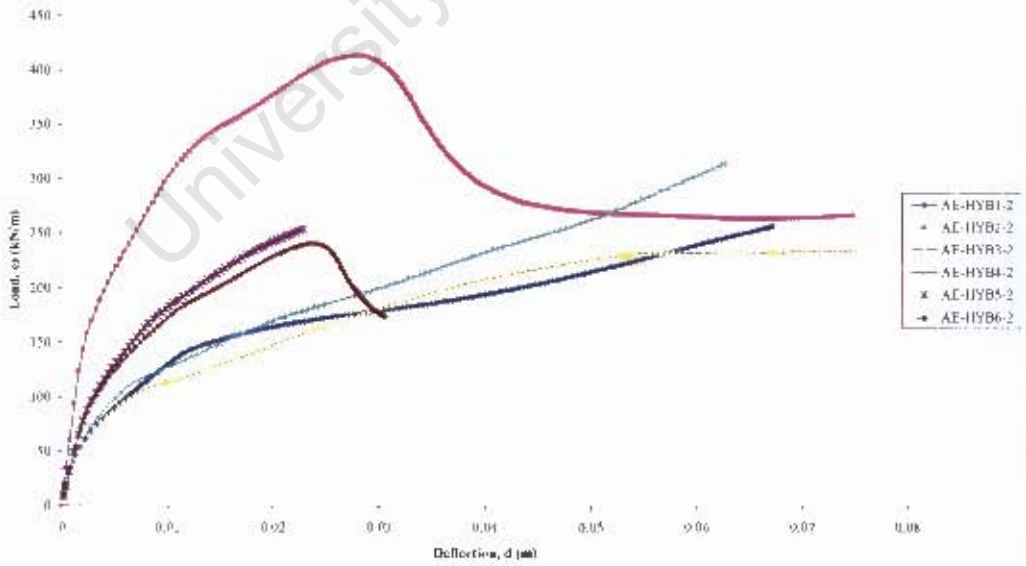

Figure 4.95 Comparison of Hybrid Load-Deflection Curves

Hybrids 1 and 3 (HYB1 and HYB3) have similarly shaped load-deflection curves (Figure 4.95), together with the commonly used Hybrid 4 (HYB4). Hybrids 5 and 6 (HYB5 and HYB6) again had plots similar to each other. In terms of load carrying capacity, Hybrids 5 and 6 are able to sustain higher loads with smaller deflections. The observed differences may be due to the higher strength web which does not yield prior to flange yielding. Unfortunately Hybrid 6 experiences unloading relatively quickly when compared to the other specimens. Although the Hybrid 5 analysis stopped abruptly, in all likelihood it would show the same trend. When compared to Hybrids 1 and 3, the load-deflection response of Hybrids 5 and 6 is rather surprising. It would seem that the high strength web may have a negative influence on ductility.

The most striking aspect of the ABAQUS results is the fact that Hybrid 2 (HYB2), with high strength steel web and mild steel flanges, is able to resist the highest ultimate loading as shown in Figure 4.95. This is, in fact, the one configuration which is not likely to find any applications in practice. The high strength web prevents premature web yielding but the high stresses cause extensive buckling of the compression flange as shown in Figure 4.96.

Figure 4.96 Flange Buckling in Hybrid Beam AE-HYB2-2

For the same applied load Hybrid 2 experiences lower deflections which lends supports the theory that web yielding negatively affects deflection.

Figure 4.97 shows Hybrid 1 with the bottom flange and web in material yield while stresses in the top flange are mostly below 700MPa.

Figure 4.97 Stress Distribution in Hybrid Beam AE-HYB1-2

Hybrid 5, in Figure 4.98, shows very high stresses at the bottom of the flange, near the centre of the span, where it is forced to resist more bending stresses (shear is zero at midspan). At this stage, large parts of the bottom flange have stresses greater than 248.4MPa.

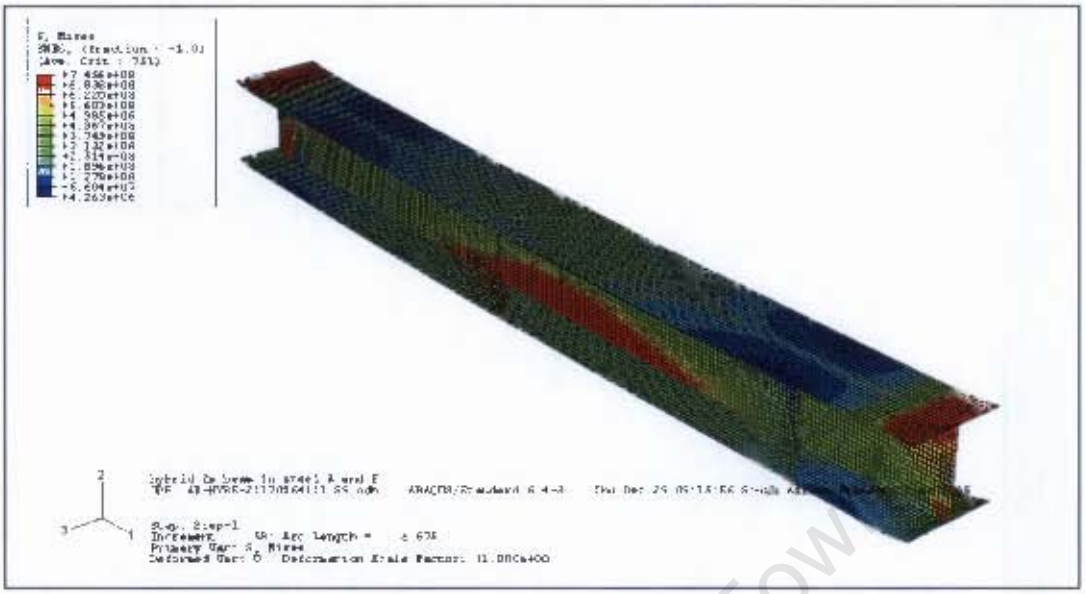

Figure 4.98 Stress Distribution in Hybrid Beam AE-HYB5-2

4.4.3 Summary of Results

From these results, it appears that hybrid 4 is a good arrangement even the large deflections would be of concern. Hybrids 1 and 2 would also be of use though there would be a small loss of strength when compared to hybrid 4. The slightly higher initial load carrying capacity of hybrid 1 suggests that this arrangement would be suited to positive moment regions while hybrid 3 would be more useful in negative moment regions.

4.5 Verification of Bending Equations

Equations predicting the strength of hybrid members have been suggested in literature (Frost and Schilling, 1964; Joint ASCE-AASHO Committee on Flexural Members, 1968) but these have not been adopted in design codes. These equations, previously introduced in Section 3.3 are presented again below. Equation 3.12 gives the web yield moment while Equations 3.13 and 3.14 predict the flange yield moment.

$$M_{yw} = \sigma_{yw} S \frac{d}{h_w} \text{ (Frost and Schilling, 1964),} \qquad 3.12$$

$$M_{yf} = \frac{2I_f}{d}\sigma_{yf} + Z_w \sigma_{yw} - \frac{t_w d^2}{12}\left(\frac{\sigma_{yw}^3}{\sigma_{yf}^2}\right) \text{ (Frost and Schilling, 1964)} \qquad 3.13$$

And

$$M_{yf} = M_y\left[\frac{12 + \beta(3\alpha - \alpha^3)}{12 + 2\beta}\right] \text{ (Joint ASCE and AASHO Committee on Flexural Members, 1968)} \qquad 3.14$$

The expressions derived for Hybrid 4 beams in Chapter 3.4 were verified against Equations 3.12 to 3.14 to determine whether they give accurate values of bending moments. Hybrid 4 beams used to conduct the verification process included the 2m beam lengths as well as all material combinations. The analysis was carried out by means of spreadsheets which have been summarised in Tables 4.17 to 4.20.

4.5.1 Verification Using the Equation Presented by Frost and Schilling (1964)

Table 4.17 Calculation of Hybrid Web and Flange Yield Moments using Equations 3.12 and 3.13

Beam	σyw	σyf	S	d	hw
AE-HYB4-2	248.4	700	2.42E+05	192	180
EF-HYB4-2	350	700	2.42E+05	192	180
BE-HYB4-2	460	700	2.42E+05	192	180
CE-HYB4-2	550	700	2.42E+05	192	180
AD-HYB4-2	248.4	690	2.42E+05	192	180
DF-HYB4-2	350	690	2.42E+05	192	180
BD-HYB4-2	460	690	2.42E+05	192	180
CD-HYB4-2	550	690	2.42E+05	192	180
AC-HYB4-2	248.4	550	2.42E+05	192	180
CF-HYB4-2	350	550	2.42E+05	192	180
BC-HYB4-2	460	550	2.42E+05	192	180
AB-HYB4-2	248.4	460	2.42E+05	192	180
BF-HYB4-2	350	460	2.42E+05	192	180
AF-HYB4-2	248.4	350	2.42E+05	192	180

(continued)

tw	I f	Z w	Myw	Myf
5	2.08E+07	4.05E+04	64.032	161.2464148
5	2.08E+07	4.05E+04	90.22222222	164.4976667
5	2.08E+07	4.05E+04	118.5777778	167.245481
5	2.08E+07	4.05E+04	141.7777778	168.7263197
5	2.08E+07	4.05E+04	64.032	159.065721
5	2.08E+07	4.05E+04	90.22222222	162.2917612
5	2.08E+07	4.05E+04	118.5777778	164.9897333
5	2.08E+07	4.05E+04	141.7777778	166.4073882
5	2.08E+07	4.05E+04	64.032	128.448614
5	2.08E+07	4.05E+04	90.22222222	131.1646088
5	2.08E+07	4.05E+04	118.5777778	132.8542503
5	2.08E+07	4.05E+04	64.032	108.614289
5	2.08E+07	4.05E+04	90.22222222	110.7293793
5	2.08E+07	4.05E+04	64.032	83.97172576

A summary of the data contained in the above Table 4.17 can be found below in Table 4.18

Table 4.18 Table 6.2 Summary of the Comparison between Analytical Results and Equation 3.12

Beam	Analytical Results [kNm]	Frost and Schilling (1964) [kNm]
AE-HYB4-2	64.0	64.0
EF-HYB4-2	90.2	90.2
BE-HYB4-2	118.6	118.6
CE-HYB4-2	141.7	141.8
AD-HYB4-2	64.0	64.0
DF-HYB4-2	90.2	90.2
BD-HYB4-2	118.6	118.6
CD-HYB4-2	141.7	141.8
AC-HYB4-2	64.0	64.0
CF-HYB4-2	90.2	90.2
BC-HYB4-2	118.6	118.6
AB-HYB4-2	64.0	64.0
BF-HYB4-2	90.2	90.2
AF-HYB4-2	64.0	64.0

From the summary in Table 4.18 it can be seen that analysis gives a value of the web yield moment which is equal to that obtained from Equation 3.12.

4.5.2 Verification Using the Equations Presented by Frost and Schilling (1964) and the Joint Joint ASCE-AASHO Committee on Flexural members (1968)

Table 4.19 Calculation of Hybrid Flange Yield Moment using Equation 3.14

Beam	σyw	σyf	hw	tw	bf	tf	
AE-HYB4-2	248.4	700	180	5	200	6	
EF-HYB4-2	350	700	180	5	200	6	
BE-HYB4-2	460	700	180	5	200	6	
CE-HYB4-2	550	700	180	5	200	6	
AD-HYB4-2	248.4	690	180	5	200	6	
DF-HYB4-2	350	690	180	5	200	6	
BD-HYB4-2	460	690	180	5	200	6	
CD-HYB4-2	550	690	180	5	200	6	
AC-HYB4-2	248.4	550	180	5	200	6	
CF-HYB4-2	350	550	180	5	200	6	
BC-HYB4-2	460	550	180	5	200	6	
AB-HYB4-2	248.4	460	180	5	200	6	
BF-HYB4-2	350	460	180	5	200	6	
AF-HYB4-2	248.4	350	180	5	200	6	

(continued)

My homog	α	Aw	Af	β	Myf
169.12875	0.354857143	900	1200	0.75	159.9195631
169.12875	0.5	900	1200	0.75	163.256224
169.12875	0.657142857	900	1200	0.75	166.1938978
169.12875	0.785714286	900	1200	0.75	167.9268511
166.712625	0.36	900	1200	0.75	157.7596384
166.712625	0.507246377	900	1200	0.75	161.074267
166.712625	0.666666667	900	1200	0.75	163.9683843
166.712625	0.797101449	900	1200	0.75	165.646122
132.886875	0.451636364	900	1200	0.75	127.4443187
132.886875	0.636363636	900	1200	0.75	130.3132249
132.886875	0.836363636	900	1200	0.75	132.3261743
111.14175	0.54	900	1200	0.75	107.8231561
111.14175	0.760869565	900	1200	0.75	110.1669392
84.564375	0.709714286	900	1200	0.75	83.49164663

The information in Table 4.19 is summarised below in Table 4.20

Table 4.20 Summary of the Comparison between Analytical Results and Equations 3.13 and 3.14

Beam	**Analytical Results [kNm]**	**Frost and Schilling (1964) [kNm]**	**Joint ASCE-AASHO Committee on Flexural members (1968) [kNm]**
AE-HYB4-2	161.0	161.2	160.0
EF-HYB4-2	164.2	164.5	163.3
BE-HYB4-2	167.0	167.2	166.2
CE-HYB4-2	168.5	168.7	167.9
AD-HYB4-2	158.8	159.1	157.8
DF-HYB4-2	162.0	162.3	161.1
BD-HYB4-2	164.7	165.0	164.0
CD-HYB4-2	166.2	166.4	165.6
AC-HYB4-2	128.2	128.4	127.4
CF-HYB4-2	131.0	131.2	130.3
BC-HYB4-2	132.7	132.9	132.3
AB-HYB4-2	108.4	108.6	107.8
BF-HYB4-2	110.6	110.7	110.2
AF-HYB4-2	83.8	84.0	83.5

As seen from Table 4.20, results from both equations compare very well with the flange yield moment obtained analytically.

4.6 Determination of New Width to Thickness Ratios

4.6.1 Width to Thickness Ratios for Flanges

A survey of studies conducted by other researchers demonstrates that flange slendernesses which produced favourable results, in terms of load-carrying and rotation capacity, ranged from 3.8 (Frost and Schilling, 1964) to 5 (McDermott, 1969). More recent studies have confirmed that flange width to thickness ratios of between 3.5 and 5 (Greco and Earls, 2003) yield good results for higher strength and hybrid beams.

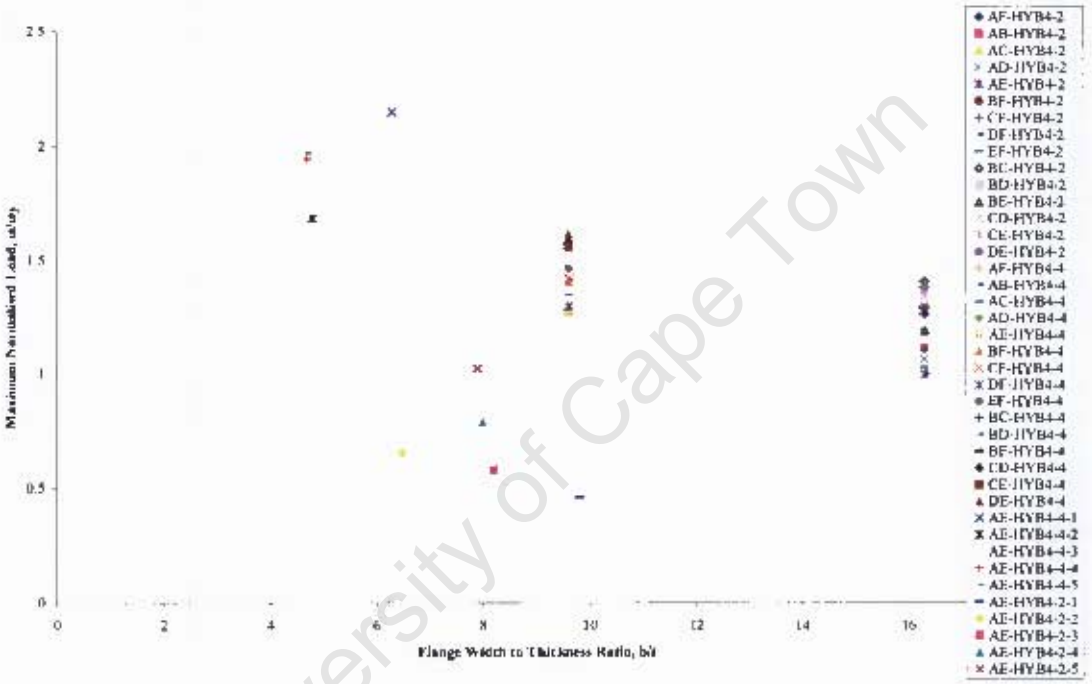

Figure 4.99 Maximum Load Sustained by Hybrid Beams as a Function of the Flange width to Thickness Ratio

Figure 4.99 above shows the flange width to thickness ratios, b/t, of all specimens included in the study plotted against the maximum non-dimensional load, $\frac{\omega}{\omega_y}$.

ω_y is the theoretical load which causes yielding of the flanges.

The largest sustained loads are possible where the b/t ratios are less than 7. This value is slightly larger than those recommended in literature. In fact, loads of up to twice the flange yield moment load were recorded for beam AE-HYB4-4-1. The load gradually decreases as slenderness increases. The other beams used to investigate the influence of flange thickness on load carrying capacity, AE-HYB4-3-2 to AE-HYB4-4-5, were

not able to reach their respective yield moments and some even started to unload before the flange yield moment had been achieved. This seems to indicate that compactness of the flanges alone does not assure higher load-carrying capacity. Suitable width to thickness ratios can also be arrived at by analytical methods as detailed below.

The relevant equation for calculation of limiting width to thickness ratios, Equation 3.11, has been reproduced below.

$$\lambda_p = \sqrt{\left(\frac{f_y.12(1-\nu^2)}{\pi^2.E.k_\sigma}\left(\frac{b}{t}\right)^2\right)} = 1.1\frac{b}{t}\sqrt{\frac{f_y}{Ek_\sigma}} \qquad 3.11$$

For class 1 plates, the Eurocode recommends a minimum value of $\lambda_{p1} = 0.46$, as detailed in Chapter 3.2.2. By adopting this lowest value of λ_{p1}, for a reference steel grade of 460MPa and with k=0.43, from Table 3.1, results in a value of 5.8 as the limiting b/t ratio for class 1 flanges. This value can be rounded up to 6. The Eurocode (Table 4.4) gives the limiting width to thickness ratio for class 1 outstand flanges as

$$\frac{c}{t} \le 9\varepsilon \qquad 4.7$$

for a material yield strength which is less than 460MPa. However, to include steels with yield strengths greater than 460MPa the equation can be modified such that it reads

$$\frac{c}{t} \le 6\varepsilon \qquad 4.8$$

Where ε was previously given as

$$\varepsilon = \sqrt{\frac{235}{f_y}} \qquad 4.9$$

it then is modified to

$$\varepsilon = \sqrt{\frac{460}{f_y}} \qquad 4.10$$

where f_y is the yield strength of the steel under investigation.

When factored to account for the 700Mpa steel using the modified Equation 4.8 and 4.10 a b/t ratio of 4.9 is obtained. This value falls within the range recommended in literature, based on experimental findings 5 (Frost and Schilling, 1964; Greco and Earls, 2003).

There are no other recommendations by which classes 2 and 3 can be located so this means flanges would fall into two broad categories, either compact or non-compact as shown in Figure 4.100. The compressive load is dimensionless ad is the ratio of the applied stress to the material yield stress.

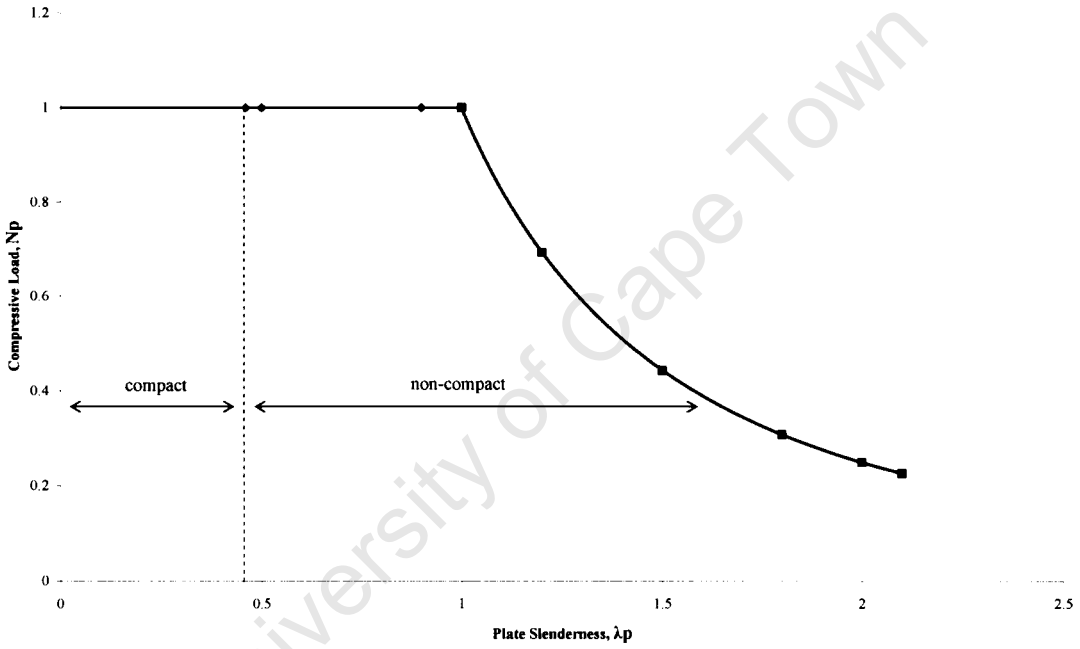

Figure 4.100 Compressive Plate Strength

4.6.2 Width to Thickness Ratios for Webs

Limiting width to thickness ratios for the webs can again be calculated through the use of Equation 3.11, and with an appropriate plate buckling factor. A value of $k_\sigma = 23.9$ from Table 3.1 is used for simply supported plates in bending. When a value of $\lambda p1 = 0.55$ is selected for the 460MPa steel grade, the resulting limiting width to thickness ratio for a compact web is 55. Web slenderness values for higher strength unstiffened webs recommended in literature range from 45 (Greco and Earls, 2003), 46 to 53 (Frost and Schilling, 1964) and 55 (Ricles et al, 1998).

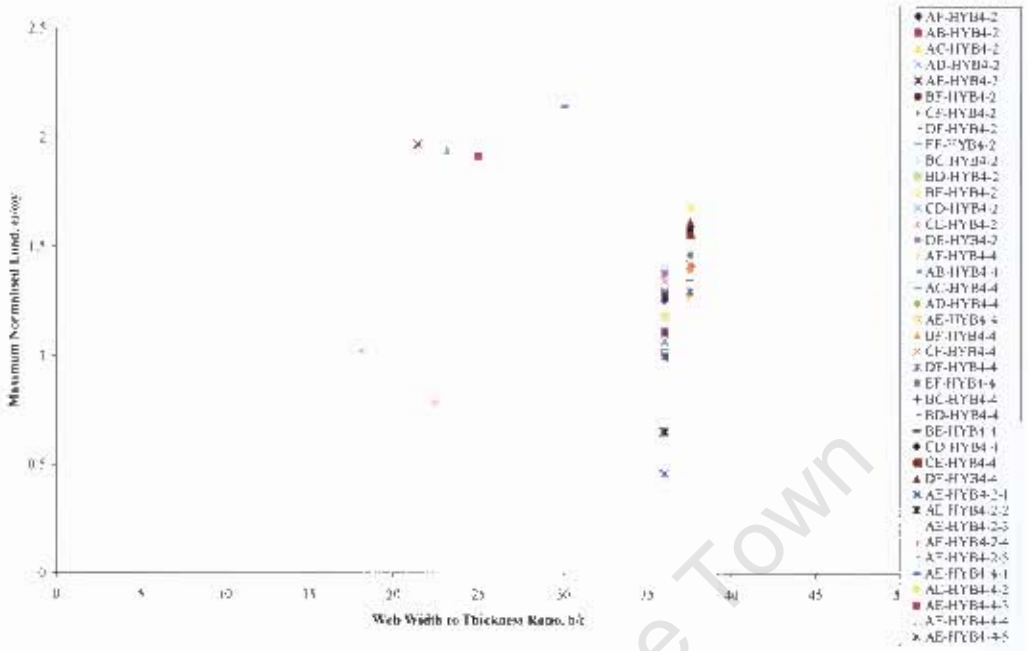

Figure 4.101 Maximum Load Sustained by Hybrid Beams as a Function of the Web Width to Thickness Ratio

Figure 4.101 shows that all hybrid webs have b/t ratios of less than 40; which is well within the limits recommended in literature. Again, suitable limits can be derived analytically.

In the Eurocode, the original equation for the limiting width to thickness ratio for an internal compression part is given as

$$\frac{c}{t} \leq 72\varepsilon \qquad 4.11$$

For steels grades with yield strengths of less than 460MPa the equation becomes

$$\frac{c}{t} \leq 55\varepsilon \qquad 4.12$$

When applied to a 700MPa steel, the new limiting width to thickness ratio is found to be 45. This value is within the recommended limits, also based on experimental findings (Rieles et al, 1998; Greco and Earls, 2003).

A section can then be classified as a compact section when both the web and the flange lie within the recommended limits. Where either the web or flange, or both, are non-compact, the entire section becomes non-compact.

In summary, proportioning hybrid flanges such that they lie within certain limits does ensure that they will carry large loads. However, it can also be seen that certain flange and web material combinations produce more favourable results than others. For example where the b/t ratio is a constant it would be expected that the hybrid beam with 700MPa flanges and 690MPa web would consistently achieve the greatest loads, but this is not always the case.

With the proposed limits recommended above it can now be seen that all the webs used in the research are compact, or class 1 and most of the flanges can now be classified as non-compact.

5 Recommendations

5.1 Conclusions

(i) Development of stresses and strains within the flanges and web from the onset of loading;

In terms of ultimate loads and deflections, the bending behaviour of unstiffened hybrid beams lies somewhere between that of an equivalent homogeneous beam made of the web steel and an equivalent beam made of the flange steel. Furthermore, due to the fact that the greater part bending stresses of a beam are resisted by the flanges, it is clear that the hybrid behaviour would more closely resemble that of the equivalent homogeneous higher strength steel.

Where the web and flange steel materials have yield strengths which are fairly close in value, hybrid beams begin to demonstrate homogeneous behaviour in that the flanges yield first, and not the webs. In addition, the characteristic strength of the hybrid, which is the flange yield moment, approaches the homogeneous beam strength which is the yield moment of the section.

The strength reserves at plastification are less for hybrid beams than for homogeneous beams which implies that 'failure' of the beam occurs soon after the ultimate load is reached. This further suggests that it would be more conservative to take the flange yield moment as the characteristic hybrid beam strength.

(ii) The influence of different width to thickness ratios on the behaviour of unstiffened hybrid beams;

Flange slenderness does influence the ultimate load-carrying capacity of hybrid beams significantly with the less slender flanges sustaining greater loads. Like homogeneous beams, short beam lengths fail by yielding, with rapid unloading. Beyond the ultimate load of the beam, instability takes the form of lateral displacement of the compression flange and web. Longer lengths experience localised yielding and buckling of the compression flange, with unloading happening gradually. Flange buckling occurs at midspan and this is particularly emphasised in this research as all flanges are classified as 'non-compact' according to the recommended slenderness limits.

(iii) The extent to which current design and recommendations that are presented in the various design codes and literature can be extrapolated for use in hybrid beam design;

Extrapolation of existing code recommendations for slenderness limits shows that some of the high strength steel webs and flanges are, technically speaking, compact. However, the fact that some of these 'compact' sections could not reach even their yield moments implies that extrapolating the existing section classification limits for hybrid beams with high strength steel flanges is not appropriate.

(iv) The effectiveness of the commonly used hybrid configuration;

Hybrid arrangement 4, HYB4, with high strength steel flanges is the most suitable arrangement as it provides extra strength to the flanges in both positive and negative bending regions. Hybrids 1 and 3 are specifically suited to positive and negative regions respectively and would effect cost savings by reducing the weight of the high strength steel required.

5.2 Recommendations

There is a need for basic design guidelines and the equations proposed by Frost and Schilling (1964) and the Joint ASCE-AASHO Committee (1968) would prove to be useful tools if included in design codes.

Modifying the limiting width to thickness ratios to accommodate high strength web and flanges would ensure that the hybrid flange yield moment is reached before buckling occurs. A flange width to thickness ratio of less than 6 would ensure greater ultimate load-carrying capacity for steels with yield stress greater than 460MPa. The proposed modification factor would then extend the limits to accommodate even 700MPa steel. The proposed web width to thickness ratio is 55 for 460MPa steel and can be similarly modified to encompass 700Mpa steel.

Only two beam lengths were investigated in this study but further research is needed in order to investigate the behaviour of longer span lengths where failure is governed by lateral torsional buckling. This would lead to formulation of guidelines for lateral bracing in unstiffened hybrid beams.

Bibliography

Bibliography

1. ABAQUS/CAE Version 6.4-3 © ABAQUS, Inc.
2. ABAQUS/CAE Version 6.5-1 © 2004 ABAQUS, Inc.
3. Adonyi, Y., Weldability Testing of the HP 70W Steel Final Report Feb. 1998, Report Prepared for the Carderock Division, Naval Surface Warfare Centre.
4. AISI-FHWA-Navy HPS Steering Committee and welding Advisory Group. Guide Specification for Highway Bridge Fabrication with HPS 70W (HPS 485W) Steel. 2nd Edition June 2003.
5. American Institute of Steel Construction Load and resistance Factor Design, AISC LRFD 1999.
6. Atkins, G., Thiessen, D. and Adonyi, Y. Welding Process Effects in Weldability Testing of Steels. Welding Journal April 2002.
7. Barth, K., White, D.W. and Bobb, B.M. Negative Bending Resistance of HPS 70W Girders. Elsevier J Constructional Steel Research Vol. 53 (2000).
8. Beg, D. and Hladnik, L. Slenderness Limit for class 3I Cross-sections made of High Strength Steel. Elsevier J Constructional Steel Research Vol. 38 (3) 1996.
9. Bjorhovde, R. Development and Use of High Performance Steel. Elsevier J Constr. Steel Research Vol. 60 (2004).
10. Carskaddan, Phillip S., Shear Buckling of Unstiffened Hybrid Beams, Journal of the Structural Division, August 1968, Volume 94, No. ST8.
11. Clarin,M., 'High Strength Steel Local Buckling and residual Stresses'.
12. Cook, R.D., Finite Element Modelling for Stress Analysis, John Wiley and Sons, © 1995 United States of America.
13. Creamer, M., Engineering News, March 4-10, 2005.
14. Datta, Ramen; Mishra, Sanak, Developing High Strength Steel, Advanced Materials and Processes, November 2001, Volume 159, Issue 11.
15. Driver, R.G., Abbas, H.H. and Sause, R. Local Buckling of Grouted and Ungrouted Internally Stiffened Double-plate HPS Webs. Elsevier J Constructional Steel Research Vol. 58 (2002).
16. Earls, C.J. Constant Moment Behaviour of High-performance Steel I-shaped Beams. Elsevier J Constructional Steel Research Vol. 57 (2001).

17. Earls, C.J. On the Inelastic Failure of High Strength Steel I-shaped Beams. Elsevier J Constructional Steel Research Vol. 49 (1) 1999.
18. Earls, Christopher J., Influence of Material effects on Structural Ductility of Compact I-Shaped Beams, Journal of Structural Engineering, November 2000.
19. Eurocode EN 1993-1-1.
20. Fortner, Brian, Forging Ahead, Civil Engineering, April 1999, Volume 69, Issue 4.
21. Frost, R. and Schilling, C., Behaviour of Hybrid Beams Subjected to Static Loads, ASCE Journal of the Structural Division, June 1964, Volume 90, No. ST3.
22. Greco, Nicola and Earls, C.J., Structural Ductility in Hybrid High Performance Steel Beams, Journal of Structural Engineering, December 2003.
23. Green, P.S., Sause, R. and Ricles, J.M. Strength and Ductility of HPS Flexural Members. Elsevier J Constructional Steel Research Vol. 58 (2002).
24. Haaijer, G., Economy of High Strength Structural Members, ASCE Journal of the Structural Division, December 1961, Volume 87, No. ST8.
25. Hibbet, Karlsson and Sorenson, Inc., ABAQUS/Standard User's Manual Version 6.3 © 2002.
26. Hibbet, Karlsson and Sorenson, Inc., ABAQUS/Standard User's Manual Version 6.3 © 2002.
27. Hibbet, Karlsson and Sorenson, Inc., Getting Started with ABAQUS/Standard Interactive Version, Version 6.3 © 2002.
28. Hibbet, Karlsson and Sorenson, Inc., Getting Started with ABAQUS/Standard Interactive Version, Version 6.3 © 2002.
29. Hildebrand, J. and Schliebner, R. Simulation, Computation and Fatigue Tests of Welded joints Between High-strength Fine-grained Steels and structural Steels. Conference Proceedings- Progress in Structural Engineering, Mechanics and Computation, Zingoni (Editor) 2004 © Taylor and Francis Group, London.
30. Howard E. Boyer (Editor), Atlas of Stress-Strain Curves, ASM International, Metals Park Ohio, © 1987.
31. Kulevan.ac.be, Accessed 27 October 2006 http://www.kuleuven.ac.be/bwk/materials/Teaching/master/wg06/l0300.htm.

32. Kulicki, John M., The Shape of Things to Come, Civil Engineering, February 2000, Volume 70, Issue 2.
33. Lagerqvist, O. and Johansson, B. Resistance of I-girders to Concentrated Loads. Elsevier J Constructinal Steel Research Vol. 39 (2) 1996.
34. Lagerqvist, O. Resistance of Bridge Girder Webs Subjected to Concentrated Forces. Elsevier J Constructional Steel Research Vol. 46 (1-30) 1998.
35. Lwin, M.M., Hamby, G. et al. High Performance Steel Designers' Guide 2nd Edition, April 2002. U.S. Department of Transportation Federal Highway Administration.
36. MacDougall, C., Driver, R. and Grondin, G., A state-of-the-Art of High Performance Steel for Bridge Design, Accessed 27 August 2004, http://www.mtq.gouv.qc.ca/fr/publications/ministere/llcolloque/high-performance.pdf.
37. Madonna, Aveni, High Performance Steel Used in Box Girder Bridge Design, Civil Engineering, July 2001, Volume 71, Issue 7.
38. Mans, Patrick; Yakel, Aaron J.; Azizinamini, Atorod , Full-Scale Testing of Composite Plate Girders Constructed Using 485-MPa High-Performance Steel, Journal of Bridge Engineering, November/December 2001, Volume 6, Number 6.
39. Marquis, G.B., Steel Structures Design, Accessed 27 October 2006 http://www.lut.fi/kote/teras/Buckling.pdf.
40. Miki, C. et al. High Strength and High Performance Steels and their use in Bridge Structures. Elsevier J Constructional Steel Research Vol. 58 (2002).
41. Miki, C. et al. High Strength and High Performance Steels and their use in Bridge Structures. Elsevier J Constructional Steel Research Vol. 58 (2002).
42. Puthli, R. and Fleischer, O. Investigations on Bolted Connections for High Strength Steel Members. Elsevier J Constructional Steel Research Vol. 57 (2001).
43. Report of the Subcommittee 1 on Hybrid Beams and Girders, Joint ASCE-AASHO Committee on Flexural Members, ASCE Journal of the Structural Division, June 1968, Volume 94. No. ST6.
44. Sause, Richard; Fahnstock, Larry A., Strength and Ductility of HPS_100W I-Girders in Negative Flexure, Journal of Bridge Engineering, September/October 2001.

45. South African National Standards, SANS 10162-1, 2004.
46. Thomas, S.J. and Earls, C.J., Cross-Sectional Compactness and Bracing Requirements for HPS483W Girders, Journal of Structural Engineering, December 2003.
47. Tryland, T., Hopperstad, O.S. and Langseth, M., Steel Girders Subjected to Concentrated Loading- Validation of Numerical Simulations. Elsevier J Constructional Steel Research Vol. 50 (1999).
48. Wasserman, Edward P., Optimisation of HPS-70W Applications, Journal of Bridge Engineering, Volume 7 , Number 1, January 2002.
49. Wassermann, Edward; Azizinamini, Atorod; Pate, Henry; Greer, William, Making the Grade, Civil Engineering, April 1998, Volume 68, Issue 4.